Gradient Elasticity Modelling and Analysis for the Mechanics of Unidirectional and Bidirectional Fiber Reinforced Composites

by

MohammadMahdi Zeidi

A thesis submitted in partial fulfillment of the requirement for the degree of

Master of Science

Department of Mechanical Engineering

University of Alberta

ABSTARCT

The mechanics of fiber-reinforced solids have consistently been the subject of intense study that significantly advances our knowledge and practice in materials science and engineering. The subject leads to two major branches of researches involving either the direct investigation of local behaviors of an individual fiber—matrix system including interfacial region or the development of continuum theory through which the overall microscopic behavior of fibers is adequately taken into account in the model of deformations. The former relies on massive identification procedures, which most often require huge computational resources. Nonetheless, this approach was used successfully in the analysis of the mechanics of composite materials. Continuum-based approaches offer the advantages of the continuum descriptions and the associated mathematical framework. In this thesis, a continuum-based model is presented for the mechanics of unidirectional and bidirectional composites subjected to finite plane deformations (flexure and extension). This is framed in the development of a constitutive relation within which the constraint of material incompressibility is augmented. The elastic resistance of the fibers is accounted for via the computation of variational derivatives along the lengths of fibers. The equilibrium equation and necessary boundary conditions are derived by virtue of the principles of virtual work statement. A rigorous derivation of the corresponding linear theory is developed and used to obtain analytical solution for small deformations superposed on large. Also, The solutions of the resulting Partial Differential Equations (PDEs) are obtained using the Finite Element Analysis (FEA), which demonstrate excellent correspondence with existing theoretical and experimental results. The numerical results are compared with the results in literatures (FEniCS Project) showing a good agreement. The proposed model can serve as an alternative 2D Cosserat theory of nonlinear elasticity.

PREFACE

Four peer-reviewed journal papers were combined to compose the main body of thesis:

Chapter 2 of this thesis has been published as: Zeidi, M., Kim, C.I., (2018). Finite plane deformations of elastic solids reinforced with fibers resistant to flexure: complete solution. **Archive of Applied Mechanics**, 88(5), 819-835, http://doi.org/10.1007/s00419-018-1344-3

Chapter 3 as: Zeidi, M., Kim, C.I., (2017). Mechanics of fiber composites with fibers resistant to extension and flexure. **Mathematics and Mechanics of Solids**, http://doi.org/10.1177/1081286517728543

Chapter 4 as: Zeidi, M., Kim, C.I., (2018). Mechanics of an elastic solid reinforced with bidirectional fiber in finite plane elastostatics: complete analysis. **Continuum Mechanics and Thermodynamics**, 30(3), 573-592, http://doi.org/10.1007/s00161-018-0623-0

Chapter 5 as: Kim, C.I., Zeidi, M., (2018). Gradient elasticity theory for fiber composites with fibers resistant to extension and flexure. **International Journal of Engineering Science**, https://doi.org/10.1016/j.ijengsci.2018.06.002

ACKNOWLEDGEMENTS

TABLE OF CONTENTS

LIST OF FIGURES

LIST OF TABLES

Chapter 1

Introduction and Background

We begin this chapter with a brief introduction of fiber-reinforced composites. In section 1.1, we discuss the strain gradient theory and some examples about continuum-based models with strain gradient in bending and torsion. Furthermore, section 1.2 provides historical background of higher-order gradient theory and explains Piola's contributions and his followers (Truesdell, Mindlin and Toupin). Also, generalized continua is presented in sections 1.3 and 1.4. In section 1.5, we illustrate application of higher order theory in crack/fatigue, soft materials and fiber reinforced composite. Lastly, we will demonstrate goals and advantages of this thesis in section 1.6.

1.1   Introduction

The mechanics of materials with distinct microstructures has consistently been the subject of intense study ([1]-[2]) due to their practical importance in materials science and engineering. It is widely believed that, for many materials, the microstructure of a material governs the overall mechanical responses of materials [3]-[4]. Fiber-reinforced composites are a particular case of such materials where fibers; microstructure of the composite; are embedded in a matrix material. In practice, these fibers are often presumed to be densely distributed so as to render the idealization of continuous distribution which further leads to the continuum description of fiber-composites via a homogenization procedure. Within this prescription, the composites can be regarded as a special type of anisotropic materials

where the response function depends on the first gradient of deformations, typically augmented by the constraints of bulk compressibility or fiber inextensibility. In the latter case, the resulting prediction models are often so constrained that the corresponding deformation fields are essentially kinematically determinate, particularly those arise in fibers ([5]-[6]). Nonetheless, continuum-based approaches were used widely in the analysis of the mechanics of composite materials for their advantage in the continuum descriptions and the associated mathematical frame work ([5]-[7]).

The continuum theory, which accounts microstructural effects of fibers on elastic materials, has gained renewed attention in recent years ([8]-[9]). This includes the refinement of the first-order continuum theory by considering the higher gradient of deformations in an effort to describe the more detailed characterization of the continua with microstructure. In the case of fiber composites, this means the incorporation of the bending resistance of the fibers into the models of deformations. This is framed in the setting of the nonlinear strain-gradient theory ([10]-[11]) of anisotropic elasticity where the bending resistance of fibers is assigned to the changes in curvature of fibers explicitly [8]. The latter is obtained via the computation of the second gradient of deformations in which the fibers are regarded as continuous curves defined in convected coordinates. Current applications of the general theory are discussed in [12]-[13], and mathematical aspects of the subject are presented in [14]-[15]. A theory for an elastic solid with fiber's resistant to flexure, stretch and twist is developed in [16] under the simplified setting of the constraint Cosserat theory. In addition, authors in [17]-[18] discussed second-gradient theory of elasticity for the mechanics of meshed structures and examined shear strain distributions of the meshed structure subjected to the plane bias extension. The majority of the aforementioned studies have been conducted in the limited scope that either inextensible fibers or single family of fibers are considered. Moreover, although recent studies [17]-[19] and [20] reveal that the second-gradient theory accurately predicts the smooth transitions of shear strain

fields of meshed structures undergoing bias extensions, the compatible results in the case of general fiber composites remain absent from the literature.

As we discussed above about strain-gradient application and advantages in the modeling and analysis for the mechanics of fiber-reinforced composite, hear we present this theory briefly:

When the deformations are small, the second gradient of the deformation can be neglected. In this case, the relation between stresses and spatial derivatives of displacement is linear. Due to this linear relation, tractions can be defined by the unit area of undeformed body. Hence, when applied forces are determined, we can find corresponding stress fields and displacements by solving a Boundary Value Problem (BVP) explicitly.

The main interests in the finite elasticity are controllable (exact) deformations. The common approach to the aforementioned problem is utilizing inverse method. This method was originally developed by Rivilin [21] at first. When the body is compressible, only pure homogeneous deformation is admissible (see Ericksen [22]). Therefore, it is obvious that we have to use approximate methods. These methods are:

- The first method is that we use polynomial form of strain energy as a function of strain invariants [2]. This assumption is based on small deformations and no restrictions are imposed on rotations.

- The second method is that we assume deformations are small but not infinitesimal. Thus, the perturbation theory can be used. This method is formulated and is used for several problems in nonlinear elasticity (see for example [2]-[6]).

Rivilin [21] developed a new method which called the second gradient elasticity using up to the second order of deformation gradient (see Figure 1.4). In his method, it is assumed that classical theory is not accurate enough because it only takes up to first (linear) order of deformations which can not capture large deformations. With some mathematical procedures, Rivilin decreases surface traction

$$X = X(\xi^1, \xi^2) \qquad\qquad x = x(\xi^1, \xi^2)$$

$$\frac{\partial x^i}{\partial X^P} = \frac{\partial x^i}{\partial \xi^\alpha} \frac{\partial \xi^\alpha}{\partial X^P}$$
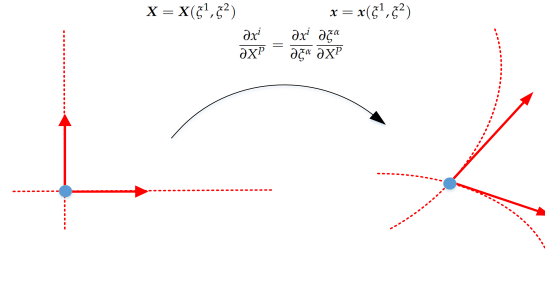
Figure 1.1: Rate of changes in lengths/angles via first gradient

$$\frac{\partial^2 x^i}{\partial X^P \partial X^Q} = \frac{\partial}{\partial X^Q} \left(\frac{\partial x^i}{\partial \xi^\alpha} \frac{\partial \xi^\alpha}{\partial X^P} \right)$$

$$\frac{\partial^2 x^i}{\partial X^P \partial X^Q} = \underbrace{\frac{\partial^2 x^i}{\partial \xi^\beta \partial \xi^\alpha}}_{\text{def. hessian}} \frac{\partial \xi^\beta}{\partial X^Q} \frac{\partial \xi^\alpha}{\partial X^P} + \frac{\partial x^i}{\partial \xi^\alpha} \underbrace{\frac{\partial^2 \xi^\alpha}{\partial X^Q \partial X^P}}_{\text{inv. ref. hessian}}$$
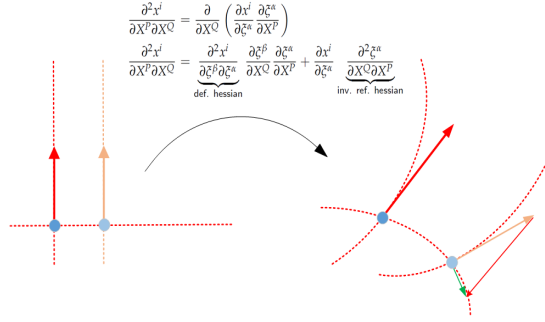
Figure 1.2: Rate of changes in length via second gradient

BVP to the system of two equations which describes the mechanics of homogeneous isotropic, elastic and compressible materials. Figures 1.1 and 1.2 show differences between the first and second gradient theory. Higher order gradient theory accounts relative rotation at each material point of an elastic body. Mathematically, we can define stress-strain relation for both classical and higher order gradient continua as given in Eq. (1.1).

$$\text{Classical continua} \implies \sigma = f(\varepsilon)$$

$$\text{Higher order gradient continua} \implies \sigma = f(\varepsilon, \nabla \varepsilon, ...) \qquad (1.1)$$

Also figure 1.3 shows comparison of the extension test by using the first gradient (linear) and second gradient approaches [23]. First gradient approach results are close to the fishnet theory which considers fiber composites as lattice (interlocked fibers). The results of second gradient theory have a good agreement with the experimental results, where the first gradient simulations were not able to produce accurate results. The main advantage of second gradient elasticity-based analysis

in the case of bias extension test is to capture transition zones (transitions between red and green zones and also between blue and green zones as shown in figure 1.3). In chapter 5, we will present a more detailed numerical and analytical comparisons which clearly indicate that the our proposed model successfully predicts the smooth transitions of the shear strain fields unlike those described by the first-order theory where a significant discontinuity is present.
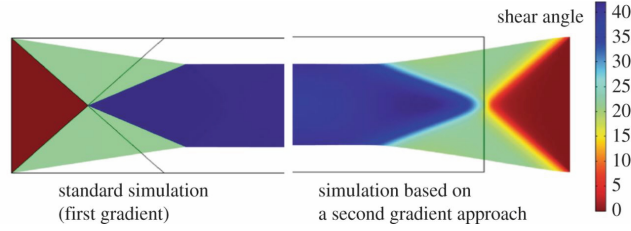
Figure 1.3: First vs. second gradient elasticity comparsion (Picture taken from: [23])

1.1.1 Examples of models with strain gradient

Examples of models, which are proposed in the case of strain gradient theory, will be discussed in this section. By using this models, it is possible to incorporate size effects in torsion and bending analysis.

–Linear elastic material behavior:

$$\sigma = E(\epsilon - l^2 \nabla^2 \epsilon) \quad \text{where } l = \text{material parameter.} \tag{1.2}$$

–Bending:

$$\sigma = E(\epsilon - c.\mathbf{sign}(\epsilon)\nabla\epsilon) \quad \text{where } c = \text{gradient coefficient.} \tag{1.3}$$

–Torsion:

$$\sigma = G(\quad -c_1(\nabla \ .\nabla \ )^{0.5} - c_2\nabla^2 \ ) \quad \text{where } c_1, c_2 = \text{gradient coefficients.} \tag{1.4}$$

1.2 Higher-order gradient theory historical background

This section provides historical background of higher-order gradient theory developments and explains Piola's contributions and also his followers: Truesdell, Mindlin and Toupin.

1.2.1 Piola

Piola was born in Milan on 1794 and received his doctorate degree in mathematics at University of Pavia. Piola devoted all of his significant scientific life in demonstrating that the virtual work statement is the most effective and suitable method for developing new models which are able to show good agreement with experimental data and also can forecast the existence of unknown phenomena in Continuum Mechanics. In this part, Piola's idea and his contributions are illustrated:

Piola suggests the variational principles in the modeling and analysis of continuum mechanics. In his point of view, Lagrange's method is the most effective method. To support this argument, he expresses similarity between the theory of differential curves and rational mechanics. Piola states that Lagrange reduced all problems from rational mechanics into the energy minimization problems which require variational analysis. He also states that the variational principle reduces the probability of being misled ([24]). He generalized the theory of deformable bodies (methods of Lagrange). Piola has not considered the particular case of linearized deformation measures. He characterized the continuum models for which the state of deformation can be expressed by Green deformation measure and its derivatives with respect to Lagrangian referential coordinates.

1.2.2 Truesdell

Truesdell was born in California on 1919 and completed his doctorate degree at Princeton University. He developed foundational rational mechanics in order to establish mathematical models for continuum mechanics. Also, he had some developments in the rational thermodynamics.

It is stated in [24] that Truesdell did not fully understand the ideas of Lagrange and also Piola. Authors in [24] also mentioned that Truesdell does not recall the fact that Piola has proven the direct relevance between the principle of virtual work and the balance of momentum (Piola's theorem). Further, it is concluded in [24] that Truesdell exaggerated the concept of Cauchy in the procedure of founding continuum models. However, as shown by Piola, Mindlin, Sedov and Germain, the role of the Cauchy stress is not pivotal as Truesdell believed [24].

1.2.3 Mindlin and Toupin

Mindlin was born in New York on 1906 and studied mathematics at the Columbia University. In 1963, Mindlin generalized the classical continuum theory of elastic body (see section 1.3). One year after Mindlin, Toupin considered this method in the couple-stresses theories (simplified micropolar elasticity with constrained microrotations).

Mindlin and Toupin's efforts are based on the virtual work statement and the principle of least action. They established the most appropriate continuum models for the modelling of complex mechanical systems [25]-[26].

In [27], Mindlin incorporates the gradient of virtual deformation up to the third order. He suggests a model for internal work where the work is expanded by internal interactions on virtual displacement. He then introduces set of three stress tensors which are the first, second and third-order gradient of virtual displacement through which he finds admissible contact interactions. Mindlin's results are PDEs with admissible boundary conditions. Mindlin uses functional analysis and

differential geometry in his theory.

1.3 Generalized continuum theory

Due to the rationalization of continuum mechanics by Truesdell (see section 1.2), generalized continuum theory was very popular on 1960s. Nowadays, researches regarding these theories are very popular due to their application in tissue engineering, biomechanics and biological membranes.

Two major approaches were developed in order to generalize the classical continuum theory by incorporating the length scale into the models of deformations. First approaches is to include additional degree of freedom (DOF) into the models of deformations. Second methods are developed based on the observation that strain energy function is combined with high-order gradients (Couple stress theory). Several researchers, for example: Toupin, Mindlin and Koiter adopted these theory and formulated continuum based models which are in opposition to the independent director fields theory that Truesdell and Cosserat proposed.

Voigt in [3] considered continua with additional DOF at each material point (three microrotations DOF). Voigt believed that each point in the body is acting as a rigid body. The other approach is to consider the microstructures of materials so that it can accommodate the bending and extension of the material points.
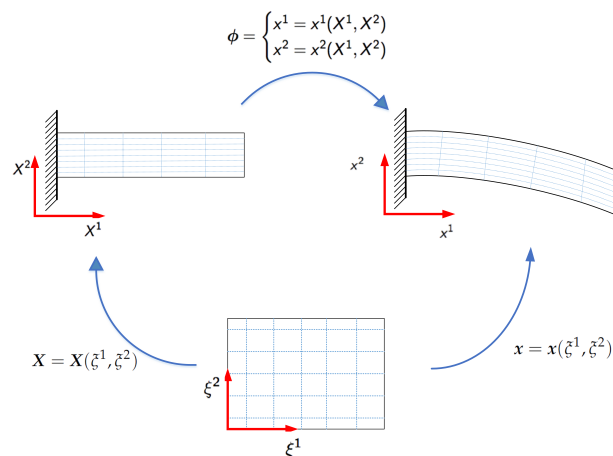
Figure 1.4: Starin grdaient

Eugène Cosserat and François Cosserat proposed this idea in [28]. They considered a triad of directors at each point, in addition to position. The gradients of director were constrained so that only rotational motions are considered. This allows micro-rotations at each point which is dependent on the position. This is completely different with the higher-order gradient theory where position and director fields can be independent.

Toupin and Noll developed coupled-stress theory in [10]. They mentioned that only the first-order deformation gradient appears in the constitutive relation which is not accurate enough for their point of view. They proposed that, constitutive dependence need to be extended in order to include higher-order gradients fields. More specifically, when the gradients are considered up to N-th order, the corresponding function describing materials is necessarily N-order differentiable. In addition, Reissner [29] developed finite deformation theory based on the model suggested by Toupin.

In summary, the differences between classical continua and generalized continua are:

1. **Classical Continua:**

- 3 displacement components $\implies (u_1, u_2, u_3)$
- Symmetric stress tensor $\implies \sigma = \sigma^T$

  —Not able to fully cover the macro and nano scales,

  —Size-effects cannot be captured.

2. **Microstructured continua:**

- 3 displacements and 3 microrotations $\implies (u_1, u_2, u_3, \varphi_1, \varphi_2, \varphi_3)$
- Asymmetric stress tensor $\implies \sigma \neq \sigma^T$

  —Introduce material *length scale.*

  —Popular due to their application in modeling and analysis of the biomedical, tissue and biological systems.
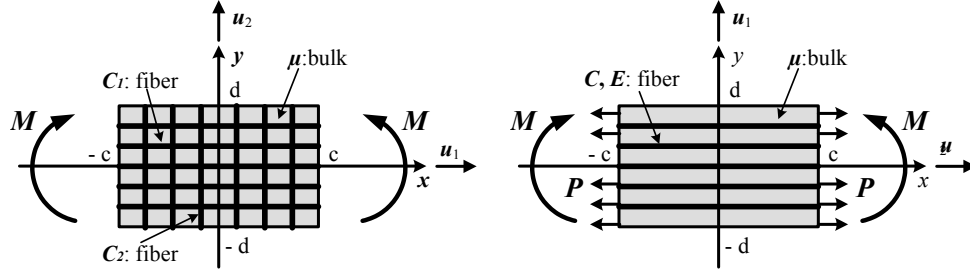
Figure 1.5: Schematic for bidirectional and unidirectional fiber

1.4 Gradient elasticity theory for fibre-reinforced composites

Adkins is the first researcher who developed theory of fibre-reinforced composite (Figure 1.5). He considered inextensible fibers distributed on surfaces and subsequently extended his theory to the case where fibers are distributed uniformly in a medium [30]. This model can be considered as special cases of Spencer's theory which we explain in the next paragraph.

Spencer developed a more comprehensive theory of fibre-reinforced composite [1]. He used nonlinear anisotropic elasticity in which the constraints of incompressibility and fiber inexetensibity are imposed. In his model, fiber's bending and shear motion are excluded. Later, Spencer and Soldatos [8], based on the nonlinear strain gradient ([10]-[11] and [31]), developed the theory which is capable of accommodating fibers elastic resistance against to twist and shear. Using the nonlinear strain gradient theory, Del'Isolla and Steigmann [9] considered fabrics where the gradient is determined from the surface deformation. Finally, Steigmann [16] eliminated constraints of fibers by means of modeling them as Kirchhoff rods. He established the theory of fiber reinforced composites where fiber's resistant to bending and shear is incorporated. In this theory, the fibers can bend and stretch.

In the case fiber reinforced composites, bending energy in higher order theory has a finite value which causes smooth transition in contrast to the first order theory that bending energy is infinite as shown in figure 1.6.

Figure 1.6: Comparsion classical and higher order theory

1.5   Higher-order gradient theory application

- **Fiber reinforced composites:**

It is necessary to consider the fibre bending stiffness by means of the dependence of the deformation energy (see figure 1.6) on the second deformation gradient ([2]-[6]). Because first-order gradient models can not capture all needed information (e.g. microstructure rotations of material; see section 1.4). The mechanical behavior of fibre-reinforced composites can be expressed by:

1. Considering each fibre as a Euler or Timoshenko beam,

2. Modelling interactions between the fibers by using *elastic*, *visco-elastic* or *visco-plastic* constraints [24].

This model has some disadvantages such as:

1. Need super-fast calculating devices,

2. No efficient analytical and semi-analytical optimization processes are available.

In result, when bending resistance of the fibers is considered explicitly based on higher-order gradient theory, we are able to capture general behaviors of fiber composites.

- **Living Tissues:**

Due to the complex nature of living tissues, they need to be described with high-order gradient models [32]. Bone tissues are recommended to be analyzed and modelled (see Figure 1.7) by using continuum models which incorporate microstructure [33]. Moreover, the biological activity of living parts of bone tissues produces a continuous remodelling of them. Living tissues can be modeled as composites with one family of statistically oriented continuous fibers. The fibre's orientation (statistical orientation) can be expressed by using probability distribution density function. With this assumption, we can model living tissue with the theory of fiber reinforced composite which discussed in section 1.4 (see Federico [34]). Authors in [34] mentioned that for modelling tendons and ligaments, we can use one family of fibers and also for modelling intervertebral disc and adventitial layer of blood vessel, we have to use two families of fibers [34].
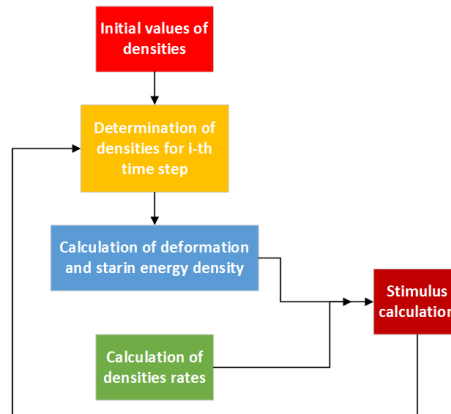
Figure 1.7: Analysis of bone remodeling with substitute material

Such phenomena have been studied in [35] in details. Bone tissues are created with a multiscale structure and thus can show unwanted behaviors, such as:

1. Mechanical instabilities,

2. Internal boundary layer formation for deformation.

- **Meta-materials in biological applications:**

Tissue can be constructed by adding an artificial, biocompatible and biodegradable material. It is preferable that the added material has the same mechanical and

chemical behaviors in compare to the natural tissue in order to retain mechanical and chemical behaviors in the optimum state. This principle is used in [36] where it is shown that how the microstructural responses of a hypothetical biodegradable material may positively influence the remodeling process in a reconstructed bone tissue (see Fig. 1.8). This opens an important possible fields of researches in this theory. The synthesis of tailored meta-materials is becoming a more and more popular research subject.
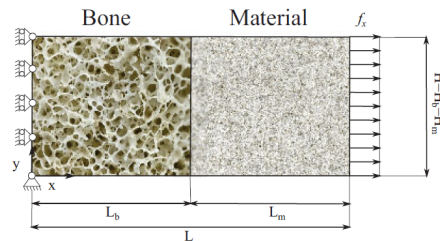
Figure 1.8: Schematic of 2D model bone tissue (Picture taken from: [36])

A metamaterial is a material, designed to have a chemical and mechanical behavior that can not be find in nature. The designed metamaterials are necessarily to exhibit mechanical behaviors which have to favor their role as a scaffold on new bone tissue which need to be formed by a deposit process. Moreover, they need to be biocompatible so that they do not interfere with the physiological remodeling and reconstruction activities of cells present in tissue. Their mechanical behavior need to be optimized by using high-order theory in order to describe bone tissue remodeling processes. Bone tissue remodeling is a process which the skeleton is periodically renewed to retain the bone's biochemical and biomechanical behaviors. This process is done by removing continuously damaged bone tissue and creating new one. This Process consists below stages as shown in Fig. 1.9 (see [37]):

–Quinesence,

–Resorption,

–Reversal,

–Formation,

–Mineralization.
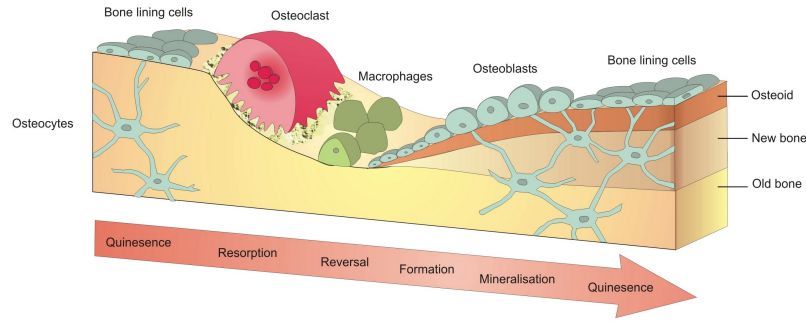
Figure 1.9: Bone remodeling (Picture taken from: [38])

- **Crack and damage:**

First order gradient models have been considered to model the crack and plastic deformations of media [39]. Many numerical and conceptual problems arise in the [39] show the possibility of singular solutions (see [40]). Higher-order gradient models are used to formulate well-established models, in which the localization of the material regions where crack is nucleated, has been determined by using the higher-order gradient (see [41]). In [41], Francfort made the formulation of variational analysis for modelling crack and damages. The results in Francfort's paper show that employing higher-order gradient terms are necessary for this application and it helps us to obtain the more accurate descriptions of crack-matrix systems (without singularity issues) [24].

1.6   Goals and Motivations

As we discussed in sections 1.1-1.5, the classical continuum theory (first gradient) can not describe microstructure continua. In order to make our results close to the experimental data and also to increase accuracy of them, we have to use higher gradient theory. In this thesis, we consider bending resistance of the fibers, based on nonlinear strain gradient theory. In result, we can capture general behaviors of fiber composites. By using complicated models in the case of fiber reinforced composite, we need to apply rigorous and advanced numerical and analytical techniques in order to solve governing system of nonlinear coupled equations. The

ultimate goal of this study is to develop continuum-based models and solve the corresponding analytical and numerical solutions of Partial Differential Equations (PDEs) which are obtained from the gradient elasticity theory for the mechanics of bidirectional and unidirectional fibers with fibers resistant to flexure and stretches. In this thesis, we eliminate constraints of fibers by means of modeling them as Kirchhoff rods so that the fibers can bend and stretch within the medium.[16]. We develop a continuum-based model for the mechanics of fiber-reinforced subjected to finite plane deformations. The procedures for developing this model are given in chapter 2-5. We first define Kinematics and Equilibrium equations by using the principles of virtual work statement and then successively find governing system of nonlinear coupled fourth order PDEs in the case of Neo-Hookian type materials. Neo-Hookian materials was proposed by Mindlin on 1948 and is a hyperelastic material model that can be used for prevising the nonlinear stress-strain behavior of materials. Then, we solve governing equations both analytically and numerically via Finite Element Method (FEM). In analytical solution, the derivation of the corresponding linear theory is developed and used to obtain a complete analytical solution. We develop a model which can serve as an alternative 2D Cosserat theory of nonlinear elasticity.

The challenging parts of this thesis is, obtaining analytical and numerical solutions of corresponding systems of equation and boundary conditions. This is due to the fact that the conventional methods, Fourier transform and the method of separation of variable, are not applicable. Instead, we adapt modified separation of variable methods and successfully obtain complete analytical solutions for the small deformations superposed on large which we will explain in detail in chapter 3 to 5. Also, due to the complex nature of the resulting PDEs, it was not possible to obtain solutions using the commercial numerical softwares (e.g. COMSOL, Maple, Abaqus and Mathematica). To overcome the difficulties, we developed our own numerical schemes through which complete numerical solutions are obtained. The detailed procedures are given in chapter 2 to 5.

1.7 Structure of Thesis

This thesis consists four main chapters plus introduction and conclusion chapters and also each chapter starts with an abstract. The main chapters present:

Chapter 2, discusses a continuum model that can accommodate *unidirectional* fiber's elastic resistance to *flexure*. The fibers are regarded as continuously distributed spatial rods of Kirchhoff type such that the kinematics are based on their position field and a director field. Furthermore, we seek a complete model describing the finite plane deformations of elastic solids reinforced with fibers resistant to flexure. Hence, we assume that the fiber's directional field remains in a plane, with no components in the out of plane direction, and the corresponding deformations and all material properties are independent of the out of plane coordinate. Within this prescription, we consider a special case of a Neo-Hookian material reinforced with a single family of fibers.

Chapter 3, presents mechanics of *unidirectional* fiber reinforced composites with fiber resistant to *flexure* and *extension*. The results are also compared with the experimental data demonstrating that the proposed model successfully predicts the deformed configuration of a crystalline nanocellulose fiber composite subjected to three-point bending.

A continuum-based model in the analysis of an elastic solid, reinforced with *bidirectional* fibers are developed in chapter 4. The results are then compared with several experimental data demonstrating that the proposed model successfully predicts the deformed configurations of a crystalline nanocellulose fiber composite subjected to three-point bending and also corresponds with the experimental results for T700S carbon–E glass fiber composites.

Chapter 5, illustrates the mechanics of *bidirectional* fiber reinforced composites with fiber resistant to *flexure* and *extension*. More importantly, the proposed model assimilates, in the case of bidirectional fiber reinforced composites, the plane bias extension test and successfully predicts the smooth transitions of the corresponding shear strain fields, as opposed to the first-gradient theory, where the resulting

shear strain appears to be discontinued. In addition, we develop a compatible linear theory within the description of superposed incremental deformations. By employing *adapted iterative reduction and eigenfunction expansion* methods (modified separation of variables method), a complete analytical solution is obtained.

Chapter 6, summarizes all chapters and illustrates potential future research that may be used in the future research.

Throughout all chapters, we make use of a number of well-established symbols and conventions such as $\mathbf{A}^T$, $\mathbf{A}^{-1}$, $\mathbf{A}^*$ and $\mathsf{tr}(\mathbf{A})$. These are the transpose, the inverse, the cofactor and the trace of a tensor $\mathbf{A}$, respectively. The tensor product of vectors is indicated by interposing the symbol $\otimes$, and the Euclidian inner product of tensors $\mathbf{A}$, $\mathbf{B}$ is defined by $\mathbf{A} \cdot \mathbf{B} = \mathsf{tr}(\mathbf{A}\mathbf{B}^T)$; the associated norm i$\sqrt{\mathbf{A} \cdot \mathbf{A}}$. The symbol "$|\cdot|$" is used to denote the usual Euclidian norm of vectors. Latin and Greek indices take values in $\{1, 2\}$ and, when repeated, are summed over their ranges. Lastly, the notation $F_{\mathbf{A}}$ stands for the tensor-valued derivatives of a scalar-valued function $F(\mathbf{A})$.

Chapter 2

Mechanics of unidirectional fiber-reinforced composite with fiber resistant to flexure

In section 2.1, we develop kinematics and equilibrium equation. Furthermore, we consider a special case of a Neo-Hookian material reinforced with a single family of fibers in section 2.1.1. Via the method of virtual work and the computation of variational derivatives along the length of a fiber, the corresponding Euler equilibrium equation, in the form of coupled Partial Differential Equations, is derived. In section 2.2, we present an analysis for the derivation of the necessary boundary conditions. In sections 2.3 and 2.4, a set of numerical solutions is obtained via a finite element analysis. Lastly, in sections 2.5 and 2.6, the development of linear theory and analytical solution of the present model are discussed.

2.1   Kinematics and Equilibrium Equations

We consider from [8] that the energy density for a fiber-reinforced solid is of the form

$$
\begin{aligned}
W(\mathbf{F}, \mathbf{G}) &= \widehat{W}(\mathbf{F}) + W(\mathbf{G}), \\
W(\mathbf{G}) &\equiv \frac{1}{2} C(\mathbf{F}) \left| \mathbf{g} \right|^2,
\end{aligned}
\tag{2.1}
$$

where F is the gradient of the deformation function $(\chi(X))$ and G is the second gradient of the deformation $(G = \nabla F)$. Further, C refers to the material property of fibers which, in general, independent of the deformation gradient $(C = C(F))$. The advantage of adopting above form of energy function is that the bending energy of the fibers is solely accounted by the strain gradient so that it allows one to compute energy variations induced by first gradient (F) and second gradient (G) in a separate manner. This approach has been widely and successfully used in the relevant studies ([15], [16] and [47]).

The orientation of a particular fiber is given by

$$\lambda = |\mathbf{d}| \text{ and } \boldsymbol{\tau} = \lambda^{-1}\mathbf{d} \tag{2.2}$$

where

$$\mathbf{d} = \mathbf{FD}, \tag{2.3}$$

in which $\mathbf{D}$ is the unit tangent to the fiber trajectory in the reference configuration. Eq. (2.3) can be derived by taking the derivative of $\mathbf{r}(s) = \boldsymbol{\chi}(\mathbf{X}(s))$, upon making the identifications $\mathbf{D} = \mathbf{X}'(s)$ and $\mathbf{d} = \mathbf{r}'(s)$. Here primes refer to derivatives with respect to arclength along a fiber in the reference configuration (i.e. $(*)' = d(*)/ds$). The expression for geodesic curvature of an arc $\mathbf{r}(s)$ is then obtained from Eq. (2.3) as

$$\mathbf{g} = \mathbf{r}'' = \frac{d(\mathbf{r}'(s))}{ds} = \frac{\partial(\mathbf{FD})}{\partial\mathbf{X}}\frac{d\mathbf{X}}{ds} = \nabla[\mathbf{FD}]\mathbf{D}. \tag{2.4}$$

Further, by using the chain rule, the compatibility condition of $\mathbf{F}$ is given by

$$G_{iAB} = F_{iA,B} = F_{iB,A} = G_{iBA}. \tag{2.5}$$

In this chapter, we adopt the framework of the virtual work statement $\dot{E} = P$ in the derivation of equilibrium equations. From (Eq. 2.1), the potential energy of

the system is given by

$$E = \int_w W(\mathbf{F}, \mathbf{G}) dA. \tag{2.6}$$

To accommodate the bulk incompressibility condition, we consider the following energy functional

$$
\begin{aligned}
E &= \int_w U(\mathbf{F}, \mathbf{G}, p) \, dA, \\
U(\mathbf{F}, \mathbf{G}, p) &= W(\mathbf{F}, \mathbf{G}) - p(J - 1),
\end{aligned}
\tag{2.7}
$$

where J is determinant of F and p is a Lagrange-multiplier field.

The derivation of the Euler equation and boundary conditions in second-gradient elasticity is well studied [10]-[11] and [46]. Here, we reproduce the results for the sake of clarity and completeness of the proposed model. The induced variation of the energy is then evaluated as

$$\dot{E} = \int_w \dot{U}(\mathbf{F}, \mathbf{G}, p) \, dA, \tag{2.8}$$

where

$$\dot{U}(\mathbf{F}, \mathbf{G}, p) = W_{\mathbf{F}} \cdot \dot{\mathbf{F}} + \mathbf{W}_{\mathbf{G}} \cdot \dot{\mathbf{G}} - p\dot{J}, \tag{2.9}$$

and subscripts denote corresponding partial derivatives. We note here that, within the framework of the forgoing model, the fiber's extensibility can be accounted through the variational computation of the energy density function with respect to ε. In other words, the energy density function is required to be a function of ε in addition to F, G and ρ to accommodate fiber's extensibility. The corresponding energy variation is computed as

$$\dot{U}(\mathbf{F}, \mathbf{G}, p, \varepsilon) = W_F \dot{\mathbf{F}} + W_\varepsilon \dot{\varepsilon} + W_{\mathbf{G}} \cdot \dot{\mathbf{G}}, \tag{2.10}$$

$$\dot{\varepsilon} \stackrel{(6)}{=} \left[\frac{1}{2}\left(\lambda^2 - 1\right)\dot{\ }\right] = \dot{\lambda}\lambda. \tag{2.11}$$

and

$$\dot{\lambda}\lambda = \mathbf{FD} \cdot \dot{\mathbf{FD}} = tr(\mathbf{FD} \otimes \dot{\mathbf{FD}}) = tr((\mathbf{FD} \otimes \mathbf{D})\dot{\mathbf{F}}^T) = \mathbf{F}[\mathbf{D} \otimes \mathbf{D}] \cdot \dot{\mathbf{F}}. \qquad (2.12)$$

The above computations are excluded from the present study in an effort to obtain mathematically tractable equations. Now, since $\dot{J} = J_F \cdot \dot{F} = F^* \cdot \dot{F}$, Eq. (2.8) yields

$$\dot{E} = \int_w [(W_{\mathbf{F}} - p\mathbf{F}^*) \cdot \dot{\mathbf{F}} + W_{\mathbf{G}} \cdot \dot{\mathbf{G}}]dA. \qquad (2.13)$$

Also, from Eq. (2.5), $W_{\mathbf{G}} \cdot \dot{\mathbf{G}}$ can be rewritten as

$$\frac{\partial W}{\partial G_{iAB}}\dot{G}_{iAB} = \frac{\partial W}{\partial G_{iAB}}u_{i,AB} = \left(\frac{\partial W}{\partial G_{iAB}}u_{i,A}\right)_{,B} - \left(\frac{\partial W}{\partial G_{iAB}}\right)_{,B}u_{i,A}, \qquad (2.14)$$

where $u = \dot{\chi}$ is the variation of the position field. By substituting Eq. (2.14) into Eq. (2.13), we find

$$\dot{E} = \int_w [\left(\frac{\partial W}{\partial F_{iA}} - pF_{iA}^*\right) \cdot \dot{F}_{iA} + \left(\frac{\partial W}{\partial G_{iAB}}u_{i,A}\right)_{,B} - \left(\frac{\partial W}{\partial G_{iAB}}\right)_{,B}u_{iA}]dA, \qquad (2.15)$$

the above becomes

$$\dot{E} = \int_w [\frac{\partial W}{\partial F_{iA}} - pF_{iA}^* - \left(\frac{\partial W}{\partial G_{iAB}}\right)_{,B}]\dot{F}_{iA}dA + \int_{\partial w}\left(\frac{\partial W}{\partial G_{iAB}}u_{i,A}\right)N_BdS, \qquad (2.16)$$

where N is the rightward unit normal to the boundary curve ∂w in the sense of the Green-stoke's theorem. If we assume the material response is uniform, Eq. (2.1) furnishes

$$W_{\mathbf{G}} \cdot \dot{\mathbf{G}} = C\mathbf{g} \cdot \dot{\mathbf{g}}, \qquad (2.17)$$

and

$$W_{\mathbf{G}} = C\mathbf{g} \otimes \mathbf{D} \otimes \mathbf{D}. \qquad (2.18)$$

21

For initially straight fibers (i.e. $\nabla D = 0$), $Div(W_{\mathbf{G}})$ reduces to

$$
\begin{aligned}
Div(W_{\mathbf{G}}) &= Cg_{i,B}D_A D_B (\mathbf{e}_i \otimes \mathbf{E}_A), \\
\left(\frac{\partial W}{\partial G_{iAB}} \right)_{,B} &= Cg_{i,B}D_A D_B.
\end{aligned}
\tag{2.19}
$$

Consequently, Eq. (2.16) becomes

$$
\dot{E} = \int_w P_{iA} \dot{F}_{iA} dA + \int_{\partial w} Cg_i D_A D_B u_{i,A} N_B dS,
\tag{2.20}
$$

where

$$
P_{iA} = \frac{\partial W}{\partial F_{iA}} - pF_{iA}^* - Cg_{i,B}D_B D_A.
\tag{2.21}
$$

Therefore, the corresponding Euler equation can be obtained as follows

$$
P_{iA,A} = 0
\tag{2.22}
$$

2.1.1 Neo-Hookian Materials

In the case of Neo-Hookian materials, the energy density function is given by

$$
\begin{aligned}
\widehat{W}(\mathbf{F}) &= \frac{\mu}{2} tr(\mathbf{C}) = \frac{\mu}{2} tr(\mathbf{F}^T \mathbf{F}) = \frac{\mu}{2} \mathbf{F} \cdot \mathbf{F} \\
W(\mathbf{F}, \mathbf{G}) &= \frac{\mu}{2} \mathbf{F} \cdot \mathbf{F} + \frac{1}{2} C |\mathbf{g}|^2
\end{aligned}
\tag{2.23}
$$

where μ and C are the material constant of the matrix and fiber, respectively. We mention here that the Neo-Hookian model is suitable for deformation analysis involving large rotation and small extension such as bending analysis [48]. Accord-

ingly, from Eqs. (2.21-2.22), the corresponding Euler equation can be obtained as

$$
\begin{aligned}
P_{iA,A} &= \mu F_{iA,A} - p_{,A} F_{iA}^* - C g_{i,AB} D_A D_B = 0, & (2.24) \\
F_{iA,A}^* &= 0
\end{aligned}
$$

If a fiber-reinforced material consists of a single family of fibers ($D = E_1$, $D_1 = 1$, $D_2 = 0$) and subjected to plane deformations, Eq. (2.24) reduces to

$$
\mu F_{iA,A} - p_{,A} F_{iA}^* - C g_{i,11} = 0 \text{ for } i, A = 1, 2, \tag{2.25}
$$

and

$$
\begin{aligned}
g_i &= F_{i1,1} = G_{i11}, & (2.26) \\
F_{iA} &= \frac{\partial \chi_i}{\partial X_A} \text{ and } F_{iA}^* = \varepsilon_{ij} \varepsilon_{AB} F_{jB},
\end{aligned}
$$

where ε_{ij} is the 2D permutation. Therefore, Eq. (2.26) together with the incompressibility condition furnishes a PDE system solving for χ_1, χ_2 and p.

$$
\begin{aligned}
\mu \left(\chi_{1,11} + \chi_{1,22} \right) - p_{,1} \chi_{2,2} + p_{,2} \chi_{2,1} - C \chi_{1,1111} &= 0, \\
\mu \left(\chi_{2,11} + \chi_{2,22} \right) + p_{,1} \chi_{1,2} - p_{,2} \chi_{1,1} - C \chi_{2,1111} &= 0, \\
\chi_{1,1} \chi_{2,2} - \chi_{1,2} \chi_{2,1} &= 1. \tag{2.27}
\end{aligned}
$$

2.2   Boundary Conditions

From Eq. (2.16), we have

$$
\dot{E} = \int_w P_{iA} \dot{F}_{iA} dA + \int_{\partial w} \left(\frac{\partial W}{\partial G_{iAB}} u_{i,A} \right) N_B dS, \tag{2.28}
$$

where

$$P_{iA} = \frac{\partial W}{\partial F_{iA}} - pF_{iA}^* - \left(\frac{\partial W}{\partial G_{iAB}}\right)_{,B}. \qquad (2.28\text{-}1)$$

Decomposing the above as in (2.15) (i.e. $P_{iA}u_{i,A} = (P_{iA}u_i)_{,A} - P_{iA,A}u_i$), the above yields

$$\dot{E} = \int_{\partial w} P_{iA}u_i N_A dS - \int_w P_{iA,A}u_i dA + \int_{\partial w} \left(\frac{\partial W}{\partial G_{iAB}}u_{i,A}\right) N_B dS, \qquad (2.29)$$

and hence the Euler equation $P_{iA,A} = 0$ which hold in w. With this satisfied, Eq. (2.29) reduces to

$$\dot{E} = \int_{\partial w} P_{iA}u_i N_A dS + \int_{\partial w} \left(\frac{\partial W}{\partial G_{iAB}}u_{i,A}\right) N_B dS. \qquad (2.30)$$

Now, we make use of the normal-tangent decomposition of ∇u as;

$$\nabla \mathbf{u} = \nabla \mathbf{u}(\mathbf{T} \otimes \mathbf{T}) + \nabla \mathbf{u}(\mathbf{N} \otimes \mathbf{N}) = \mathbf{u}' \otimes \mathbf{T} + \mathbf{u}_{,\mathbf{N}} \otimes \mathbf{N} \qquad (2.31)$$

where $T = X'(s) = k \times N$ is the unit tangent to ∂w; and $u' = du(X(s))/ds$ and $u_{,N}$ are the tangential and normal derivatives of u on ∂w (i.e. $u_i' = u_{i,A}T_A$, $u_{i,N} = u_{i,A}N_A$). Thus, Eq. (2.30) can be rewritten as

$$\dot{E} = \int_{\partial w} P_{iA}u_i N_A dS + \int_{\partial w} \frac{\partial W}{\partial G_{iAB}} \left(u_i' T_A N_B + u_{i,N} N_A N_B\right) dS. \qquad (2.32)$$

Since

$$\frac{\partial W}{\partial G_{iAB}}T_A N_B u_i' = \left(\frac{\partial W}{\partial G_{iAB}}T_A N_B u_i\right)' - \left(\frac{\partial W}{\partial G_{iAB}}T_A N_B\right)' u_i, \qquad (2.32\text{-}1)$$

we obtain

$$
\begin{aligned}
\dot{E} \;=\;& \int_{\partial w} \left\{ P_{iA}N_A - \left(\frac{\partial W}{\partial G_{iAB}} T_A N_B \right)' \right\} u_i dS \\
&+ \int_{\partial w} \frac{\partial W}{\partial G_{iAB}} u_{i,N} N_A N_B dS + \int_{\partial w} \left(\frac{\partial W}{\partial G_{iAB}} T_A N_B u_i \right)' dS. \quad (2.33)
\end{aligned}
$$

In view of Eq. (2.18) (i.e. $W_{\mathbf{G}} = Cg \otimes D \otimes D$), the above furnishes

$$
\begin{aligned}
\dot{E} \;=\;& \int_{\partial w} \left\{ P_{iA}N_A - (Cg_i D_A T_A D_B N_B)' \right\} u_i dS \\
&+ \int_{\partial w} Cg_i D_A N_A D_B N_B u_{i,N} dS - \sum \| Cg_i D_A T_A D_B N_B u_i \|, \quad (2.34)
\end{aligned}
$$

where the double bar symbol refers to the jump across the discontinuities on the boundary ∂w (i.e. $\| * \| = (*)^+ - (*)^-$) and the sum refers to the collection of all discontinuities. According to virtual work statement ($\dot{E} = P$), the admissible mechanical powers are given by

$$
P = \int_{\partial w_t} t_i u_i dS + \int_{\partial w} m_i u_{i,N} dS + \sum f_i u_i. \quad (2.35)
$$

By comparing Eqs. (2.34) and (2.35), we obtain

$$
\begin{aligned}
\mathbf{t} \;&=\; \mathbf{PN} - \frac{d}{ds} \left[C\mathbf{g}(\mathbf{D} \cdot \mathbf{T})(\mathbf{D} \cdot \mathbf{N}) \right], \\
\mathbf{m} \;&=\; C\mathbf{g}(\mathbf{D} \cdot \mathbf{N})^2, \\
\mathbf{f} \;&=\; C\mathbf{g}(\mathbf{D} \cdot \mathbf{T})(\mathbf{D} \cdot \mathbf{N}). \quad (2.36)
\end{aligned}
$$

which are expressions of edge tractions, edge moments and the corner forces, respectively. For example, if the fiber's directions are either normal or tangential to

the boundary, Eq. (2.36) further reduces to

$$
\begin{aligned}
t_i &= P_{iA}N_A, \\
m_i &= Cg_i D_A N_A D_B N_B, \\
f_i &= 0,
\end{aligned}
\tag{2.37}
$$

where

$$
P_{iA} = \mu F_{iA} - pF_{iA}^* - Cg_{i,B}D_A D_B, \quad g_i = F_{iA,B}D_A D_B.
\tag{2.38}
$$

2.3 Finite element analysis of the 4th order coupled PDE

It is not trivial to demonstrate numerical analysis procedures for coupled PDE systems, especially for those with high order terms, since the piece wise linear function adopted in FE analysis has limited differentiability up to second order. For pre processing, Eq. (2.27) can be recast as

$$
\begin{aligned}
0 &= \mu\left(R + \chi_{1,22}\right) - A\chi_{2,2} + B\chi_{2,1} - CR_{,11}, \\
0 &= \mu\left(Q + \chi_{2,22}\right) + A\chi_{1,2} - B\chi_{1,1} - CQ_{,11}, \\
0 &= Q - \chi_{1,11}, 0 = R - \chi_{2,11}, \\
0 &= A - \mu(\chi_{1,11} + \chi_{1,22}) - CR_{,11}, \\
0 &= B - \mu(\chi_{2,11} + \chi_{2,22}) - CQ_{,11},
\end{aligned}
\tag{2.39}
$$

where $Q = \chi_{1,11}$ and $R = \chi_{2,11}$. By employing the Picard iterative process, the non-linear terms in the above can be treated as

$$
\begin{aligned}
- A_{initial}\chi_{2,2} + B_{initial}\chi_{2,1} &\implies -A_0\chi_{2,2} + B_0\chi_{2,1}, \\
A_{initial}\chi_{1,2} - B_{initial}\chi_{1,1} &\implies A_0\chi_{1,2} - B_0\chi_{1,1},
\end{aligned}
\tag{2.40}
$$

where the values of A and B continue to be refreshed based on their previous estimations (e.g. A_1 and B_1 are updated by their previous values A_0 and B_0) as iteration progresses. Thus, we write

$$
\begin{aligned}
- A_{N-1}\chi_{2,2}^{N-1} + B_{N-1}\chi_{2,1}^{N-1} &\implies -A_N\chi_{2,2}^N + B_N\chi_{2,1}^N, \\
A_{N-1}\chi_{1,2}^{N-1} - B_{N-1}\chi_{1,1}^{N-1} &\implies A_N\chi_{1,2}^N - B_N\chi_{1,1}^N,
\end{aligned}
\tag{2.41}
$$

where N is the number of iterations. The weak form of Eq. $(2.39)_1$ is given by

$$
0 = \int_\Omega w_1(\mu\left(R + \chi_{1,22}\right) - A\chi_{2,2} + B\chi_{2,1} - CR_{,11})d\Omega,
\tag{2.42}
$$

By applying integration by parts (e.g. $\mu \int_{\Omega^e} w_1\chi_{1,22}d\Omega = -\mu \int_{\Omega^e} w_{1,2}\chi_{1,2}d\Omega + \mu \int_{\Omega^e} w_1\chi_{1,2}Nd\Gamma$) and the Green-stoke's theorem, the above becomes

$$
\begin{aligned}
0 &= \int_{\Omega^e} (\mu w_1 R - \mu w_{1,2}\chi_{1,2} - w_1 A_0\chi_{2,2} + w_1 B_0\chi_{2,1} + Cw_{1,1}R_{,1})d\Omega \\
&+ \int_{\partial\Gamma^e} \mu w_1\chi_{1,2}Nd\Gamma - \int_{\partial\Gamma^e} Cw_1 R_{,1}Nd\Gamma,
\end{aligned}
\tag{2.43}
$$

Similarly, we obtain

$$
\begin{aligned}
0 &= \int_{\Omega} (\mu w_1 R - \mu w_{1,2}\chi_{1,2} - w_1 A_0 \chi_{2,2} + w_1 B_0 \chi_{2,1} + C w_{1,1} R_{,1}) d\Omega \\
&\quad + \int_{\partial\Gamma} \mu w_1 \chi_{1,2} N d\Gamma - \int_{\partial\Gamma} C w_1 R_{,1} N d\Gamma, \\
0 &= \int_{\Omega} (\mu w_2 Q - \mu w_{2,2}\chi_{2,2} + + w_2 A_0 \chi_{1,2} - w_2 B_0 \chi_{1,1} + C w_{2,1} Q_{,1}) d\Omega \\
&\quad + \int_{\partial\Gamma} \mu w_2 \chi_{2,2} N d\Gamma - \int_{\partial\Gamma} C w_2 Q_{,1} N d\Gamma, \\
0 &= \int_{\Omega} (w_3 Q + w_{3,1}\chi_{1,1}) d\Omega - \int_{\partial\Gamma} w_3 \chi_{1,1} N d\Gamma, \\
0 &= \int_{\Omega} (w_4 R + w_{4,1}\chi_{2,1}) d\Omega - \int_{\partial\Gamma} w_4 \chi_{2,1} N d\Gamma, \\
0 &= \int_{\Omega} (w_5 A + \mu w_{4,1}\chi_{1,1} - \mu w_{5,2}\chi_{1,2} + C w_{4,1} R_{,1}) d\Omega - \int_{\partial\Gamma} \mu w_5 \chi_{1,1} N d\Gamma \\
&\quad + \int_{\partial\Gamma} \mu w_5 \chi_{1,2} N d\Gamma - \int_{\partial\Gamma} C w_5 R_{,1} N d\Gamma, \\
0 &= \int_{\Omega} (w_6 B + \mu w_{6,1}\chi_{2,1} - \mu w_{6,2}\chi_{2,2} + C w_{5,1} Q_{,1}) d\Omega - \int_{\partial\Gamma} \mu w_6 \chi_{2,1} N d\Gamma \\
&\quad + \int_{\partial\Gamma} \mu w_6 \chi_{2,2} N d\Gamma - \int_{\partial\Gamma} C w_6 Q_{,1} N d\Gamma, \quad (2.44)
\end{aligned}
$$

where Ω, $\partial\Gamma$ and N are the domain of interest, the associated boundary, and the rightward unit normal to the boundary $\partial\Gamma$ in the sense of the Green-stoke's theorem, respectively. The unknowns, χ_1, χ_2, Q, R, A and B can be written in the form of Lagrangian polynomial such that

$$
(*) = \sum_{j=1}^{n} [(*)_j \Psi_j] \text{ and } n = 1,\ 2,\ 3,\ 4, \quad (2.45)
$$

where Ψ_i are the shape functions for the 4-node rectangular element.

$$
\begin{aligned}
\Psi_1(\xi, \eta) &= \frac{(\xi - 1)(\eta - 1)}{4} \\
\Psi_2(\xi, \eta) &= \frac{(\xi + 1)(1 - \eta)}{4} \\
\Psi_3(\xi, \eta) &= \frac{(\xi + 1)(\eta + 1)}{4} \\
\Psi_4(\xi, \eta) &= \frac{(1 - \xi)(\eta - 1)}{4}
\end{aligned}
\tag{2.46}
$$

and

$$
\begin{array}{llll}
\frac{\partial \Psi_1}{\partial \xi} = \frac{(\eta - 1)}{4} & \frac{\partial \Psi_2}{\partial \xi} = \frac{(1 - \eta)}{4} & \frac{\partial \Psi_3}{\partial \xi} = \frac{(\eta + 1)}{4} & \frac{\partial \Psi_4}{\partial \xi} = \frac{-(\eta + 1)}{4} \\
\frac{\partial \Psi_1}{\partial \eta} = \frac{(\xi - 1)}{4} & \frac{\partial \Psi_2}{\partial \eta} = \frac{-(\xi + 1)}{4} & \frac{\partial \Psi_3}{\partial \eta} = \frac{(\xi + 1)}{4} & \frac{\partial \Psi_4}{\partial \eta} = \frac{(1 - \xi)}{4}
\end{array}
$$

Also we have:

$$
\begin{aligned}
J &= \begin{bmatrix} \frac{\partial x}{\partial \xi} & \frac{\partial y}{\partial \xi} \\ \frac{\partial x}{\partial \eta} & \frac{\partial y}{\partial \eta} \end{bmatrix} = \begin{bmatrix} \frac{\partial \Psi_1}{\partial \xi} & \frac{\partial \Psi_2}{\partial \xi} & \frac{\partial \Psi_3}{\partial \xi} & \frac{\partial \Psi_4}{\partial \xi} \\ \frac{\partial \Psi_1}{\partial \eta} & \frac{\partial \Psi_2}{\partial \eta} & \frac{\partial \Psi_3}{\partial \eta} & \frac{\partial \Psi_4}{\partial \eta} \end{bmatrix} \begin{bmatrix} x_1 & y_1 \\ x_2 & y_2 \\ x_3 & y_3 \\ x_4 & y_4 \end{bmatrix} \\
d\Omega &= J.d\xi.d\eta
\end{aligned}
\tag{2.47}
$$

Accordingly, the corresponding test function w_m is expressed by

$$
w_m = \sum_{i=1}^{n} w_m^i \Psi_i \text{ and } m = 1, \ 2, \ 3, ...6,
\tag{2.48}
$$

where w_m^i is weight of the test function. In view of Eq. (2.45), the first of Eq. $(2.44)_1$ can be rewritten as

$$
\begin{aligned}
0 \;=\; & \sum_{j=1}^{n}\{\int_{\Omega}(\mu\Psi_i\Psi_j + C\Psi_{i,1}\Psi_{j,1})d\Omega\}R_j - \sum_{j=1}^{n}\{\int_{\Omega}(\mu\Psi_{i,2}\Psi_{j,2})d\Omega\}\chi_{1j} \\
& -\sum_{j=1}^{n}\{\int_{\Omega}(\Psi_i A_0\Psi_{j,2} + \Psi_i B_0\Psi_{j,1})d\Omega\}\boldsymbol{\chi}_2^j \\
& +\int_{\partial\Gamma}(\mu\Psi_i\chi_{1,2})Nd\Gamma - \int_{\partial\Gamma}(C\Psi_i R_{,1})Nd\Gamma,
\end{aligned}
\tag{2.49}
$$

and similarly for the rest of equations. In addition, for the local stiffness matrix, we find

$$
\begin{bmatrix}
K_{11}^{11} & K_{12}^{11} & K_{13}^{11} & K_{14}^{11} \\
K_{21}^{11} & K_{22}^{11} & K_{23}^{11} & K_{24}^{11} \\
K_{31}^{11} & K_{32}^{11} & K_{33}^{11} & K_{34}^{11} \\
K_{41}^{11} & K_{42}^{11} & K_{43}^{11} & K_{44}^{11}
\end{bmatrix}_{Local}
\begin{bmatrix}
\chi_1^1 \\
\chi_1^2 \\
\chi_1^3 \\
\chi_1^4
\end{bmatrix}_{Local}
=
\begin{bmatrix}
F_1^1 \\
F_2^1 \\
F_3^1 \\
F_4^1
\end{bmatrix}_{Local},
\tag{2.50}
$$

or alternatively,

$$
\left[K_{ij}^{11}\right]\{\chi_1^i\} = \{F_i^1\}.
\tag{2.51}
$$

Here

$$
\left[K_{ij}^{11}\right] = \int_{\Omega}(\mu\Psi_{i,2}\Psi_{j,2})d\Omega,
\tag{2.52}
$$

$$
\{F_i^1\} = -\mu\int_{\partial\Gamma^e}\Psi_i\chi_{1,2}Nd\Gamma + C\int_{\partial\Gamma^e}\Psi_i R_{,1}Nd\Gamma,
\tag{2.53}
$$

and similarly for the rest of components (e.g. $\left[K_{ij}^{21}\right]\{\chi_2^i\} = \{F_i^2\}$). Finally, we assemble the local stiffness matrices and obtain the following systems of equations

in the Global form.

$$
\begin{bmatrix}
\begin{bmatrix} K_{ij}^{11} \end{bmatrix} & \begin{bmatrix} K_{ij}^{12} \end{bmatrix} & \begin{bmatrix} K_{ij}^{13} \end{bmatrix} & \begin{bmatrix} K_{ij}^{14} \end{bmatrix} & \begin{bmatrix} K_{ij}^{15} \end{bmatrix} & \begin{bmatrix} K_{ij}^{16} \end{bmatrix} \\
\begin{bmatrix} K_{ij}^{21} \end{bmatrix} & \begin{bmatrix} K_{ij}^{22} \end{bmatrix} & \begin{bmatrix} K_{ij}^{23} \end{bmatrix} & \begin{bmatrix} K_{ij}^{24} \end{bmatrix} & \begin{bmatrix} K_{ij}^{25} \end{bmatrix} & \begin{bmatrix} K_{ij}^{26} \end{bmatrix} \\
\begin{bmatrix} K_{ij}^{31} \end{bmatrix} & \begin{bmatrix} K_{ij}^{32} \end{bmatrix} & \begin{bmatrix} K_{ij}^{33} \end{bmatrix} & \begin{bmatrix} K_{ij}^{34} \end{bmatrix} & \begin{bmatrix} K_{ij}^{35} \end{bmatrix} & \begin{bmatrix} K_{ij}^{36} \end{bmatrix} \\
\begin{bmatrix} K_{ij}^{41} \end{bmatrix} & \begin{bmatrix} K_{ij}^{42} \end{bmatrix} & \begin{bmatrix} K_{ij}^{43} \end{bmatrix} & \begin{bmatrix} K_{ij}^{44} \end{bmatrix} & \begin{bmatrix} K_{ij}^{45} \end{bmatrix} & \begin{bmatrix} K_{ij}^{46} \end{bmatrix} \\
\begin{bmatrix} K_{ij}^{51} \end{bmatrix} & \begin{bmatrix} K_{ij}^{52} \end{bmatrix} & \begin{bmatrix} K_{ij}^{53} \end{bmatrix} & \begin{bmatrix} K_{ij}^{54} \end{bmatrix} & \begin{bmatrix} K_{ij}^{55} \end{bmatrix} & \begin{bmatrix} K^{ij56} \end{bmatrix} \\
\begin{bmatrix} K_{ij}^{61} \end{bmatrix} & \begin{bmatrix} K_{ij}^{62} \end{bmatrix} & \begin{bmatrix} K_{ij}^{63} \end{bmatrix} & \begin{bmatrix} K_{ij}^{64} \end{bmatrix} & \begin{bmatrix} K_{ij}^{65} \end{bmatrix} & \begin{bmatrix} K_{ij}^{66} \end{bmatrix}
\end{bmatrix}_{Global}
\begin{bmatrix}
\{\chi_1^i\} \\
\{\chi_2^i\} \\
Q_i \\
R_i \\
A_i \\
B_i
\end{bmatrix}_{Global}
=
\begin{bmatrix}
\{F_i^1\} \\
\{F_i^2\} \\
\{F_i^3\} \\
\{F_i^4\} \\
\{F_i^5\} \\
\{F_i^6\}
\end{bmatrix}_{Global}
\tag{2.54}
$$

2.4 Numerical Solution Result

For demonstration purpose, we consider a rectangular fiber composite where one end is fixed and the other end is subjected to uniform bending in order to examine fibers' reinforcing effects against to flexure. We also note here that data are obtained under the normalized setting (e.g. $\frac{C}{\mu} = 150$, $\frac{M}{\mu} = 5[L]^3$). The convergence criteria are set for both non-linear terms and the deformed profiles at $y = 0$.

$$
\begin{aligned}
|A_{n+1} - A_n| &= e_1 \leq \varepsilon, \ |B_{n+1} - B_n| = e_2 \leq \varepsilon, \tag{2.55} \\
\varepsilon &= \text{maximum error} = 10^{-10}
\end{aligned}
$$

It is clear from Table. 2.1 and Fig. 2.2 that our numerical solution demonstrates fast convergence within 20 iterations. The deformation profile and contour show smooth transitions as they approach the boundary (Figs. 2.3-2.5). In addition, Fig. 2.4. indicates that magnitude of deformation decreases with increasing fiber's bending stiffness.

Table 2.1: Maximum numerical error with respect to the number of iterations.

Number of iterations	Maximum error
1	$1.0e + 00$
5	$4.5e - 03$
10	$2.5e - 06$
17	$6.2e - 11$
30	$5.8e - 23$
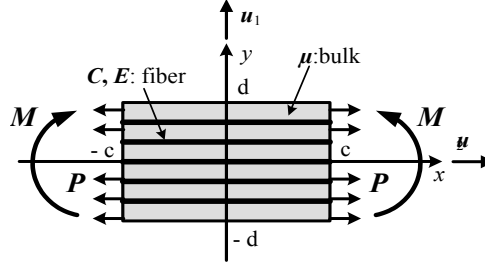
Figure 2.1: Schematic for unidirectional fiber with moment boundary condition.

2.5 Linear Theory

We consider superposed "*small*" deformations as

$$\boldsymbol{\chi} = \boldsymbol{\chi}_o + \varepsilon \dot{\boldsymbol{\chi}}; |\varepsilon| \ll 1, \tag{2.56}$$

where $(*)_o$ denote configuration of $*$ evaluated at $\varepsilon = 0$ and $(\dot{*}) = \partial(*)/\partial\varepsilon$. In particular, we denote $\dot{\boldsymbol{\chi}} = \mathbf{u}$. Here caution needs to be taken that the present notation is not confused with the one used for the variational computation. Then, the deformation gradient tensor can be written by

$$\mathbf{F} = \mathbf{F}_o + \varepsilon \nabla \mathbf{u}, \ \text{where} \dot{\mathbf{F}} = \nabla \mathbf{u}. \tag{2.57}$$

We assume that the body is initially undeformed and stress free at $\varepsilon = 0$ (i.e. $\mathbf{F}_o = \mathbf{I}$ and $\mathbf{P}_o = \mathbf{0}$). Then, Eq. (2.57) becomes

$$\mathbf{F} = \mathbf{I} + \varepsilon \nabla \mathbf{u}, \tag{2.58}$$

32
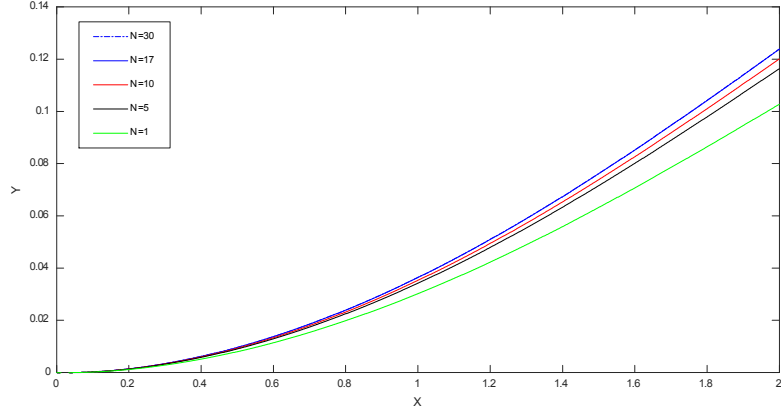
Figure 2.2: Convergence of the numerical solutions at $y = 0$.
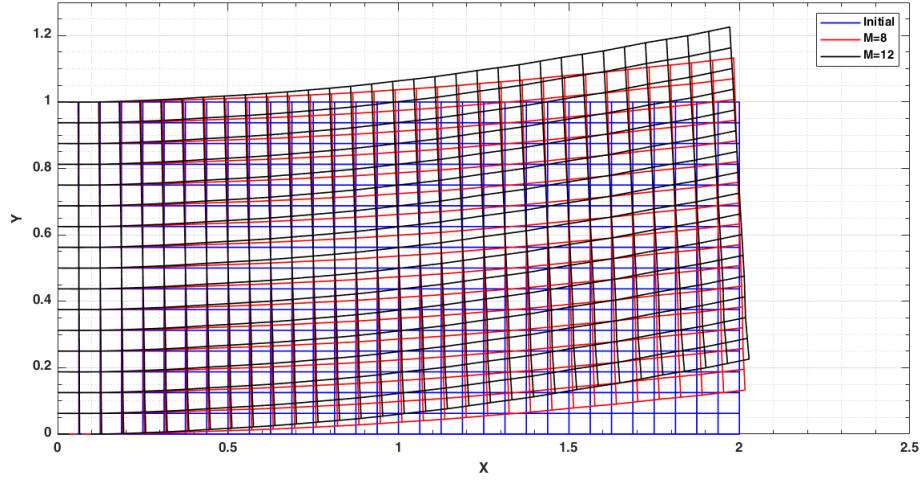
Figure 2.3: Deformed configurations with respect to M/μ when $C/\mu = 150$.

and successively obtain

$$\mathbf{F}^{-1} = \mathbf{I} - \varepsilon \nabla \mathbf{u} + o(\varepsilon), \qquad (2.59)$$

$$J = \det \mathbf{F} = 1 + \varepsilon \operatorname{div} \mathbf{u} + o(\varepsilon). \qquad (2.60)$$

Further, in view of Eq. (2.56), Eq. (2.22) can be rewritten as

$$Div(\mathbf{P}) = Div(\mathbf{P}_o) + \varepsilon Div(\dot{\mathbf{P}}) + o(\varepsilon) = \mathbf{0}. \qquad (2.61)$$
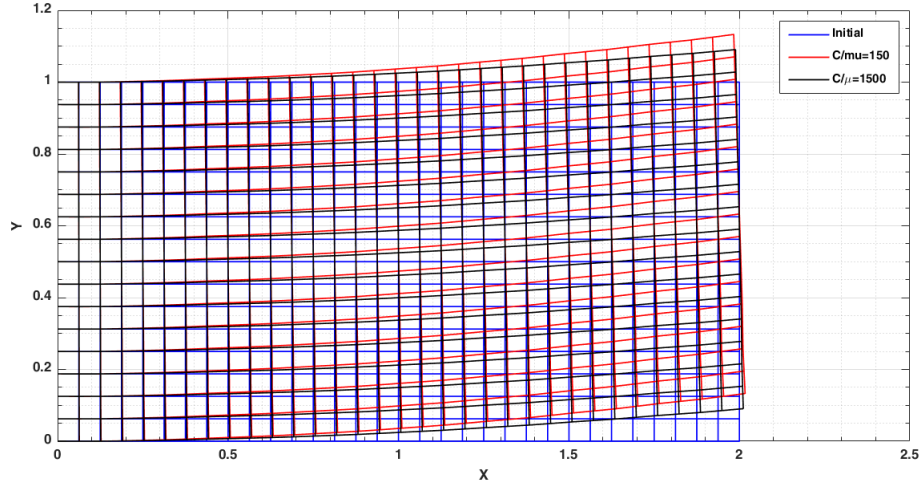
Figure 2.4: Deformed configurations with respect to C/μ when $M/\mu = 8$.
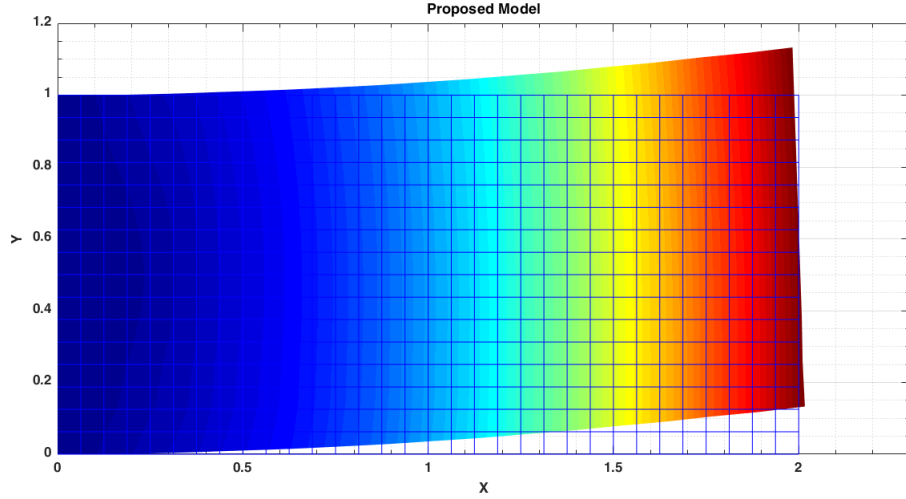
Figure 2.5: Deformation contour $\left(\sqrt{\chi_1^2 + \chi_2^2}\right)$ when $C/\mu = 150$ and $M/\mu = 8$.

Dividing the above by ε and let $\varepsilon \to 0$, we obtain

$$Div(\dot{\mathbf{P}}) = 0 \tag{2.62}$$

which serves as the linearized Euler equation. Now, from Eq. (2.21), we evaluate the variation of $\mathbf{P}$ with respect to ε as

$$\dot{\mathbf{P}} = W_{\mathbf{FF}}\dot{\mathbf{F}} - \dot{p}\mathbf{F}_o^* - p_o\dot{\mathbf{F}}^* - C\nabla\dot{\mathbf{g}}(\mathbf{D} \otimes \mathbf{D}) \tag{2.63}$$

34

where, in the case of Neo-Hookian material (Eq. (2.23)); $W_{\mathbf{FF}} = \mu(\mathbf{e}_i \otimes \mathbf{E}_A \otimes \mathbf{e}_i \otimes \mathbf{E}_A)$. Thus Eq. (2.62-2.63) furnishes

$$Div(\mu\dot{\mathbf{F}}) - Div(\dot{p}\mathbf{F}_o^*) - Div(p_o\dot{\mathbf{F}}^*) - Div(C\nabla\dot{\mathbf{g}}(\mathbf{D} \otimes \mathbf{D})) = 0. \qquad (2.64)$$

However, from Eq. (2.56), terms in the above further deduce to $Div(\mu\dot{\mathbf{F}}) = Div(\mu\nabla\mathbf{u}) = \mu u_{i,AA}\mathbf{e}_i$,

$$\begin{aligned} Div(\dot{p}\mathbf{F}_o^*) &= \mathbf{F}_o^*\nabla\dot{p} = \mathbf{I}\nabla\dot{p}, \qquad (2.65)\\ Div(\mathbf{F}^*) &= 0, \end{aligned}$$

where $\mathbf{I}\nabla\dot{p}$ is on the current basis ($\mathbf{I}\nabla\dot{p} = \dot{p}_{,i}\mathbf{e}_i$) and

$$Div(p_o\dot{\mathbf{F}}^*) = p_o Div(\mathbf{F}^*)^{\cdot} = 0, \ p_o = \mu = \text{constant} \qquad (2.66)$$

We note that $p_o = \mu$ to recover initial stress free state at $\varepsilon = 0$ (i.e. $\mathbf{P}_o = \mu\mathbf{F}_o - p\mathbf{F}_o^* - C\nabla\mathbf{g}_o(\mathbf{D} \otimes \mathbf{D}) = \mathbf{0}$). In addition, since $\mathbf{g} = \nabla[\mathbf{FD}]\mathbf{D}$, we obtain in the case of initially straight fibers ($\nabla\mathbf{D} = 0$)

$$\begin{aligned} Div(C\nabla\dot{\mathbf{g}}(\mathbf{D} \otimes \mathbf{D})) &= CDiv[u_{i,ABC}D_A D_B D_C D_D\mathbf{e}_i \otimes \mathbf{E}_D]\\ &= Cu_{i,ABCD}D_A D_B D_C D_D\mathbf{e}_i \qquad (2.67)\\ \dot{\mathbf{F}} &= \nabla\mathbf{u} \end{aligned}$$

Consequently, from Eqs. (2.64-2.67), the linearized Euler equation is given by

$$\mu u_{i,AA} - \dot{p}_{,i} - Cu_{i,ABCD}D_A D_B D_C D_D = 0, \qquad (2.68)$$

Further, the corresponding bulk incompressibility condition reduces to

$$(J-1)^{\cdot} = \mathbf{F}_o^* \cdot \dot{\mathbf{F}} = \mathrm{div}\,\mathbf{u} = \mathbf{0}. \tag{2.69}$$

For a single family of fibers (i.e. $\mathbf{D} = \mathbf{E}_1$, $D_1 = 1$, $D_2 = 0$), the Eq. (2.68) becomes

$$\dot{p}_{,i} = \mu u_{i,AA} - C u_{i,1111} \text{ for } i, A = 1, 2 \tag{2.70}$$

which, together with Eq. (2.69), serves as a compatible linear model of Eq. (2.27) for small deformations. Finally, the boundary conditions in Eq. (2.26) can be linearized similarly as the above $(\mathbf{t} = \mathbf{t}_o + \varepsilon \dot{\mathbf{t}} + o(e))$

$$
\begin{aligned}
\dot{\mathbf{t}} &= \dot{\mathbf{P}}\mathbf{N} - \frac{d}{ds}\left[C\dot{\mathbf{g}}(\mathbf{D}\cdot\mathbf{T})(\mathbf{D}\cdot\mathbf{N})\right], \\
\dot{\mathbf{m}} &= C\dot{\mathbf{g}}(\mathbf{D}\cdot\mathbf{N})^2, \\
\dot{\mathbf{f}} &= C\dot{\mathbf{g}}(\mathbf{D}\cdot\mathbf{T})(\mathbf{D}\cdot\mathbf{N}).
\end{aligned}
\tag{2.71}
$$

In particular, if the fiber's directions are either normal or tangential to the boundary $((\mathbf{D}\cdot\mathbf{T})(\mathbf{D}\cdot\mathbf{N}) = 0)$, Eq. (2.71) further reduces to

$$
\begin{aligned}
\dot{t}_i &= \dot{P}_{iA} N_A, \\
\dot{m}_i &= C\dot{g}_i D_A N_A D_B N_B, \\
\dot{f}_i &= 0.
\end{aligned}
\tag{2.72}
$$

where

$$
\begin{aligned}
\dot{P}_{iA} &= \mu u_{i,A} - \dot{p}(F_{iA}^*)_o - p_o \dot{F}_{iA}^* - C\dot{g}_{i,B} D_A D_B, \tag{2.73} \\
\dot{g}_i &= u_{i,AB} D_A D_B.
\end{aligned}
$$

and

$$(F_{iA}^*)_o = \delta_{iA}, \because (F_{iA})_o = \delta_{iA} \text{ at } \varepsilon = 0. \tag{2.74}$$

Lastly, since $J\partial F_{jB}^*/\partial F_{iA} = F_{jB}^* F_{iA}^* - F_{iB}^* F_{jA}^*$ at $\mathbf{F}_o = \mathbf{I}$ we obtain

$$(\partial F_{jB}^*/\partial F_{iA})_o = \delta_{jB}\delta_{iA} - \delta_{iB}\delta_{jA} \tag{2.75}$$

$$(\mathbf{F}_{\mathbf{F}}^*[\dot{\mathbf{F}}])_{jB} = (\delta_{jB}\delta_{iA} - \delta_{iB}\delta_{jA})u_{i,A}.$$

Thus yields

$$\dot{F}_{iA}^* = (Div\mathbf{u})\delta_{iA} - u_{A,i} = -u_{A,i}. \tag{2.76}$$

where $Div\mathbf{u} = 0$ from the Linearized incompressibility condition. In the superposed incremental deformations, there is no clear distinction between current and deformed configuration.

2.6 Solution to the linearized problem

We introduce scalar field ϕ as

$$\mathbf{u} = \mathbf{k} \times \nabla\phi, \ \mathbf{k}(\text{unit normal}); \ u_i = \varepsilon_{\lambda i}\phi_{,\lambda} \tag{2.77}$$

so that Eq. (2.69) can be automatically satisfied ($\phi_{,12} - \phi_{,21} = 0$). From Eq. (2.77), the linearized Euler equation Eq. (2.70) can be rewritten as

$$\dot{p}_{,i} = \mu\varepsilon_{\lambda i}(\phi_{,\lambda 11} + \phi_{,\lambda 22}) - C\varepsilon_{\lambda i}\phi_{,\lambda 1111} \tag{2.78}$$

By utilizing the compatibility condition for $\dot{p}_{,i}$ ($\dot{p}_{,ij} = \dot{p}_{,ji}$), we obtain the following ODE as;

$$\mu(\phi_{,1111} + 2\phi_{,1122} + \phi_{,2222}) - C(\phi_{,11} + \phi_{,22})_{,1111} = 0 \tag{2.79}$$

The above further reduces to

$$\Delta H - \alpha H_{,1111} = 0, \text{ where } H = \Delta\phi \text{ and } \alpha = \frac{C}{\mu} > 0. \tag{2.80}$$

The general solution for the above equation can be found as (when: $1 - 4\frac{C}{\mu}m^2 < 0$)

$$\begin{aligned}
\phi = {}& \sum_{m=1}^{\infty}[\{e^{a_m x}(A_m \cos b_m x + B_m \sin b_m x) + e^{-a_m x}(C_m \cos b_m x + D_m \sin b_m x)\} \\
& \times (E_m \cos my + F_m \sin my)] + K,
\end{aligned} \tag{2.81}$$

where K is a solution of Laplace's equation $(\Delta K = 0)$ given by

$$K = \sum_{n=1}^{\infty}[(G_n \cosh nx + H_n \sinh nx)(I_n \cos ny + J_n \sin ny)] \tag{2.82}$$

and m is separation constants. We note here that the case of $1 - 4\frac{C}{\mu}m^2 > 0$ is excluded, since the strength of fibers is usually far more stronger than those of bulk materials and therefore physically less meaningful. The unknown constant real numbers $A_m, B_m, C_m, D_m, E_m, F_m, G_n, H_n, I_n$, and J_n can be completely determined by imposing admissible boundary conditions depicted in Eqs. (2.72-2.76). The corresponding stress and displacement fields can be also determined through Eqs. (2.73) and (2.77-2.78) $(u_1 = -\phi_{,2}, u_2 = \phi_{,1})$. For example, in the case of symmetric bending where (Fig. 2.1)

$$\dot{\mathbf{m}} = \dot{m}_1\mathbf{e}_1 + \dot{m}_2\mathbf{e}_2, \quad \dot{m}_1 = 5 \approx \sum_{n=1}^{30}\frac{20}{\pi n}(-1)^{\frac{n-1}{2}}\cos(\frac{\pi n}{2d})y\mathbf{e}_1, \quad \dot{m}_2 = 0 \tag{2.83}$$

and

$$\mathbf{D} = D_1\mathbf{E}_1 + D_2\mathbf{E}_2, \quad D_1 = 1, \ D_2 = 0. \tag{2.84}$$
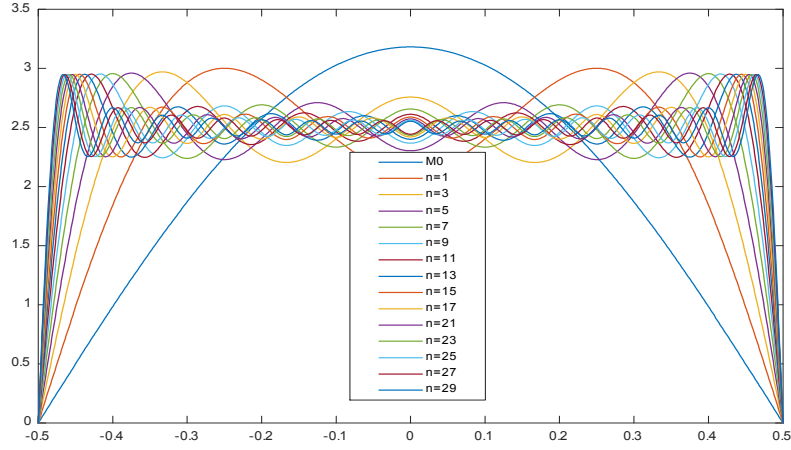
Figure 2.6: Fourier series convergence

We find

$$
\begin{aligned}
\phi(x,y) &= \sum_{n=1}^{30} [\{e^{a_m x}\left(-C_m \cos b_m x + D_m \sin b_m x\right) + e^{-a_m x}\left(C_m \cos b_m x + D_m \sin b_m x\right)\} \\
&\quad \times (\sin\left(\frac{\pi n}{2d}\right) y)], \\
m &= \frac{\pi n}{2d}, \alpha = \frac{C}{\mu}, \\
a_m &= \frac{\sqrt{2m\sqrt{\alpha}+1}}{2\sqrt{\alpha}}, \ b_m = \frac{\sqrt{2m\sqrt{\alpha}-1}}{2\sqrt{\alpha}},
\end{aligned}
\tag{2.85}
$$

and unknown C_m and D_m can be determined via:

$$
\begin{aligned}
\dot{m}_1 &= Cu_{1,11} = -\phi_{,211} = \sum_{n=1}^{30} \frac{20}{\pi n}(-1)^{(n-1)/2}\cos(\frac{\pi n}{2d})y \\
\dot{m}_2 &= Cu_{2,11} = \phi_{,111} = 0.
\end{aligned}
\tag{2.86}
$$

2.7   Results for Linearized Problem

Using the symmetry condition across $x = 0$ and the second of Eq. (2.86), we obtain $A_m = -C_m$ and $B_m = D_m$. So, the unknowns in Eq. (2.85) are completely determined. The applied moment is approximated using Fourier series (Eq. (2.83)) indicating fast convergence (30 iterations) and corresponding results are summarized through Fig. 2.7-2.9. Despite the presence of sharp corners, where singular behaviors of response functions are observed, the obtained solution demonstrates smooth and continuous deformation profiles with sufficient sensitivities to the parameters C and M (Figs. 2.7-2.8). The corresponding deflections are inversely correlated with fibers' strength C/μ (Fig. 2.8), while a positive correlation exists between the deflections and applied bending moments (Fig. 2.7). Analytical solution shows good agreement with FEM solution for the small deformation, while larger values of M induce a significant discrepancy between the linear and nonlinear solution (Fig. 2.9). This is mainly due to the fact that the presented linear model accounts only the leading order terms as depicted in Eq. (2.56-2.57).
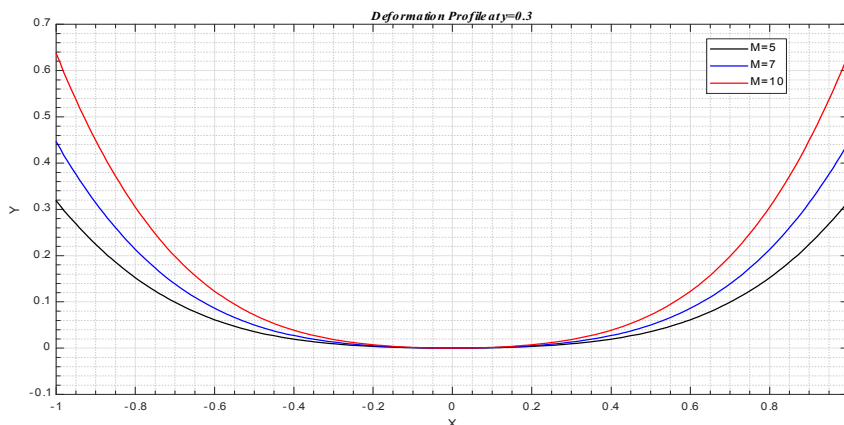
Figure 2.7: Deformation profiles with respect to M/μ when $C/\mu = 150$.
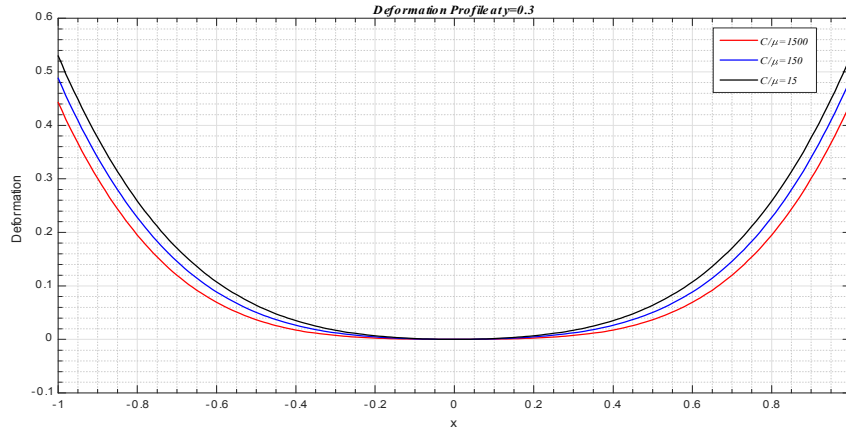
Figure 2.8: Deformation profiles with respect to C/μ when $M/\mu = 5$.
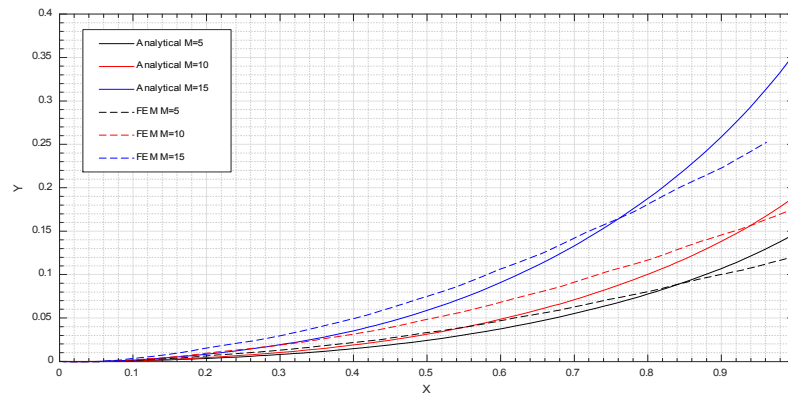
Figure 2.9: Nonlinear vs. linear solutions of the bending problem with $C/\mu = 150$.
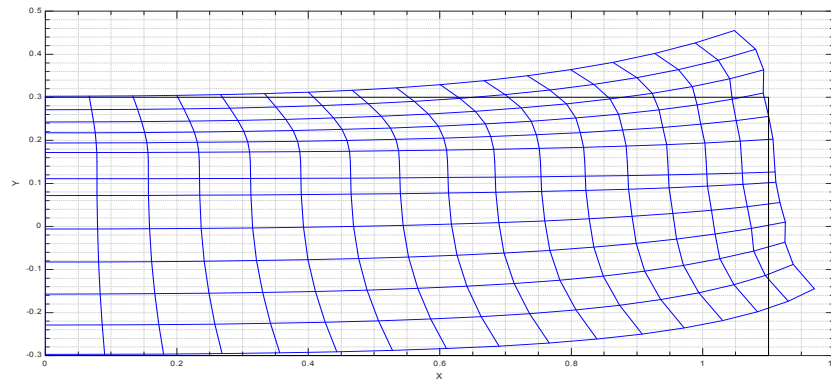
Figure 2.10: Deformed configuration when $C/\mu = 150$ and $M/\mu = 5$.

41

Chapter 3

Mechanics of unidirectional fiber-reinforced composite with fiber resistant to flexure and stretch

The kinematics and constitutive framework are presented in section 3.1. Via the computation of variational derivatives and the virtual-work statement, in section 3.2, the corresponding equilibrium equation is derived. In section 3.2.1, we also consider an example in the case of Neo-Hookian materials. A set of numerical solutions is obtained via a finite element analysis in sections 3.3 and 3.4. The results are also compared with the experimental data demonstrating that the proposed model successfully predicts the deformed configuration of a Crystalline Nanocellulose fiber composite subjected to 3 point bending. In section 3.5, a rigorous analysis is conducted regarding the necessary boundary conditions. A linear theory and analytical solution are presented in sections 3.6 and 3.7

3.1   Kinematics and Constitutive Framework

The present model is a special case of the work of [16] in which the author developed a model incorporating fibers' resistant to twist in addition to flexure and stretch. More precisely, the suggested model intends for the analysis of plane finite deformations of elastic solids reinforced with fibers resistant to extension and flex-

ure. We propose that the mechanical response of the fiber material is governed by the following strain energy function

$$
\begin{aligned}
W(\mathbf{F}, \mathbf{G}) &= \widehat{W}(\mathbf{F}) + W(\mathbf{G}), \\
W(\mathbf{G}) &\equiv \frac{1}{2} C(\mathbf{F}) |\mathbf{g}|^2,
\end{aligned}
\tag{3.1}
$$

where $\mathbf{F}$ is the gradient of the deformation function and $\mathbf{G}$ is the second gradient of the deformation ($\mathbf{G} = \boldsymbol{\nabla}\mathbf{F}$). Eq. (3.1) is consistent with the model proposed by Spencer [8] that, in the case of a single family of fibers, the dependence of the strain energy on $\mathbf{G}$ occurs through $\mathbf{g}$. The orientation of a particular fiber are given by

$$
\lambda = |\mathbf{d}| \text{ and } \lambda\boldsymbol{\tau} = \mathbf{d}; \ \lambda \equiv \frac{ds}{dS} \text{ and } \boldsymbol{\tau} \equiv \frac{d\mathbf{r}(s)}{ds},
\tag{3.2}
$$

where

$$
\mathbf{d} = \mathbf{F}\mathbf{D},
\tag{3.3}
$$

in which $\mathbf{D}$ is the unit tangent to the fiber trajectory in the reference configuration. Eq. (3.3) can be derived by taking the derivative of $\mathbf{r}(s) = \boldsymbol{\chi}(\mathbf{X}(s))$, upon making the identifications $\mathbf{D} = \mathbf{X}'(s)$ and $\mathbf{d} = \mathbf{r}'(s)$. Here primes refer to derivatives with respect to arclength along a fiber in the reference configuration ($(*)' = d(*)/dS$). The expression for geodesic curvature of an arc is then obtained from Eq. (3.3) as

$$
\mathbf{g} \equiv \mathbf{r}'' = (\mathbf{F}\mathbf{D})' = \mathbf{F}'\mathbf{D} + \mathbf{F}\mathbf{D}' = \mathbf{F}'\mathbf{D} = \frac{d\mathbf{F}}{d\mathbf{X}}(\frac{d\mathbf{X}}{ds}\otimes\mathbf{D}) = \mathbf{G}(\mathbf{D}\otimes\mathbf{D}),
\tag{3.4}
$$

for initially straight fibers (i.e. $\mathbf{D}' = 0$). Also, Eqs. (3.2-3.3) furnish

$$
\lambda^2 = \mathbf{F}\mathbf{D} \cdot \mathbf{F}\mathbf{D} = \mathbf{F}^T\mathbf{F}\mathbf{D} \cdot \mathbf{D} = \mathbf{C}\mathbf{D} \cdot \mathbf{D} = \mathbf{C} \cdot \mathbf{D} \otimes \mathbf{D}.
\tag{3.5}
$$

The compatibility condition of $\mathbf{F}$ can be seen as

$$G_{iAB} = F_{iA,B} = F_{iB,A} = G_{iBA}. \tag{3.6}$$

Let suppose $C(\mathbf{F}) = C$ and

$$\widehat{W}(\mathbf{F}) = W(I, \varepsilon), \text{ where } I = tr\mathbf{C} = \lambda_1^2 + \lambda_2^2 \text{ and } \varepsilon = \frac{1}{2}\left(\lambda^2 - 1\right) = \frac{1}{2}\left(\mathbf{C} \cdot \mathbf{D} \otimes \mathbf{D} - 1\right). \tag{3.7}$$

We then have

$$W(I, \varepsilon, \mathbf{g}) = W(I, \varepsilon) + \frac{1}{2}C|\mathbf{g}|^2 = W(\mathbf{F}, \mathbf{G}), \tag{3.8}$$

To compute response functions $\partial W/\partial F_{iA}$ and $\partial W/\partial G_{iAB}$ for the use in the Euler equation and natural boundary conditions, we use the chain rule

$$\frac{\partial W}{\partial F_{iA}}\dot{F}_{iA} + \frac{\partial W}{\partial G_{iAB}}\dot{G}_{iAB} = \dot{W}, \tag{3.9}$$

where the superposed dot refers to derivatives with respect to a parameter at a certain fixed value ($\epsilon = 0$) that labels a one parameter family of deformations. Accordingly, in view of Eq. (3.8) we have that

$$\dot{W} = \dot{W}(I, \varepsilon, \mathbf{g}) = W_I \dot{I} + W_\varepsilon \dot{\varepsilon} + W_{\mathbf{g}} \cdot \dot{\mathbf{g}}, \tag{3.10}$$

in which we have used the fact that W depends on the deformation through I, ε and $\mathbf{g}$; ultimately $\mathbf{F}$ and $\mathbf{G}$. To derive the required expressions, we use (3.7) and derive

$$\dot{I} = [tr(\mathbf{C})]^{\cdot} = (\mathbf{I} \cdot \mathbf{C})^{\cdot} = \mathbf{I} \cdot \dot{\mathbf{C}} = 2\mathbf{F} \cdot \dot{\mathbf{F}}, \tag{3.11}$$

and $(\lambda^2)^{\cdot} = (\mathbf{FD} \cdot \mathbf{FD})^{\cdot}$ then

$$\dot{\varepsilon} = \dot{\lambda}\lambda = \mathbf{FD} \cdot \dot{\mathbf{FD}} = tr(\mathbf{FD} \otimes \dot{\mathbf{FD}}) = tr((\mathbf{FD} \otimes \mathbf{D})\dot{\mathbf{F}}^T) = \mathbf{FD} \otimes \mathbf{D} \cdot \dot{\mathbf{F}}. \tag{3.12}$$

Thus we obtain

$$
\begin{aligned}
\dot{W} &= 2W_I \mathbf{F}\cdot\dot{\mathbf{F}} + W_\varepsilon \dot{\lambda}\lambda + C\mathbf{g}\cdot\dot{\mathbf{g}} \\
&= 2W_I \mathbf{F}\cdot\dot{\mathbf{F}} + W_\varepsilon \mathbf{F}\mathbf{D}\otimes\mathbf{D}\cdot\dot{\mathbf{F}} + C\mathbf{g}\cdot\dot{\mathbf{g}}.
\end{aligned}
\tag{3.13}
$$

But from (3.1)

$$
\dot{W}(\mathbf{G}) = W_{\mathbf{G}}\cdot\dot{\mathbf{G}} \equiv (\frac{1}{2}C(\mathbf{F})\,|\mathbf{g}|^2\,\dot{)} = C\mathbf{g}\cdot\dot{\mathbf{g}}.
\tag{3.14}
$$

Also, invoking (3.4), the above yields

$$
W_{\mathbf{G}}\cdot\dot{\mathbf{G}} = C\mathbf{g}\cdot\dot{\mathbf{g}} = \dot{\mathbf{G}}\cdot(C\mathbf{g}\otimes\mathbf{D}\otimes\mathbf{D}),
\tag{3.15}
$$

where $\dot{\mathbf{g}}=\dot{\mathbf{G}}(\mathbf{D}\otimes\mathbf{D}), \dot{\mathbf{D}}=0$ for initially straight fibers. Thus we derive that

$$
\frac{\partial W}{\partial G_{iAB}} = Cg_i D_A D_B.
\tag{3.16}
$$

In order to accommodate bulk incompressibility, we introduce an augmented energy potential as

$$
U(I,\varepsilon,\mathbf{g},p) = W(I,\varepsilon,\mathbf{g}) - p(J-1).
\tag{3.17}
$$

Then

$$
\dot{U} = \dot{W} - \dot{p}(J-1) - p\dot{J} = \dot{W} - p\dot{J}, \; \dot{p}(J-1) = 0 \text{ for } J = 1.
\tag{3.18}
$$

Further, since $\dot{J} = \frac{\partial J}{\partial \mathbf{F}}\cdot\dot{\mathbf{F}} = J\,(\mathbf{F}^{-1})^T\cdot\dot{\mathbf{F}} = \mathbf{F}^*\cdot\dot{\mathbf{F}}$, combining (3.13) and (3.18) furnishes

$$
\dot{U} = 2W_I \mathbf{F}\cdot\dot{\mathbf{F}} + W_\varepsilon \mathbf{F}\mathbf{D}\otimes\mathbf{D}\cdot\dot{\mathbf{F}} - p\mathbf{F}^*\cdot\dot{\mathbf{F}} + C\mathbf{g}\cdot\dot{\mathbf{g}}.
\tag{3.19}
$$

But from (3.14), the above can be written as

$$
\dot{U} = (2W_I \mathbf{F} + W_\varepsilon \mathbf{F}\mathbf{D}\otimes\mathbf{D} - p\mathbf{F}^*)\cdot\dot{\mathbf{F}} + W_{\mathbf{G}}\cdot\dot{\mathbf{G}}.
\tag{3.20}
$$

45

3.2 Equilibrium

The derivation of the Euler equation and boundary conditions in second-gradient elasticity is well studied [10]-[11] and [46]. We reproduce here for the sake of clarity and completeness of the proposed model; in particular, the connections between the applied loads and the deformations. The weak form of the equations of equilibrium is given by the virtual-work statement

$$\dot{E} = P, \tag{3.21}$$

where P is the virtual work of the applied loads and the superposed dot refers to the variational derivative;

$$E = \int_{\Omega} U(\mathbf{F}, \mathbf{G}) \, dA, \tag{3.22}$$

is the strain energy. We note hear that conservative loads are characterized by the existence of a potential L such that $P = \dot{L}$, and in the present case, the problem of determining equilibrium deformations is reduced to the problem of minimizing the potential energy $E - L$. We have

$$\dot{E} = \int_{\Omega} \dot{U}(\mathbf{F}, \mathbf{G}) \, dA, \tag{3.23}$$

where $\dot{U}$ is given by (3.20). Writing

$$W_{\mathbf{G}} \cdot \dot{\mathbf{G}} = \frac{\partial W}{\partial G_{iAB}} \dot{G}_{iAB} = \frac{\partial W}{\partial G_{iAB}} \dot{F}_{iA,B} = \frac{\partial W}{\partial G_{iAB}} u_{i,AB}; \ u_i \equiv \dot{r}_i = \dot{\chi}_i,$$

$$\frac{\partial W}{\partial G_{iAB}} u_{i,AB} = \left(\frac{\partial W}{\partial G_{iAB}} u_{i,A} \right)_{,B} - \left(\frac{\partial W}{\partial G_{iAB}} \right)_{,B} u_{i,A}, \tag{3.24}$$

we have

$$\int_{\Omega} W_{\mathbf{G}} \cdot \dot{\mathbf{G}} dA = \int_{\Omega} \left(\frac{\partial W}{\partial G_{iAB}} u_{i,A} \right)_{,B} dA - \int_{\Omega} \left(\frac{\partial W}{\partial G_{iAB}} \right)_{,B} u_{i,A} dA. \tag{3.25}$$

By virtue of Green-Stokes theorem, (3.25) can be rewritten as

$$\int W_{\mathbf{G}} \cdot \dot{\mathbf{G}} dA = \int_{\partial\Omega} \frac{\partial W}{\partial G_{iAB}} u_{i,A} N_B dS - \int_{\Omega} \left(\frac{\partial W}{\partial G_{iAB}} \right)_{,B} u_{i,A} dA, \qquad (3.26)$$

where $\mathbf{N}$ is the rightward unit normal to $\partial\Omega$. In addition, from (3.15)

$$\begin{aligned}
\int W_{\mathbf{G}} \cdot \dot{\mathbf{G}} dA &= \int \frac{\partial W}{\partial G_{iAB}} u_{i,A} N_B dS - \int C g_{i,B} D_A D_B \dot{F}_{iA} dA, \\
&= -\int_{\Omega} C\nabla \mathbf{g}(\mathbf{D} \otimes \mathbf{D}) \cdot \dot{\mathbf{F}} \, dA + \int_{\partial\Omega} W_{\mathbf{G}}^T [\dot{\mathbf{F}}]^T \cdot \mathbf{N} dS. \quad (3.27)
\end{aligned}$$

By combining (3.20), (3.23), and (3.27), we obtain

$$\dot{E} = \int_{\Omega} \mathbf{P} \cdot \dot{\mathbf{F}} \, dA + \int_{\partial\Omega} W_{\mathbf{G}}^T [\dot{\mathbf{F}}]^T \cdot \mathbf{N} dS, \qquad (3.28)$$

where

$$\mathbf{P} = 2W_I \mathbf{F} + W_\varepsilon \mathbf{F}(\mathbf{D} \otimes \mathbf{D}) - p\mathbf{F}^* - C\nabla \mathbf{g}(\mathbf{D} \otimes \mathbf{D}), \qquad (3.29)$$

and hence the Euler equation

$$Div(\mathbf{P}) = 0, \qquad (3.30)$$

3.2.1   Neo-Hookian Type Materials

In the case of incompressible Neo-Hookian type materials with augmented extensibility, the energy density function can be expressed as

$$W = \mu I + \frac{1}{2} E \varepsilon^2 \qquad (3.31)$$

Thus (3.5), (3.7) and (3.29) yield

$$\mathbf{P} = 2\mu\mathbf{F} + \frac{1}{2} E(\mathbf{FD} \cdot \mathbf{FD} - 1)\mathbf{F}(\mathbf{D} \otimes \mathbf{D}) - p\mathbf{F}^* - C\nabla \mathbf{g}(\mathbf{D} \otimes \mathbf{D}), \qquad (3.32)$$

and the corresponding Euler equation is obtained as

$$
\begin{aligned}
P_{iA,A} &= 2\mu F_{iA,A} + \frac{1}{2}E(F_{iB,A}F_{jC}F_{jD} + F_{iB}F_{jC,A}F_{jD} + F_{iB}F_{jC}F_{jD,A})D_A D_B D_C D_D \\
&\quad - \frac{1}{2}EF_{iB,A}D_A D_B - p_{,A}F_{iA}^* - Cg_{i,AB}D_A D_B = 0.
\end{aligned}
\tag{3.33}
$$

If a fiber-reinforced material consists of a single family of fibers (i.e. $\mathbf{D} = \mathbf{E}_1$, $D_1 = 1$, $D_2 = 0$) and subjected to plane deformations, (3.33) further reduces to

$$
\begin{aligned}
P_{iA,A} &= 2\mu F_{iA,A} + \frac{1}{2}E(F_{i1,1}F_{j1}F_{j1} + F_{i1}F_{j1,1}F_{j1} + F_{i1}F_{j1}F_{j1,1}) \\
&\quad - \frac{1}{2}EF_{i1,1} - p_{,A}F_{iA}^* - Cg_{i,11} = 0 \quad \text{for } i, \ A = 1, 2,
\end{aligned}
\tag{3.34}
$$

and

$$
g_i = F_{i1,1}, \quad F_{iA} = \frac{\partial \chi_i}{\partial X_A} \quad \text{and} \quad F_{iA}^* = \varepsilon_{ij}\varepsilon_{AB}F_{jB},
\tag{3.35}
$$

where ε_{ij} is the 2-D permutation; $\varepsilon_{12} = -\varepsilon_{21} = 1, \varepsilon_{11} = -\varepsilon_{22} = 0$. Therefore, Eq. (3.35) together with the incompressibility condition ($\det \mathbf{F} = 1$) furnish a coupled PDE system:

$$
\begin{aligned}
0 &= 2\mu(\chi_{1,11} + \chi_{1,22}) - p_{,1}\chi_{2,2} + p_{,2}\chi_{2,1} - C\chi_{1,1111} - \frac{1}{2}E\chi_{1,11} \qquad (3.36) \\
&\quad + \frac{1}{2}E(3\chi_{1,11}\chi_{1,1}\chi_{1,1} + \chi_{1,11}\chi_{2,1}\chi_{2,1} + 2\chi_{2,11}\chi_{1,1}\chi_{2,1}), \\
0 &= 2\mu(\chi_{2,11} + \chi_{2,22}) - p_{,2}\chi_{1,1} + p_{,1}\chi_{1,2} - C\chi_{2,1111} - \frac{1}{2}E\chi_{2,11} \\
&\quad + \frac{1}{2}E(3\chi_{2,11}\chi_{2,1}\chi_{2,1} + \chi_{2,11}\chi_{1,1}\chi_{1,1} + 2\chi_{1,11}\chi_{2,1}\chi_{1,1}), \\
1 &= \chi_{1,1}\chi_{2,2} - \chi_{1,2}\chi_{2,1}.
\end{aligned}
$$

3.3 FEA of the 4th order coupled PDE

It is not trivial to demonstrate numerical analysis procedures for coupled PDE systems, especially for those with high order terms. For pre processing, Eq. (3.36)

can be expressed as

$$
\begin{aligned}
0 &= \mu\left(R + \chi_{1,22}\right) - A\chi_{2,2} + B\chi_{2,1} - CR_{,11} - \frac{1}{2}EQ \\
&\quad + \frac{1}{2}E(3Q\chi_{1,1}\chi_{1,1} + Q\chi_{2,1}\chi_{2,1} + 2R\chi_{1,1}\chi_{2,1}), \\
0 &= \mu\left(Q + \chi_{2,22}\right) + A\chi_{1,2} - B\chi_{1,1} - CQ_{,11} - \frac{1}{2}ER \\
&\quad + \frac{1}{2}E(3R\chi_{2,1}\chi_{2,1} + R\chi_{1,1}\chi_{1,1} + 2Q\chi_{2,1}\chi_{1,1}), \\
0 &= C\chi_{2,2} - D\chi_{1,2} - 1, \ 0 = Q - \chi_{1,11}, \\
0 &= R - \chi_{2,11}, \ 0 = C - \chi_{1,1}, \ 0 = D - \chi_{2,1}, \\
0 &= A - \mu(\chi_{1,11} + \chi_{1,22}) - CR_{,11}, \\
0 &= B - \mu(\chi_{2,11} + \chi_{2,22}) - CQ_{,11}, \tag{3.37}
\end{aligned}
$$

where $Q = \chi_{1,11}$, $R = \chi_{2,11}$, $C = \chi_{1,1}$ and $D = \chi_{2,1}$. The non-linear terms in the above can be replaced by

$$
\begin{aligned}
-A\chi_{2,2} + B\chi_{2,1} &\implies -A_0\chi_{2,2} + B_0\chi_{2,1} \\
A\chi_{1,2} - B\chi_{1,1} &\implies A_0\chi_{1,2} - B_0\chi_{1,1} \\
C\chi_{2,2} - D\chi_{2,1} &\implies C_0\chi_{2,2} - D_0\chi_{2,1}, \tag{3.38}
\end{aligned}
$$

where the values of A, B and C continue to be refreshed based on their previous estimations (A_o, B_o and C_o) as iteration progresses. Therefore, the weak form of

Eq. (3.37) is obtained by

$$
\begin{aligned}
0 &= \int_\Omega (\mu w_1 R - \mu w_{1,2}\chi_{1,2} - w_1 A_0 \chi_{2,2} + w_1 B_0 \chi_{2,1} + C w_{1,1} R_{,1} - \frac{1}{2} E w_1 Q \\
&\quad + \frac{1}{2} E w_1 (3QC_0^2 + QD_0^2 + 2RC_0 D_0)) d\Omega + \int_{\partial\Gamma} (\mu w_1 \chi_{1,2}) N d\Gamma - \int_{\partial\Gamma} (C w_1 R_{,1}) N d\Gamma, \\
0 &= \int_\Omega (\mu w_2 Q - \mu w_{2,2}\chi_{2,2} + + w_2 A_0 \chi_{1,2} - w_2 B_0 \chi_{1,1} + C w_{2,1} Q_{,1} - \frac{1}{2} E w_2 R \\
&\quad + \frac{1}{2} w_2 E (3RD_0^2 + RC_0^2 + 2QD_0 C_0)) d\Omega + \int_{\partial\Gamma} (\mu w_2 \chi_{2,2}) N d\Gamma - \int_{\partial\Gamma} (C w_2 Q_{,1}) N d\Gamma, \\
0 &= \int_\Omega C_0 w_3 \chi_{2,2} - D_0 w_3 \chi_{1,2} - w_3) d\Omega, \\
0 &= \int_\Omega (w_4 Q + w_{4,1}\chi_{1,1}) d\Omega - \int_{\partial\Gamma} (w_4 \chi_{1,1}) N d\Gamma, \\
0 &= \int_\Omega (w_5 R + w_{5,1}\chi_{2,1}) d\Omega - \int_{\partial\Gamma} (w_5 \chi_{2,1}) N d\Gamma, \\
0 &= \int_\Omega (w_6 C - w_6 \chi_{1,1}) d\Omega, \ 0 = \int_\Omega (w_7 D - w_7 \chi_{2,1}) d\Omega, \\
0 &= \int_\Omega (w_8 A + \mu w_{8,1}\chi_{1,1} - \mu w_{8,2}\chi_{1,2} + C w_{8,1} R_{,1}) d\Omega - \int_{\partial\Gamma} (\mu w_8 \chi_{1,1}) N d\Gamma \\
&\quad + \int_{\partial\Gamma} (\mu w_8 \chi_{1,2}) N d\Gamma - \int_{\partial\Gamma} (C w_8 R_{,1}) n d\Gamma, \\
0 &= \int_\Omega (w_9 B + \mu w_{9,1}\chi_{2,1} - \mu w_{9,2}\chi_{2,2} + C w_{9,1} Q_{,1}) d\Omega - \int_{\partial\Gamma} (\mu w_9 \chi_{2,1}) N d\Gamma \\
&\quad + \int_{\partial\Gamma} (\mu w_9 \chi_{2,2}) N d\Gamma - \int_{\partial\Gamma} (C w_9 Q_{,1}) N d\Gamma, \quad (3.39)
\end{aligned}
$$

where the unknowns, χ_1, χ_2, Q_1, R_1, A and B can be written in the form of Lagrangian polynomial such that $(*) = \sum_{j=1}^n [(*)_j \Psi_j(x, y)]$. Ω, $\partial\Gamma$ and $\mathbf{N}$ are the domain of interest, the associated boundary, and the rightward unit normal to the boundary $\partial\Gamma$ in the sense of the Green-stoke's theorem, respectively. The corresponding test function w is given by

$$
w = \sum w_i \Psi_i(x, y), \quad (3.40)
$$

where Ψ_i are the shape functions for the 4-node rectangular element.

$$
\begin{aligned}
\Psi_1(\xi, \eta) &= \frac{(\xi - 1)(\eta - 1)}{4} \\
\Psi_2(\xi, \eta) &= \frac{(\xi + 1)(1 - \eta)}{4} \\
\Psi_3(\xi, \eta) &= \frac{(\xi + 1)(\eta + 1)}{4} \\
\Psi_4(\xi, \eta) &= \frac{(1 - \xi)(\eta - 1)}{4}
\end{aligned}
\tag{3.41}
$$

and

$$
\begin{aligned}
\frac{\partial \Psi_1}{\partial \xi} = \frac{(\eta - 1)}{4} \quad \frac{\partial \Psi_2}{\partial \xi} = \frac{(1 - \eta)}{4} \quad \frac{\partial \Psi_3}{\partial \xi} = \frac{(\eta + 1)}{4} \quad \frac{\partial \Psi_4}{\partial \xi} = \frac{-(\eta + 1)}{4} \\
\frac{\partial \Psi_1}{\partial \eta} = \frac{(\xi - 1)}{4} \quad \frac{\partial \Psi_2}{\partial \eta} = \frac{-(\xi + 1)}{4} \quad \frac{\partial \Psi_3}{\partial \eta} = \frac{(\xi + 1)}{4} \quad \frac{\partial \Psi_4}{\partial \eta} = \frac{(1 - \xi)}{4}
\end{aligned}
$$

Also we have:

$$
J = \begin{bmatrix} \frac{\partial x}{\partial \xi} & \frac{\partial y}{\partial \xi} \\ \frac{\partial x}{\partial \eta} & \frac{\partial y}{\partial \eta} \end{bmatrix} = \begin{bmatrix} \frac{\partial \Psi_1}{\partial \xi} & \frac{\partial \Psi_2}{\partial \xi} & \frac{\partial \Psi_3}{\partial \xi} & \frac{\partial \Psi_4}{\partial \xi} \\ \frac{\partial \Psi_1}{\partial \eta} & \frac{\partial \Psi_2}{\partial \eta} & \frac{\partial \Psi_3}{\partial \eta} & \frac{\partial \Psi_4}{\partial \eta} \end{bmatrix} \begin{bmatrix} x_1 & y_1 \\ x_2 & y_2 \\ x_3 & y_3 \\ x_4 & y_4 \end{bmatrix}
\tag{3.42}
$$

$$
d\Omega = J.d\xi.d\eta
$$

Here c and d are dimensions of the domain as illustrated in Fig. 3.1. Using Lagrangian polynomial representation, the first of (3.39) can be rearranged as

$$
\begin{aligned}
0 = {} & \sum \{ \int_\Omega (\mu \Psi_i \Psi_j + C \Psi_{i,1} \Psi_{j,1}) d\Omega \} R_j - \sum \{ \int_\Omega (\mu \Psi_{i,2} \Psi_{j,2}) d\Omega \} \chi_{1j} \\
& - \sum \{ \int_\Omega (\Psi_i A_0 \Psi_{j,2} + \Psi_i B_0 \Psi_{j,1}) d\Omega \} \chi_{2j} \\
& + \sum \{ \int_\Omega - (\frac{1}{2} E \Psi_i + \frac{1}{2} E \Psi_i (3C_0^2 + D_0^2) d\Omega \} Q_j \\
& + \sum \{ \int_\Omega \frac{1}{2} E \Psi_i (2C_0 D_0)) d\Omega \} R_j + \int_{\partial \Gamma} (\mu \Psi_i \chi_{1,2}) N d\Gamma \\
& - \int_{\partial \Gamma} (C \Psi_i R_{,1}) N d\Gamma,
\end{aligned}
\tag{3.43}
$$

and similarly for the rest of equations. Consequently, we obtain the following systems of equations

$$
\begin{bmatrix}
[K^{11}] & [K^{12}] & [K^{13}] & [K^{14}] & [K^{15}] & [K^{16}] & [K^{17}] & [K^{18}] \\
[K^{21}] & [K^{22}] & [K^{23}] & [K^{24}] & [K^{25}] & [K^{26}] & [K^{27}] & [K^{28}] \\
[K^{31}] & [K^{32}] & [K^{33}] & [K^{34}] & [K^{35}] & [K^{36}] & [K^{37}] & [K^{38}] \\
[K^{41}] & [K^{42}] & [K^{43}] & [K^{44}] & [K^{45}] & [K^{46}] & [K^{47}] & [K^{48}] \\
[K^{51}] & [K^{52}] & [K^{53}] & [K^{54}] & [K^{55}] & [K^{56}] & [K^{57}] & [K^{58}] \\
[K^{61}] & [K^{62}] & [K^{63}] & [K^{64}] & [K^{65}] & [K^{66}] & [K^{67}] & [K^{68}] \\
[K^{71}] & [K^{72}] & [K^{73}] & [K^{74}] & [K^{75}] & [K^{76}] & [K^{77}] & [K^{78}] \\
[K^{81}] & [K^{82}] & [K^{83}] & [K^{84}] & [K^{85}] & [K^{86}] & [K^{87}] & [K^{88}] \\
[K^{91}] & [K^{92}] & [K^{93}] & [K^{94}] & [K^{95}] & [K^{96}] & [K^{97}] & [K^{98}]
\end{bmatrix}
\begin{bmatrix}
\chi_1 \\ \chi_2 \\ Q \\ R \\ A \\ B \\ C \\ D
\end{bmatrix}
=
\begin{bmatrix}
\{F_1\} \\ \{F_2\} \\ \{F_3\} \\ \{F_4\} \\ \{F_5\} \\ \{F_6\} \\ \{F_7\} \\ \{F_8\} \\ \{F_9\}
\end{bmatrix}
\tag{3.44}
$$

where the expressions of $[K^{ij}]$ and F_i can be obtained via the standard FEA procedures, for example;

$$
\left[K^{11}\right] = \int_\Omega (\mu \Psi_{i,2} \Psi_{j,2}) d\Omega,
\tag{3.45}
$$

and

$$
\{F_1\} = -\int_{\partial\Gamma} (\mu \Psi_i \chi_{1,2}) N d\Gamma + \int_{\partial\Gamma} (C\Psi_i R_{,1}) N d\Gamma.
\tag{3.46}
$$

3.4 Numerical Solution Result

For demonstration purpose, a set of numerical solution is obtained for a rectangular composite reinforced with a single family of fibers subjected to uniform bending and extension (Fig. 3.1).

We note here that data are obtained under the normalized setting ($\frac{C}{\mu} = 150$, $\frac{E}{\mu} = 100$, $\frac{M}{\mu} = 5[L]^3$). A comparison with experimental results is also presented when a CNC fiber composite ($C = 150GPa$, $\mu = 1GPa$) is subjected to 3 point bending at $-10mm, 0$ and $10mm$. In the test, out of plane direction is aligned with the
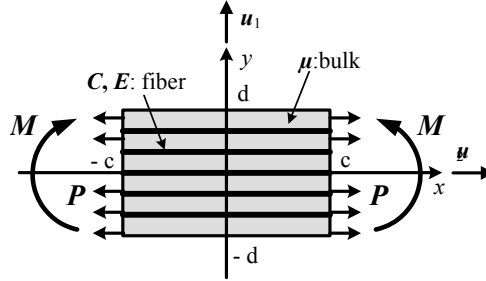
Figure 3.1: Schemetic for unidirectional fiber with moment and extension BC.
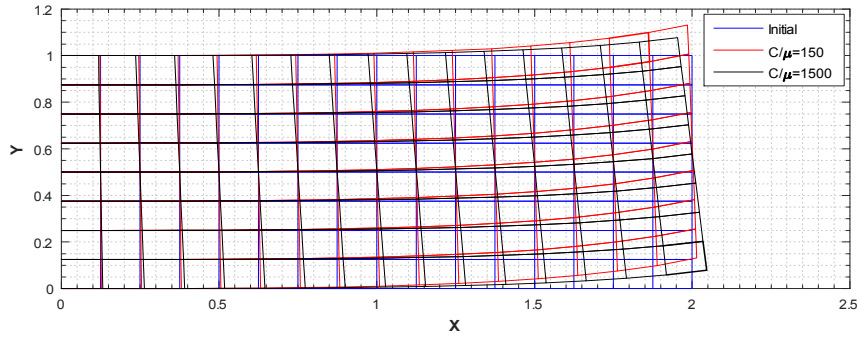
Figure 3.2: Deformed configurations with respect to C/μ when $M/\mu = 0.1E/\mu = 10$.

loading cylinder (Fig. 3.6). This is a special case of the proposed model, when $c \gg d$ and $C/\mu = 150$ with vanishing E. The results successfully predict the normal deflections and the corresponding deformation profiles of the CNC composite strip with configuration factor $= 0.526[L]^2$ between the applied load and input stress on each simulation ($\sigma_{input} \times = Load_{applied}$, Figs. 3.7-3.8). In particular, Fig. 3.7 illustrates a direct comparison with the bending experiment at maximum deflection $2.55mm$. Despite inevitable uncertainties (image processing and curve fitting), the obtained solution successfully predicts the normal deflections and the corresponding deformation profiles of the CNC composite strip.
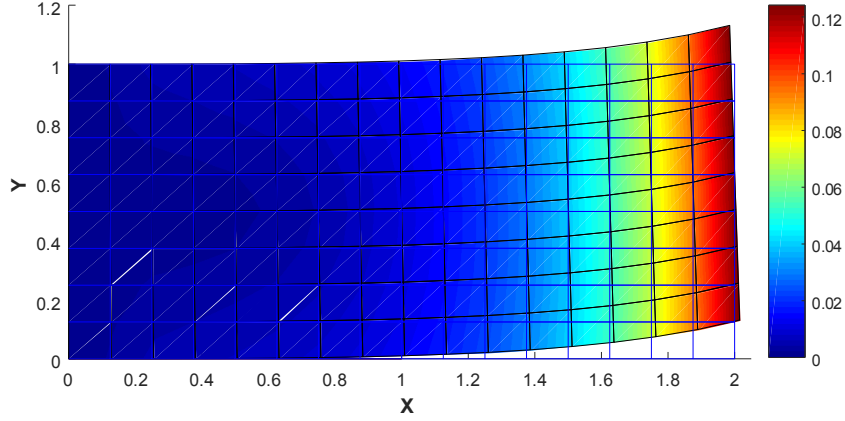
Figure 3.3: Deformed contour when $C/\mu = 150$, $E/\mu = 100$ and $M/\mu = 10$.
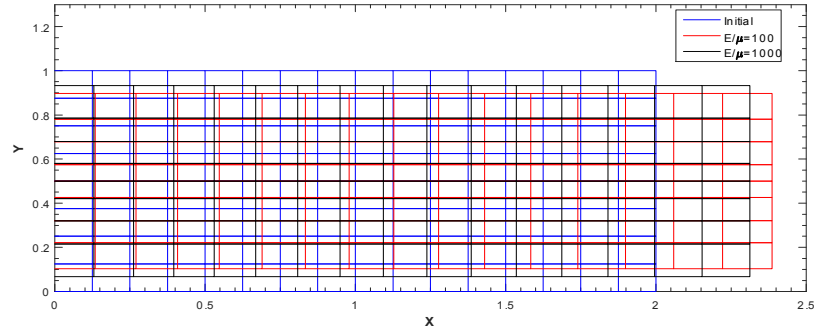
Figure 3.4: Deformed with respect to E/μ when $C/\mu = 150$, $P_{11}/\mu = 50$.

3.5 Boundary conditions

From (3.28), we have

$$\dot{E} = \int_{\Omega} P_{iA}\dot{F}_{iA}dA + \int_{\partial\Omega} \frac{\partial W}{\partial G_{iAB}}\dot{F}_{iA}N_B dS, \qquad (3.47)$$

Decomposing the above as in (3.24) furnishes

$$\dot{E} = \int_{\partial\Omega} [P_{iA}u_i N_A + \left(\frac{\partial W}{\partial G_{iAB}}u_{i,A}\right)N_B]dS - \int_{\Omega} P_{iA,A}u_i dA, \qquad (3.48)$$

With the Euler equation $(P_{iA,A} = 0)$ satisfied on Ω, we have

$$\dot{E} = \int_{\partial\Omega} P_{iA}u_i N_A dS + \int_{\partial\Omega} \left(\frac{\partial W}{\partial G_{iAB}}u_{i,A}\right)N_B dS. \qquad (3.49)$$
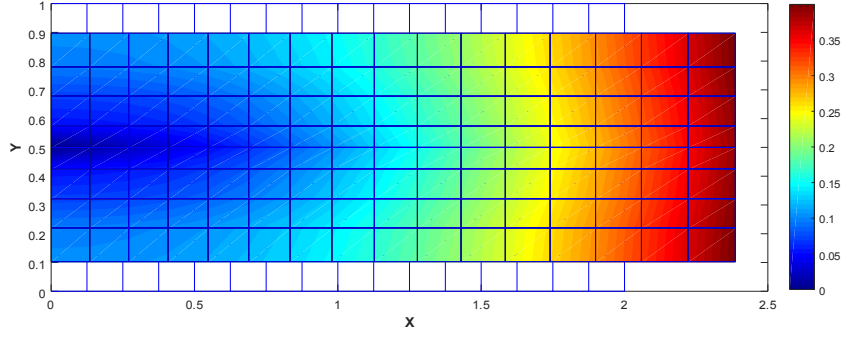
Figure 3.5: Deformation contour when $C/\mu = 150$, $E/\mu = 100$ and $P_{11}/\mu = 50$.
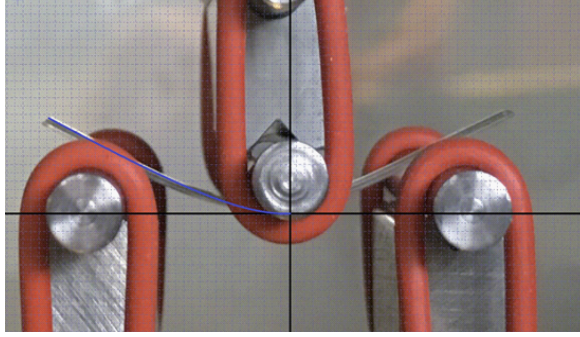
Figure 3.6: Deformation profile (image processing) at $2.55mm$: CNC fiber composite. (Dr. Ayranci and Ms. Garance)

Now, we make use of the normal-tangent decomposition of $\nabla\mathbf{u}$ as;

$$\nabla\mathbf{u} = \nabla\mathbf{u}(\mathbf{T} \otimes \mathbf{T}) + \nabla\mathbf{u}(\mathbf{N} \otimes \mathbf{N}) = \mathbf{u}' \otimes \mathbf{T} + \mathbf{u},_{\mathbf{N}} \otimes \mathbf{N} \tag{3.50}$$

where $\mathbf{T} = \mathbf{X}'(s) = \mathbf{k} \times \mathbf{N}$ is the unit tangent to ∂w; and $\mathbf{u}' = d\mathbf{u}(\mathbf{X}(s))/ds$ and $\mathbf{u},_N$ are the tangential and normal derivatives of $\mathbf{u}$ on ∂w ($u'_i = u_{i,A}T_A$, $u_{i,N} = u_{i,A}N_A$). Then, Eq. (3.49) can be rewritten as

$$\dot{E} = \int_{\partial\Omega} P_{iA}u_i N_A dS + \int_{\partial\Omega} \frac{\partial W}{\partial G_{iAB}} \left(u'_i T_A N_B + u_{i,N} N_A N_B \right) dS. \tag{3.51}$$

Since

$$\frac{\partial W}{\partial G_{iAB}} T_A N_B u'_i = \left(\frac{\partial W}{\partial G_{iAB}} T_A N_B u_i \right)' - \left(\frac{\partial W}{\partial G_{iAB}} T_A N_B \right)' u_i, \tag{3.52}$$

55
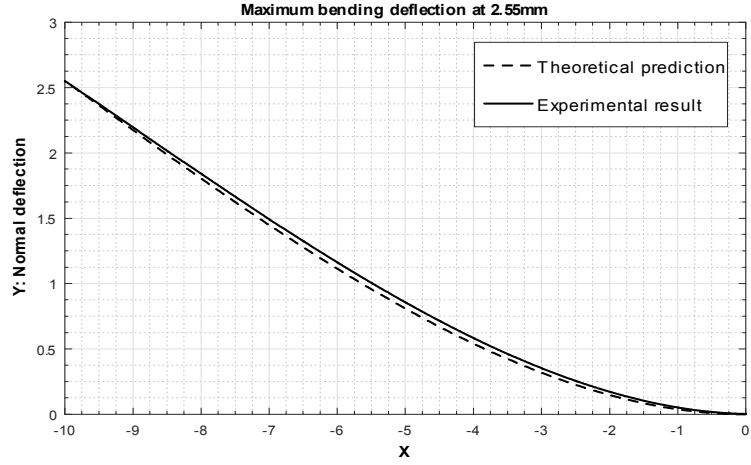
Figure 3.7: Comparison: Theoretical prediction VS Experimental result at $2.55mm$
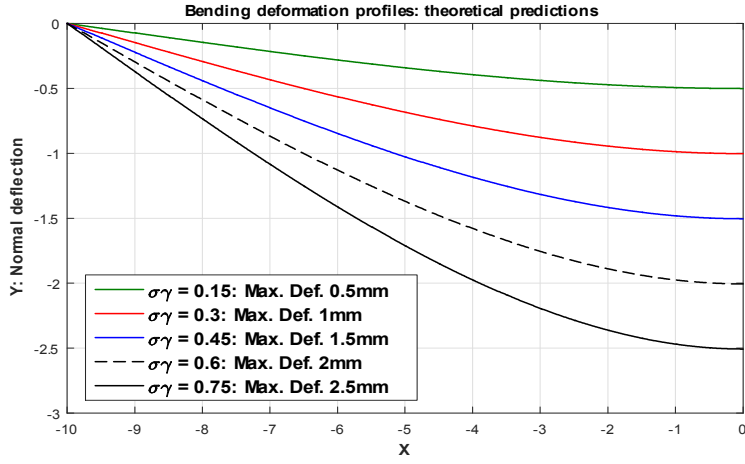
Figure 3.8: Deformation profiles with respect to σ : Theoratical prediction

we arrive at

$$
\begin{aligned}
\dot{E} \;=\; & \int_{\partial\Omega}[P_{iA}N_A - \left(\frac{\partial W}{\partial G_{iAB}}T_A N_B\right)']u_i dS + \int_{\partial\Omega}\frac{\partial W}{\partial G_{iAB}}u_{i,N}N_A N_B dS \\
& + \int_{\partial\Omega}\left(\frac{\partial W}{\partial G_{iAB}}T_A N_B u_i\right)' dS.
\end{aligned}
\tag{3.53}
$$

With the results in (3.16), the above becomes

$$
\begin{aligned}
\dot{E} \;=\; & \int_{\partial\Omega}\left\{P_{iA}N_A - (Cg_i D_A T_A D_B N_B)'\right\}u_i dS + \int_{\partial\Omega}Cg_i D_A N_A D_B N_B u_{i,N}dS \\
& - \sum\left\|Cg_i D_A T_A D_B N_B u_i\right\|,
\end{aligned}
\tag{3.54}
$$
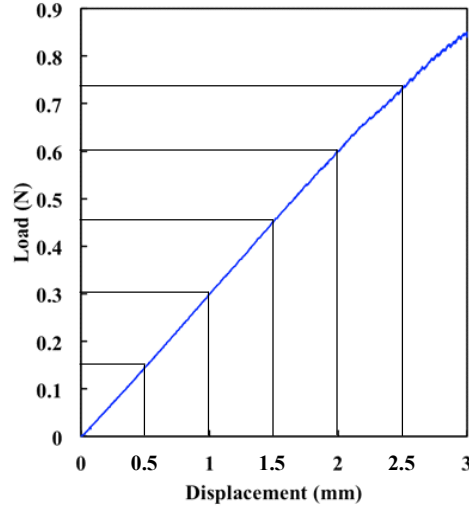
Figure 3.9: Deformation profiles with respect to σ : 3 point bending experiment. (Dr. Ayranci and Ms. Garance)

where the double bar symbol refers to the jump across the discontinuities on the boundary $\partial\Omega$ ($\|*\| = (*)^{+} - (*)^{-}$) and the sum refers to the collection of all discontinuities. It follows from (3.21) that admissible powers are of the form

$$P = \int_{\partial w_t} t_i u_i dS + \int_{\partial w} m_i u_{i,N} dS + \sum f_i u_i. \tag{3.55}$$

By comparing (3.54) and (3.55), we obtain

$$\begin{aligned}
\mathbf{t} &= \mathbf{PN} - \frac{d}{ds}\left[C\mathbf{g}(\mathbf{D}\cdot\mathbf{T})(\mathbf{D}\cdot\mathbf{N})\right], \\
\mathbf{m} &= C\mathbf{g}(\mathbf{D}\cdot\mathbf{N})^2, \\
\mathbf{f} &= C\mathbf{g}(\mathbf{D}\cdot\mathbf{T})(\mathbf{D}\cdot\mathbf{N}),
\end{aligned} \tag{3.56}$$

which are expressions of edge tractions, edge moments and the corner forces, respectively. For example, if the fiber's directions are either normal or tangential to

57

the boundary $((\mathbf{D} \cdot \mathbf{T})(\mathbf{D} \cdot \mathbf{N}) = 0)$, Eq. (3.56) further reduces to

$$
\begin{aligned}
t_i &= P_{iA}N_A, \\
m_i &= Cg_iD_AN_AD_BN_B, \\
f_i &= 0,
\end{aligned}
\tag{3.57}
$$

where

$$
\begin{aligned}
P_{iA} &= 2\mu F_{iA} + \frac{1}{2}E(F_{jC}F_{jD}D_CD_D - 1)(F_{iB}D_BD_A) - pF_{iA}^* - Cg_{i,B}D_BD_A, \\
g_i &= F_{iA,B}D_AD_B.
\end{aligned}
\tag{3.58}
$$

3.6 Linear Theory

We consider superposed "*small*" deformations as

$$
\boldsymbol{\chi} = \boldsymbol{\chi}_o + \varepsilon\dot{\boldsymbol{\chi}}; |\varepsilon| \ll 1,
\tag{3.59}
$$

where $(*)_o$ denote configuration of $*$ evaluated at $\varepsilon = 0$ and $(\dot{*}) = \partial(*)/\partial\varepsilon$. In particular, we denote $\dot{\chi} = \mathbf{u}$. Then, the deformation gradient tensor can be written by

$$
\mathbf{F} = \mathbf{F}_o + \varepsilon\nabla\mathbf{u}, \ \text{where} \dot{\mathbf{F}} = \nabla\mathbf{u}.
\tag{3.60}
$$

We assume that the body is initially undeformed and stress free at $\varepsilon = 0$ ($\mathbf{F}_o = \mathbf{I}$ and $\mathbf{P}_o = \mathbf{0}$). Then, Eq. (3.60) becomes

$$
\mathbf{F} = \mathbf{I} + \varepsilon\nabla\mathbf{u},
\tag{3.61}
$$

and successively obtain

$$
\mathbf{F}^{-1} = \mathbf{I} - \varepsilon\nabla\mathbf{u} + o(\varepsilon),
\tag{3.62}
$$

$$J = \det \mathbf{F} = 1 + \varepsilon \operatorname{div} \mathbf{u} + o(\varepsilon). \tag{3.63}$$

Further, in view of Eq. (3.59), Eq. (3.30) can be rewritten as

$$Div(\mathbf{P}) = Div(\mathbf{P}_o) + \varepsilon Div(\dot{\mathbf{P}}) + o(\varepsilon) = \mathbf{0}. \tag{3.64}$$

Divide the above by ε and let $\varepsilon \to 0$, we obtain

$$Div(\dot{\mathbf{P}}) = 0 \tag{3.65}$$

which serves as the linearized Euler equation. Now, from Eq. (3.29), we evaluate the variation of $\mathbf{P}$ with respect to ε as

$$
\begin{aligned}
\dot{\mathbf{P}} =\ & 2(W_{II}\dot{I} + W_{I\varepsilon}\dot{\varepsilon})\mathbf{F}_o + 2(W_I)_o\dot{\mathbf{F}} - \dot{p}\mathbf{F}_o^* - p_o\dot{\mathbf{F}}^* \\
& + [(W_{\varepsilon\varepsilon}\dot{\varepsilon} + W_{\varepsilon I}\dot{I})\mathbf{F}_o + (W_\varepsilon)_o\dot{\mathbf{F}} - C\nabla\dot{\mathbf{g}}](\mathbf{D} \otimes \mathbf{D}).
\end{aligned}
\tag{3.66}
$$

In view of (3.31), the above further reduces to

$$\dot{\mathbf{P}} = 2\mu\dot{\mathbf{F}} - \dot{p}\mathbf{F}_o^* - p_o\dot{\mathbf{F}}^* + [E\dot{\varepsilon}\mathbf{F}_o + E\varepsilon_o\dot{\mathbf{F}} - C\nabla\dot{\mathbf{g}}](\mathbf{D} \otimes \mathbf{D}), \tag{3.67}$$

Evaluating limits at $\varepsilon = 0$ yields

$$\dot{\mathbf{P}} = 2\mu\dot{\mathbf{F}} - \dot{p}\mathbf{I} - p_o\dot{\mathbf{F}}^* + [E\dot{\varepsilon}\mathbf{I} - C\nabla\dot{\mathbf{g}}](\mathbf{D} \otimes \mathbf{D}), \tag{3.68}$$

where $p_o = 2\mu$ to recover the initial stress free state at $\varepsilon = 0$. Thus Eqs. (3.12), (3.65) and (3.68) furnish

$$\dot{p}_{,i}\mathbf{e}_i = 2\mu\dot{F}_{iA,A}\mathbf{e}_i + E\dot{F}_{jA,B}D_A D_B D_i D_j\mathbf{e}_i - C\dot{F}_{iA,BCD}D_A D_B D_C D_D\mathbf{e}_i, \tag{3.69}$$

We note that, in the superposed incremental deformations, there is no clear distinction between current and deformed configuration. For a single family of fibers Eq. (3.69) reduces to

$$\dot{p}_{,i}\mathbf{e}_i = 2\mu u_{i,AA}\mathbf{e}_i + Eu_{1,11}\mathbf{e}_1 - Cu_{i,1111}\mathbf{e}_i. \tag{3.70}$$

In addition, the corresponding incompressibility condition reduces to

$$(J-1)^{\cdot} = \mathbf{F}_o^* \cdot \dot{\mathbf{F}} = \operatorname{div}\mathbf{u} = \mathbf{0}, \tag{3.71}$$

which, together with Eq. (3.70), serve as a compatible linear model of Eq. (3.36) for small deformations. Finally, the boundary conditions in Eq. (3.56) can be linearized similarly as the above

$$
\begin{aligned}
\dot{\mathbf{t}} &= \dot{\mathbf{P}}\mathbf{N} - \frac{d}{ds}\left[C\dot{\mathbf{g}}(\mathbf{D}\cdot\mathbf{T})(\mathbf{D}\cdot\mathbf{N}) \right], \\
\dot{\mathbf{m}} &= C\dot{\mathbf{g}}(\mathbf{D}\cdot\mathbf{N})^2, \\
\dot{\mathbf{f}} &= C\dot{\mathbf{g}}(\mathbf{D}\cdot\mathbf{T})(\mathbf{D}\cdot\mathbf{N}).
\end{aligned}
\tag{3.72}
$$

In particular, if the fiber's directions are either normal or tangential to the boundary, Eq. (3.72) further reduces to

$$
\begin{aligned}
\dot{t}_i &= \dot{P}_{iA}N_A, \\
\dot{m}_i &= C\dot{g}_i D_A N_A D_B N_B, \\
\dot{f}_i &= 0,
\end{aligned}
\tag{3.73}
$$

and

$$\dot{P}_{iA} = 2\mu\dot{F}_{iA} - \dot{p}\delta_{iA} - p_o F_{iA}^* + E\dot{F}_{jB}D_A D_B D_i D_j - C\dot{g}_{i,B}D_A D_B, \tag{3.74}$$

where $\dot{g}_i = \dot{F}_{iA,B}D_AD_B$ and $(F_{iA}^*)_o = \delta_{iA}$. Lastly, since $J\partial F_{jB}^*/\partial F_{iA} = F_{jB}^*F_{iA}^* - F_{iB}^*F_{jA}^*$ at $\mathbf{F}_o = \mathbf{I}$ we obtain

$$(\partial F_{jB}^*/\partial F_{iA})_o = \delta_{jB}\delta_{iA} - \delta_{iB}\delta_{jA} \tag{3.75}$$

$$(\mathbf{F}_{\mathbf{F}}^*[\dot{\mathbf{F}}])_{jB} = (\delta_{jB}\delta_{iA} - \delta_{iB}\delta_{jA})u_{i,A}.$$

Thus

$$\dot{F}_{iA}^* = (Div\mathbf{u})\delta_{iA} - u_{A,i} = -u_{A,i}, \tag{3.76}$$

where $Div\mathbf{u} = 0$ from the Linearized incompressibility condition.

3.7 Solution to the linearized equation

We introduce scalar field ϕ as

$$\mathbf{u} = \mathbf{k} \times \nabla\phi, \ \mathbf{k}(\text{unit normal}); \ u_i = \varepsilon_{\lambda i}\phi_{,\lambda}, \tag{3.77}$$

so that Eq. (3.71) can be automatically satisfied ($\phi_{,12} - \phi_{,21} = 0$). From (3.77), the linearized Euler equation (Eq. (3.70)) can be rewritten as

$$\dot{p}_{,i} = 2\mu\varepsilon_{\lambda i}\phi_{,\lambda AA} - E\phi_{,211}\delta_{i1} - C\varepsilon_{\lambda i}\phi_{,\lambda 1111}. \tag{3.78}$$

By utilizing the compatibility condition for $\dot{p}_{,i}$ ($\dot{p}_{,ij} = \dot{p}_{,ji}$), we obtain the following ordinary differential equation as;

$$\Delta[\Delta\phi - \frac{\alpha}{2}\phi_{,1111}] + \frac{\alpha}{2}\phi_{,1122} = 0, \ \text{where} \ \beta = \frac{E}{\mu}, \ \alpha = \frac{C}{\mu} > 0. \tag{3.79}$$

We note here that, the solution of the above equation can not be accommodated by conventional methods such as the separation of variables method, Fourier transform and polynomial solutions. In view of the solution of the modified Helmholtz

equation, we assume that ϕ takes the form of $\phi = X(x)\sin(my)$ and obtain

$$
\begin{aligned}
\phi(x,y) &= \sum_{m=1}^{\infty}[\{A_m e^{xT} + B_m e^{-xT} + e^{a_m x}(C_m \cos b_m x + D_m \sin b_m x) + \\
&\quad e^{-a_m x}(E_m \cos b_m x + F_m \sin b_m x)\} \times (\sin my)],
\end{aligned}
\tag{3.80}
$$

where

$$
a_m = (0.5(\quad \frac{\sqrt{3}}{2}\left(\frac{P}{Q}+Q\right))^2 + \left(-\frac{Q}{2}+\frac{P}{2Q}-\frac{B}{3A}\right)^2)^{0.5} + \left(-\frac{Q}{2}+\frac{P}{2Q}-\frac{B}{3A}\right))^{0.5},
$$

$$
b_m = (0.5(\quad \frac{\sqrt{3}}{2}\left(\frac{P}{Q}+Q\right))^2 + \left(-\frac{Q}{2}+\frac{P}{2Q}-\frac{B}{3A}\right)^2)^{0.5} - \left(-\frac{Q}{2}+\frac{P}{2Q}-\frac{B}{3A}\right))^{0.5},
$$

$$
m = \frac{\pi n}{2d},\ A=\frac{\alpha}{2},\ B=(1+\frac{\alpha}{2}m^2),\ D=-m^2(2+\frac{\beta}{2}),
$$

$$
Q = \left(\left(\left(\frac{D}{3A}-\frac{B^2}{9A^2}\right)^3 + \left(\frac{B^3}{27A^3}+\frac{m^4}{2A}-\frac{B.D}{6A^2}\right)^2\right)^{0.5} - \frac{B^3}{27A^3}-\frac{m^4}{2A}+\frac{BD}{6A^2}\right)^{\frac{1}{3}},
$$

$$
P = \frac{D}{3A}-\frac{1}{9}(\frac{B}{A})^2,\ T=(Q-\frac{P}{Q}-\frac{B}{3A})^{0.5}.
\tag{3.78-1}
$$

The unknown constant real numbers A_m, B_m, C_m, D_m, E_m and F_m can be completely determined by imposing admissible boundary conditions depicted in Eqs. (3.73-3.76). The corresponding stress and displacement fields can be also determined through Eqs. (3.74 and 3.77-3.78) ($u_1 = -\phi_{,2}$, $u_2 = \phi_{,1}$). In the case of symmetric bending (Fig. 3.1), we have

$$
\dot{\mathbf{m}} = \dot{m}_1\mathbf{e}_1 + \dot{m}_2\mathbf{e}_2,\ \dot{m}_1 = 5 \approx \sum_{n=1}^{30}\frac{20}{\pi n}(-1)^{\frac{n-1}{2}}\cos(\frac{\pi n}{2d})y\mathbf{e}_1,\ \dot{m}_2 = 0,
\tag{3.81}
$$

and

$$
\mathbf{D} = D_1\mathbf{E}_1 + D_2\mathbf{E}_2,\ D_1 = 1,\ D_2 = 0.
\tag{3.82}
$$

Thus

$$
\begin{aligned}
\dot{m}_1 &= Cu_{1,11} = -\phi_{,211} = \sum_{n=1}^{30} \frac{20}{\pi n}(-1)^{(n-1)/2}\cos(\frac{\pi n}{2d})y \\
\dot{m}_2 &= Cu_{2,11} = \phi_{,111} = 0,
\end{aligned}
\tag{3.83}
$$

3.8   Linearized Problem Result

The applied moment is approximated using Fourier series (Eq. (3.81)) indicating fast convergence and corresponding results are summarized through Figs. 3.11-3.10. Despite the inherent complexities of the present PDE, the solution demonstrates reasonable deformation profiles with sufficient sensitivities to the C, μ, E and M (Figs. 3.11-3.12). In addition, analytical solution shows good agreement with FEM solution for the small deformation, while larger values of M induce a significant discrepancy between them (Fig. 3.10).
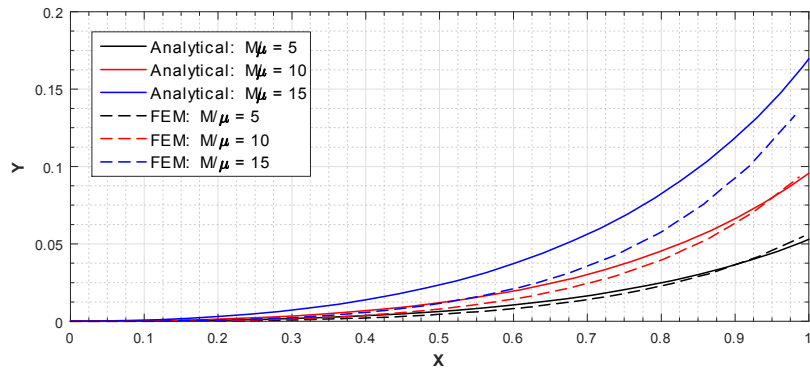
Figure 3.10: FEM VS analytical solutions of bending with $C/\mu = 150$ and $E/\mu = 100$.
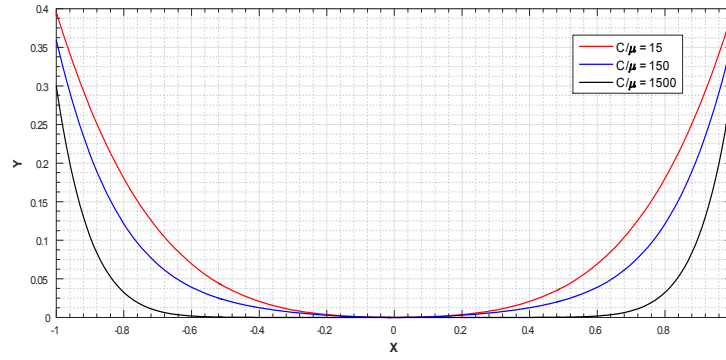
Figure 3.11: Deformation profiles when $C/\mu = 150$ and $E/\mu = 50$.
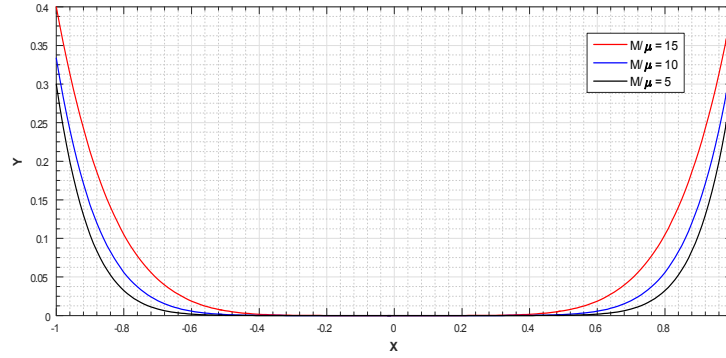
Figure 3.12: Deformation profiles when $C/\mu = 150$ and $E/\mu = 50$.
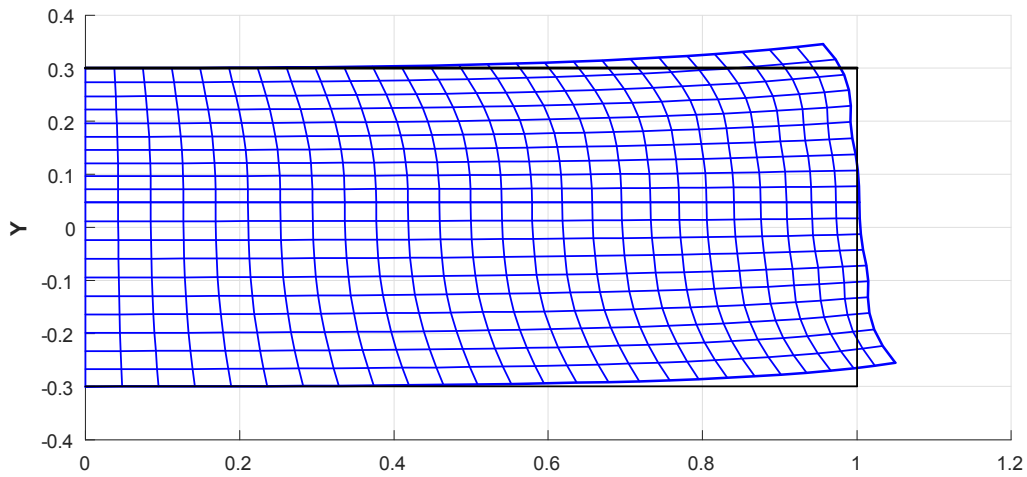
Figure 3.13: Deformed configuration when $C/\mu = 150$, $E/\mu = 100$ and $M/\mu = 5$.

Chapter 4

Mechanics of bidirectional fiber-reinforced composite with fiber resistant to flexure

Via the computation of variational derivatives along the lengths of fibers and the virtual-work statement, the corresponding Euler equilibrium equation is derived in section 4.1. . In addition, in section 4.1.1, the implementation of the model has been made for the Neo-Hookean material type. The solution of the resulting Partial Differential Equations is obtained through finite element analysis in section 4.2 and 4.3 . The results are then compared with experimental data demonstrating that the proposed model successfully predicts the deformed configurations of a Crystalline Nanocellulose fiber composite and $T700S$ carbon-E glass fiber composites. In section 4.4, we present derivation of the necessary boundary conditions. Lastly, linear theory and analytical solution are obtained in sections 4.5 and 5.6.

4.1   Kinematics and Equilibrium equations

In view of [8] and [47], we propose that the mechanical response of the fiber material is governed by the following strain energy function

$$
\begin{aligned}
W(\mathbf{F}, \mathbf{G}) &= \widehat{W}(\mathbf{F}) + W(\mathbf{G}), \\
W(\mathbf{G}) &\equiv \frac{1}{2}C_1\left(\mathbf{F}\right)\left|\mathbf{g}^1\right|^2 + \frac{1}{2}C_2\left(\mathbf{F}\right)\left|\mathbf{g}^2\right|^2,
\end{aligned}
\tag{4.1}
$$

where $\mathbf{F}$ is the gradient of the deformation function $(\boldsymbol{\chi}(\mathbf{X}))$ and $\mathbf{G}$ is the second gradient of the deformation $(\mathbf{G} = \boldsymbol{\nabla}\mathbf{F})$. The orientation of particular bidirectional fibers is given by

$$\lambda = |\boldsymbol{\eta}|, \ \mu = |\boldsymbol{\tau}| \ \text{and} \ \mathbf{l} = \boldsymbol{\eta}\lambda^{-1}, \ \mathbf{m} = \boldsymbol{\tau}\mu^{-1}. \tag{4.2}$$

$$\mathbf{FL} = \lambda\mathbf{l} \ \text{and} \ \mathbf{FM} = \mu\mathbf{m}, \tag{4.3}$$

and

$$\mathbf{F} = \lambda\mathbf{l} \otimes \mathbf{L} + \mu\mathbf{m} \otimes \mathbf{M}, \tag{4.3-1}$$

in which $\mathbf{L}$ and $\mathbf{M}$ are the unit tangent to the fiber's trajectory in the reference configuration and $\mathbf{l}$ and $\mathbf{m}$ are their counterparts in the deformed configuration. Eq. (4.3) can be derived by taking the derivative of $\mathbf{r}(s(S)) = \boldsymbol{\chi}(\mathbf{X}(S))$, upon making the identifications $\mathbf{L} = \frac{d\mathbf{X}}{dS}$ and $\mathbf{l} = \frac{d\boldsymbol{\chi}}{ds}$) and similarly for $\mathbf{M}$. In the present study, we consider initially an orthonormal set of fibers undergoing conformal deformations such that

$$\mathbf{M} \cdot \mathbf{L} = \mathbf{m} \cdot \mathbf{l} = \cos(\frac{\pi}{2}) = \mathbf{0}. \tag{4.4}$$

The expression for geodesic curvatures of a parametric curve $(\mathbf{r}(s, u))$ in s and u directions are then obtained from Eq. (4.3) as

$$\mathbf{g}^1 = \frac{d^2\mathbf{r}(S)}{dS^2} = \frac{d(\frac{\mathbf{r}(S)}{dS})}{dS} = \frac{\partial(\mathbf{FL})}{\partial\mathbf{X}}\frac{d\mathbf{X}}{dS} = \nabla[\mathbf{FL}]\mathbf{L}, \tag{4.5}$$

and

$$\mathbf{g}^2 = \frac{d^2\mathbf{r}(U)}{dU^2} = \frac{d(\frac{\mathbf{r}(U)}{dU})}{dU} = \frac{\partial(\mathbf{FM})}{\partial\mathbf{X}}\frac{d\mathbf{X}}{dU} = \nabla[\mathbf{FM}]\mathbf{M}, \tag{4.6}$$

The compatibility condition of $\nabla\mathbf{F}$ can be seen as

$$G_{iAB} = F_{iA,B} = F_{iB,A} = G_{iBA}. \tag{4.7}$$

Further, we introduce the following augmented energy functional in order to accommodate the constraint of bulk incompressibility

$$U\left(\mathbf{F}, \mathbf{G},p\right) = W(\mathbf{F}, \mathbf{G}) - p(J - 1), \tag{4.8}$$

where J is determinant of $\mathbf{F}$ and p is a Lagrange-multiplier field.

Although the variational analysis arising in second-gradient elasticity is a well established subject [10]-[11] and [46] , its implementation in the mechanics of fiber-reinforced composites, particularly in the case of bidirectional fibers, are barely studied. Here, we reformulate the results for the sake of clarity and completeness; especially, the connections between the applied loads and the deformations. The weak form of the equations of equilibrium is given by the virtual-work statement

$$\dot{E} = P, \tag{4.9}$$

where P is the virtual work of the applied loads and the superposed dot refers to the variational derivative;

$$E = \int_{\Omega} U\left(\mathbf{F}, \mathbf{G}\right) dA \tag{4.10}$$

is the strain energy. Since the conservative loads are characterized by the existence of a potential L such that $P = \dot{L}$, in the present case, the problem of determining equilibrium deformations is reduced to the problem of minimizing the potential energy $E - L$. We then have

$$\dot{E} = \int_{\Omega} \dot{U}\left(\mathbf{F}, \mathbf{G},p\right) dA, \tag{4.11}$$

where

$$\dot{U}\left(\mathbf{F}, \mathbf{G},p\right) = W_{\mathbf{F}}{\cdot}\dot{\mathbf{F}} + \mathbf{W}_{\mathbf{G}} \cdot \dot{\mathbf{G}} - p\dot{J}, \tag{4.11-1}$$

and subscripts denote corresponding partial derivatives (e.g. $W_{\mathbf{F}} = \partial W/\partial \mathbf{F}$). It is

noted here that the scenario of extensible fibers is excluded from the present study for conciseness (i.e. no variation is induced with respect to λ and μ). However, this can be easily accommodated by modifying the proposed energy density function in Eq. (4.1). Using the identity $\dot{J} = J_F \cdot \dot{\mathbf{F}} = \mathbf{F}^* \cdot \dot{\mathbf{F}}$, Eq. (4.11) becomes

$$\dot{E} = \int_\Omega [(W_{\mathbf{F}} - p\mathbf{F}^*) \cdot \dot{\mathbf{F}} + \mathbf{W_G} \cdot \dot{\mathbf{G}}] dA. \tag{4.12}$$

Also from Eq. (4.7), $W_{\mathbf{G}} \cdot \dot{\mathbf{G}}$ can be expressed as

$$\frac{\partial W}{\partial G_{iAB}} \dot{G}_{iAB} = \frac{\partial W}{\partial G_{iAB}} u_{i,AB} = \left(\frac{\partial W}{\partial G_{iAB}} u_{i,A} \right)_{,B} - \left(\frac{\partial W}{\partial G_{iAB}} \right)_{,B} u_{i,A}, \tag{4.13}$$

where $u = \dot{\chi}$ is the induced variation of the position field. Substituting the above into (4.12) yields

$$\dot{E} = \int_\Omega [\left(\frac{\partial W}{\partial F_{iA}} - pF_{iA}^* \right) \cdot \dot{F}_{iA} + \left(\frac{\partial W}{\partial G_{iAB}} u_{i,A} \right)_{,B} - \left(\frac{\partial W}{\partial G_{iAB}} \right)_{,B} u_{iA}] dA, \tag{4.14}$$

Thus, we obtain

$$\dot{E} = \int_\Omega [\frac{\partial W}{\partial F_{iA}} - pF_{iA}^* - \left(\frac{\partial W}{\partial G_{iAB}} \right)_{,B}] \dot{F}_{iA} dA + \int_{\partial\Omega} \left(\frac{\partial W}{\partial G_{iAB}} u_{i,A} \right) N_B dS, \tag{4.15}$$

where $\mathbf{N}$ is the rightward unit normal to the boundary curve $\partial\Omega$ in the sense of the Green-stoke's theorem. In general, the mechanical responses of the engineering materials are uniform that Eq. (4.1) now furnishes

$$W_{\mathbf{G}} \cdot \dot{\mathbf{G}} = C_1 \mathbf{g}^1 \cdot \dot{\mathbf{g}}^1 + C_2 \mathbf{g}^2 \cdot \dot{\mathbf{g}}^2, \tag{4.16}$$

where the expression of $W_{\mathbf{G}}$ can be found as

$$W_{\mathbf{G}} = C_1 \mathbf{g}^1 \otimes \mathbf{L} \otimes \mathbf{L} + C_2 \mathbf{g}^2 \otimes \mathbf{M} \otimes \mathbf{M}. \tag{4.17}$$

Further, in the case of initially straight fibers (i.e. $\nabla \mathbf{M} = 0,\ \nabla \mathbf{L} = 0$), $Div(W_{\mathbf{G}})$ reduces to

$$
\begin{aligned}
Div(W_{\mathbf{G}}) &= C_1 g^1_{i,B} L_A L_B (\mathbf{e}_i \otimes \mathbf{E}_A) + C_2 g^2_{i,B} M_A M_B (\mathbf{e}_i \otimes \mathbf{E}_A) \\
&= (C_1 g^1_{i,B} L_A L_B + C_2 g^2_{i,B} M_A M_B)(\mathbf{e}_i \otimes \mathbf{E}_A), \\
\left(\frac{\partial W}{\partial G_{iAB}} \right)_{,B} &= C_1 g^1_{i,B} L_A L_B + C_2 g^2_{i,B} M_A M_B.
\end{aligned}
\tag{4.17-1}
$$

Consequently, Eq. (4.15) becomes

$$
\dot{E} = \int_{\Omega} P_{iA} \dot{F}_{iA} dA + \int_{\partial \Omega} (C_1 g^1_i L_A L_B + C_2 g^2_i M_A M_B) u_{i,A} N_B dS,
\tag{4.18}
$$

where

$$
P_{iA} = \frac{\partial W}{\partial F_{iA}} - p F^*_{iA} - C_1 g^1_{i,B} L_A L_B - C_2 g^2_{i,B} M_A M_B.
\tag{4.19}
$$

The corresponding Euler equation is then obtained as

$$
P_{iA,A} = 0 \text{ or } Div(\mathbf{P}) = 0.
\tag{4.20}
$$

which hold on Ω.

4.1.1 Neo-Hookean Materials

The energy density function of the incompressible Neo-Hookean materials is given by

$$
W = \frac{\mu}{2} tr(\mathbf{C}) = \frac{\mu}{2} tr(\mathbf{F}^T \mathbf{F}) = \frac{\mu}{2} \mathbf{F} \cdot \mathbf{F}.
\tag{4.21}
$$

Thus, from Eqs. (4.19-4.20), the corresponding Euler equation can be obtained as

$$
\begin{aligned}
P_{iA,A} &= \mu F_{iA,A} - p_{,A} F^*_{iA} - C_1 g^1_{i,B} L_A L_B - C_2 g^2_{i,B} M_A M_B = 0, \\
F^*_{iA,A} &= 0 \text{ (Piola's identity).}
\end{aligned}
\tag{4.22}
$$

Now consider a fiber-reinforced material which consists of initially orthonormal set of fibers,

$$\mathbf{L} = \mathbf{E}_1, \ L_1 = 1, \ L_2 = 0, \ \mathbf{M} = \mathbf{E}_2, \ M_1 = 0, \ M_2 = 1, \qquad (4.23)$$

and is subjected to plane deformations. Within this prescription, Eq. (4.22) further reduces to

$$\mu F_{iA,A} - p_{,A} F_{iA}^* - C_1 g_{i,11}^1 - C_2 g_{i,22}^2 = 0 \text{ for } i, A = 1, 2, \qquad (4.24)$$

where

$$g_i^1 = F_{i1,1}, \ g_i^2 = F_{i2,2}, \ F_{iA} = \frac{\partial \chi_i}{\partial X_A} \text{ and } F_{iA}^* = \varepsilon_{ij} \varepsilon_{AB} F_{jB}. \qquad (4.25)$$

In the above, ε_{ij} is the 2D permutation; $\varepsilon_{12} = -\varepsilon_{21} = 1, \varepsilon_{11} = -\varepsilon_{22} = 0$. Therefore, Eq. (4.25) together with the constraint of the bulk incompressibility (det $\mathbf{F} = 1$) yields the following coupled PDE system solving for χ_1, χ_2 and p.

$$
\begin{aligned}
\mu \left(\chi_{1,11} + \chi_{1,22} \right) - p_{,1} \chi_{2,2} + p_{,2} \chi_{2,1} - C_1 \chi_{1,1111} - C_2 \chi_{1,2222} &= 0, \\
\mu \left(\chi_{2,11} + \chi_{2,22} \right) + p_{,1} \chi_{1,2} - p_{,2} \chi_{1,1} - C_1 \chi_{2,1111} - C_2 \chi_{2,2222} &= 0, \\
\chi_{1,1} \chi_{2,2} - \chi_{1,2} \chi_{2,1} &= 1. \qquad (4.26)
\end{aligned}
$$

4.2 FEA of the 4th order coupled PDE

It is not trivial to demonstrate numerical analysis procedures for coupled PDE systems, especially for those with high order terms due to the C^1 continuity of the

corresponding *Hilbert* space. For pre processing, Eq. (4.26) can be recast as

$$\mu\left(R+F\right)-A\chi_{2,2}+B\chi_{2,1}-C_1R_{,11}-C_2F_{,22}=0,$$

$$\mu\left(Q+G\right)+A\chi_{1,2}-B\chi_{1,1}-C_1Q_{,11}-C_2G_{,22}=0,$$

$$C\chi_{2,2}-D\chi_{1,2}-1=0,\ \ Q-\chi_{1,11}=0,$$

$$R-\chi_{2,11}=0,\ \ C-\chi_{1,1}=0,\ \ D-\chi_{2,1}=0,$$

$$F-\chi_{1,22}=0,\ \ G-\chi_{2,22}=0,$$

$$A-\mu(\chi_{1,11}+\chi_{1,22})-C_1R_{,11}-C_2F_{,22}=0,$$

$$B-\mu(\chi_{2,11}+\chi_{2,22})-C_1Q_{,11}-C_2G_{,22}=0. \tag{4.27}$$

where $Q=\chi_{1,11}$, $R=\chi_{2,11}$, $F=\chi_{1,22}$, $G=\chi_{2,22}$, $C=\chi_{1,1}$ and $D=\chi_{2,1}$. The non-linear terms in the above can be treated as

$$-A\chi_{2,2}+B\chi_{2,1}\ \ \Longrightarrow\ \ -A_0\chi_{2,2}+B_0\chi_{2,1},$$

$$A\chi_{1,2}-B\chi_{1,1}\ \ \Longrightarrow\ \ A_0\chi_{1,2}-B_0\chi_{1,1},$$

$$C\chi_{2,2}-D\chi_{2,1}\ \ \Longrightarrow\ \ C_0\chi_{2,2}-D_0\chi_{2,1}, \tag{4.28}$$

where the values of A, B and C continue to be refreshed based on their previous estimations (A_0, B_0, C_0) as iteration progresses. Therefore, the weak form of Eq.

(4.27) is obtained by

$$
\begin{aligned}
0 &= \int_{\Omega} (\mu w_1 R - \mu w_1 F - w_1 A_0 \chi_{2,2} + w_1 B_0 \chi_{2,1} + C_1 w_{1,1} R_{,1} + C_2 w_{1,2} F_{,2}) d\Omega \\
&\quad - \int_{\partial \Gamma} (C_1 w_1 R_{,1} + C_2 w_1 F_{,2}) N d\Gamma, \\
0 &= \int_{\Omega} (\mu w_2 Q - \mu w_2 G + w_2 A_0 \chi_{1,2} - w_2 B_0 \chi_{1,1} + C_1 w_{2,1} Q_{,1} + C_2 w_{2,2} G_{,2}) d\Omega \\
&\quad - \int_{\partial \Gamma} (C_1 w_2 Q_{,1} + C_2 w_2 G_{,2}) N d\Gamma, \\
0 &= \int_{\Omega} C_0 w_3 \chi_{2,2} - D_0 w_3 \chi_{1,2} - w_3) d\Omega, \ 0 = \int_{\Omega} (w_4 Q + w_{4,1} \chi_{1,1}) d\Omega - \int_{\partial \Gamma} (w_4 \chi_{1,1}) N d\Gamma, \\
0 &= \int_{\Omega} (w_5 R + w_{5,1} \chi_{2,1}) d\Omega - \int_{\partial \Gamma} (w_5 \chi_{2,1}) N d\Gamma, \ 0 = \int_{\Omega} (w_6 C - w_6 \chi_{1,1}) d\Omega, \\
0 &= \int_{\Omega} (w_7 D - w_7 \chi_{2,1}) d\Omega, \ 0 = \int_{\Omega} (w_8 F + w_{8,2} \chi_{1,2}) d\Omega - \int_{\partial \Gamma} (w_8 \chi_{1,2}) N d\Gamma, \\
0 &= \int_{\Omega} (w_9 G + w_{9,2} \chi_{2,2}) d\Omega - \int_{\partial \Gamma} (w_9 \chi_{2,2}) N d\Gamma, \\
0 &= \int_{\Omega} (w_{10} A + \mu w_{10,1} \chi_{1,1} - \mu w_{10,2} \chi_{1,2} + C_1 w_{10,1} R_{,1}) d\Omega - \int_{\partial \Gamma} (\mu w_{10} \chi_{1,1}) N d\Gamma + \\
&\quad \int_{\partial \Gamma} (\mu w_{10} \chi_{1,2}) N d\Gamma - \int_{\partial \Gamma} (C_1 w_{10} R_{,1} + C_2 w_{10} F_{,2}) N d\Gamma, \\
0 &= \int_{\Omega} (w_{11} B + \mu w_{11,1} \chi_{2,1} - \mu w_{11,2} \chi_{2,2} + C_1 w_{11,1} Q_{,1}) d\Omega - \int_{\partial \Gamma} (\mu w_{11} \chi_{2,1}) N d\Gamma + \\
&\quad \int_{\partial \Gamma} (\mu w_{11} \chi_{2,2}) N d\Gamma - \int_{\partial \Gamma} (C_1 w_{11} Q_{,1} + C_2 w_{11} G_{,2}) N d\Gamma, \quad (4.29)
\end{aligned}
$$

where the unknowns (e. g. χ_1, χ_2, Q_1, R_1, A, B etc...) can be written in the form of Lagrangian polynomial such that $(*) = \sum_{j=1}^{n} [(*)_j \Psi_j]$. Ω, $\partial \Gamma$ and $\mathbf{N}$ are the domain of interest, the associated boundary, and the rightward unit normal to the boundary $\partial \Gamma$ in the sense of the Green-stoke's theorem, respectively. The corresponding test function w is given by

where Ψ_i are the shape functions for the 4-node rectangular element.
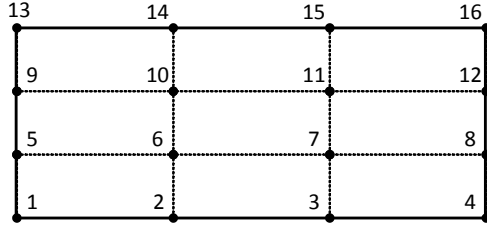
Figure 4.1: Schematic of 16 nodes rectangular element

$$
\begin{bmatrix}
1 & 5 & 9 & 13 \\
2 & 6 & 10 & 14 \\
3 & 7 & 11 & 15 \\
4 & 8 & 12 & 16
\end{bmatrix}
=
\begin{bmatrix}
f_1 \\
f_2 \\
f_3 \\
f_4
\end{bmatrix}
\begin{bmatrix} g_1 & g_2 & g_3 & g_4 \end{bmatrix},
\qquad (4.30)
$$

where

$$
\begin{aligned}
f_1(x) &= \frac{\left(x - \frac{c}{3}\right)\left(x - \frac{2c}{3}\right)(x - c)}{\left(-\frac{c}{3}\right)\left(-\frac{2c}{3}\right)(-c)}, \quad
f_2(x) = \frac{(x)\left(x - \frac{2c}{3}\right)(x - c)}{\left(\frac{c}{3}\right)\left(-\frac{c}{3}\right)\left(-\frac{2c}{3}\right)}, \\
f_3(x) &= \frac{(x)\left(x - \frac{c}{3}\right)(x - c)}{\left(\frac{2c}{3}\right)\left(\frac{c}{3}\right)\left(-\frac{c}{3}\right)}, \quad
f_4(x) = \frac{(x)\left(x - \frac{c}{3}\right)\left(x - \frac{2c}{3}\right)}{\left(\frac{c}{3}\right)\left(\frac{2c}{3}\right)(c)} \\
g_1(y) &= \frac{\left(y - \frac{d}{3}\right)\left(y - \frac{2d}{3}\right)(y - d)}{\left(-\frac{d}{3}\right)\left(-\frac{2d}{3}\right)(-d)}, \quad
g_2(y) = \frac{(y)\left(y - \frac{2d}{3}\right)(y - d)}{\left(\frac{d}{3}\right)\left(-\frac{d}{3}\right)\left(-\frac{2d}{3}\right)}, \\
g_3(y) &= \frac{(y)\left(y - \frac{d}{3}\right)(y - d)}{\left(\frac{2d}{3}\right)\left(\frac{d}{3}\right)\left(-\frac{d}{3}\right)}, \quad
g_4(y) = \frac{(y)\left(y - \frac{d}{3}\right)\left(y - \frac{2d}{3}\right)}{\left(\frac{d}{3}\right)\left(\frac{2d}{3}\right)(d)}. \qquad (4.31\text{-}1)
\end{aligned}
$$

The assignment of each shape function is illustrated in Fig. 4.1

Using Lagrangian polynomial representation, the first of Eq. (4.29) can be rewritten as

$$
\begin{aligned}
0 &= \sum_{i,\,j=1}^{n} \left\{ \int_{\Omega} (\mu \Psi_i \Psi_j + C_1 \Psi_{i,1} \Psi_{j,1}) d\Omega \right\} R_j + \sum_{i,\,j=1}^{n} \left\{ \int_{\Omega} (\mu \Psi_i \Psi_j + C_2 \Psi_{i,2} \Psi_{j,2}) d\Omega \right\} F_j - \\
&\quad \sum_{i,\,j=1}^{n} \left\{ \int_{\Omega} (\Psi_i A_0 \Psi_{j,2} + \Psi_i B_0 \Psi_{j,1}) d\Omega \right\} \chi_{2j} - \int_{\partial\Gamma} (C_1 \Psi_i R_{,1} + C_2 \Psi_i F_{,2}) N d\Gamma. \quad (4.31)
\end{aligned}
$$

and similarly for the rest of equations. Finally, we obtain the systems of equations $[\mathbb{K}][\mathbb{E}] = [\mathbb{F}]$. Here $[\mathbb{K}]$ and $[\mathbb{F}]$ are $[11 \times 10]$ and $[10 \times 1]$ matrices, respectively

and $[\mathbb{E}]$ is $[11 \times 1]$ matrix with unknowns (χ_1, χ_2, Q_1, R_1, A, B etc...). The expressions of $[K^{ij}]$ and $[F_i]$ can be obtained via the standard Finite Element Analysis procedures. For example,

$$K^{11} = \int_{\Omega} (\mu \Psi_i \Psi_j + C_2 \Psi_{i,2} \Psi_{j,2}) d\Omega, \qquad (4.32)$$

and

$$F_1 = \int_{\partial\Gamma} (C_1 \Psi_i R_{,1} + C_2 \Psi_i F_{,2}) N d\Gamma. \qquad (4.33)$$

We mention here that other numerical scheme may be adopted such as the methods presented in [96]-[97]. Fig. 4.2. illustrate performance comparison between the presented method and the one adopted in [97] which shows good agreement over the domain of interest. The deformation profiles and contours in Figs. 4.4-4.5 are the predictions from both the proposed numerical scheme and the method in [96] and [99]. Again, they produce almost identical predictions when performed in the analogous settings. Lastly, the presented numerical scheme demonstrates fast convergence within 70 iterations (Fig. 4.5).
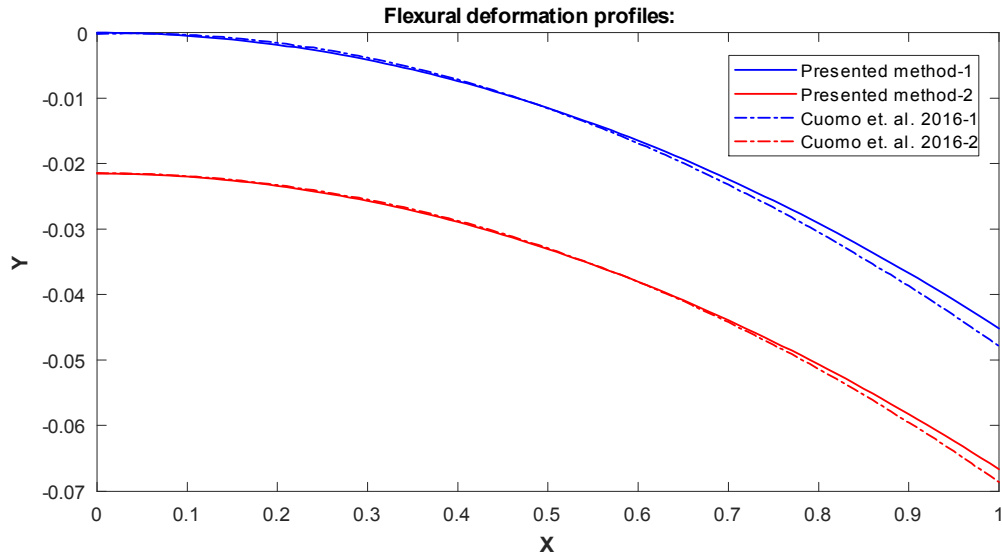
Figure 4.2: Performance comparison: Proposed method VS Cuomo et. al. 2016
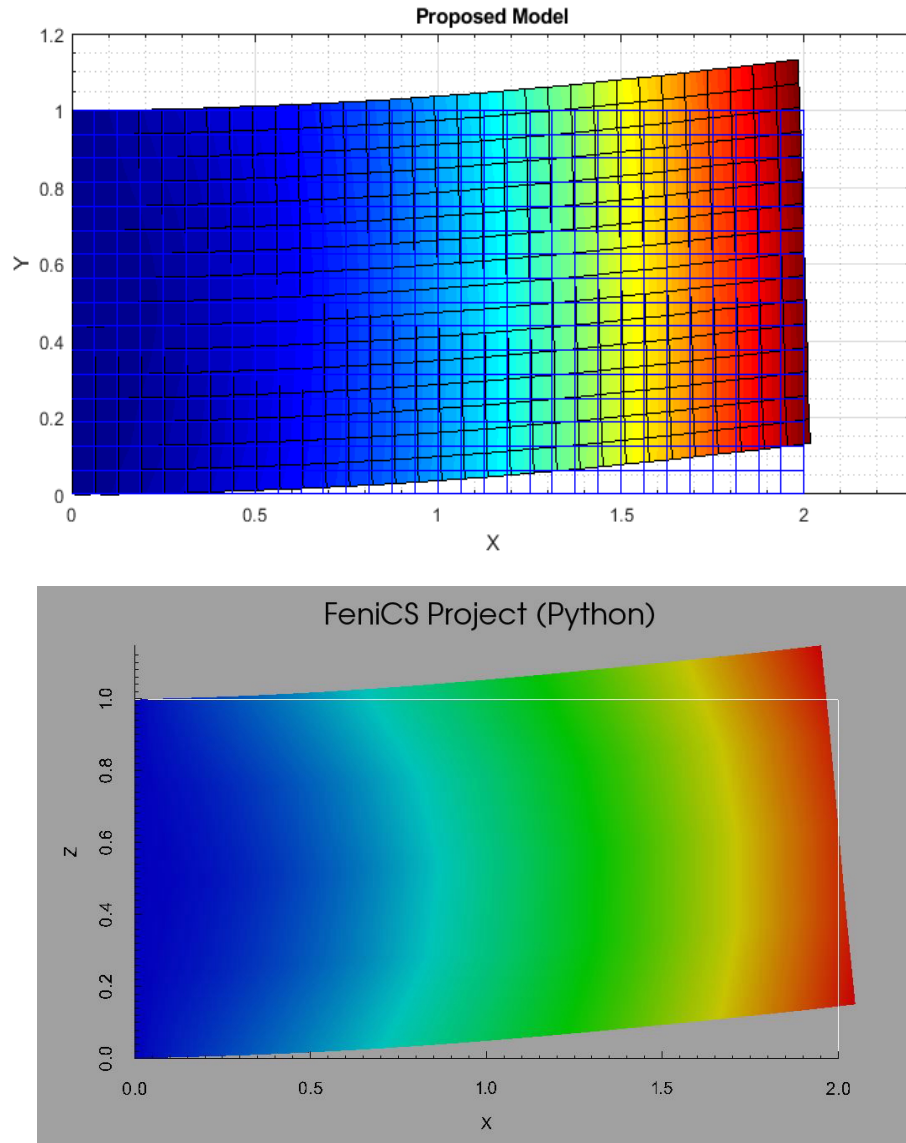
Figure 4.3: Deformation contours: Proposed method VS Abali et. al. 2017

4.3 Numerical Solution Result

For demonstration purposes, a set of numerical solutions is obtained for a rectangular composite reinforced with bidirectional fibers (orthonormal) subjected to uniform bending (see Fig. 4.6.). In the simulation, a half problem is considered in which the corresponding boundary conditions are given as $\chi_{1,11} = -M/\mu$, $\chi_{2,11} = 0$, $\chi_2 = 0$ and $\chi_1 = 0$ at $x = 0$, and $\chi_{1,11} = -M/\mu$, $\chi_{2,11} = 0$, $\chi_{2,1} = 0$ and $\chi_{1,1} = 0$ at $x = c$. Similar boundary conditions are employed for the upper $(y = d)$
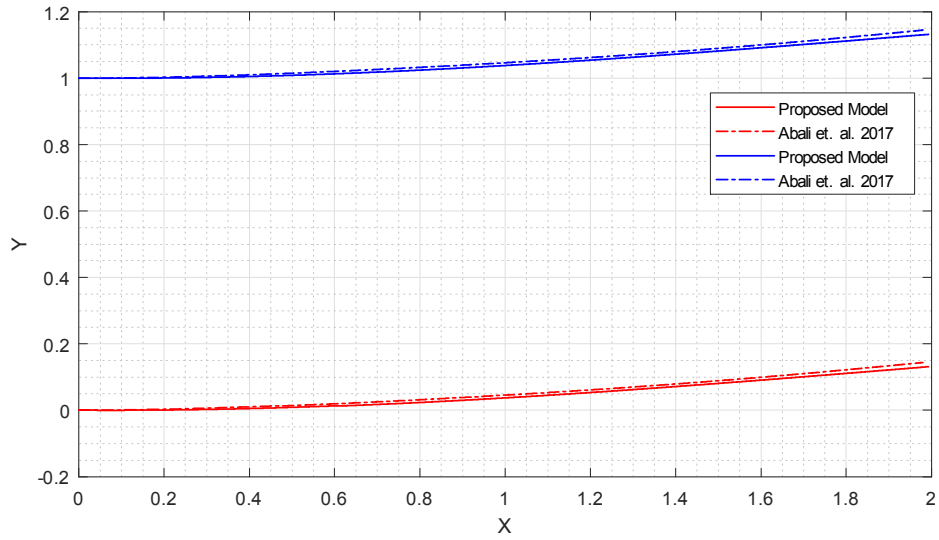
Figure 4.4: Deformation profiles: Proposed method VS Abali et. al. 2017

Figure 4.5: Convergence analysis.

and bottom $(y = -d)$ faces except boundary moments where we impose zero moment in order to assimilate flexural deformations (see, [88]-[89]). The results in Figs. 4.7-4.8 clearly indicate the effects of the second-gradient of the deformations on the resulting deformed configurations.
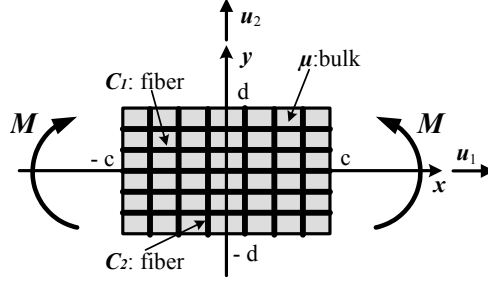
Figure 4.6: Schematic of problem for bidirectional fiber reinforced with moment (M) boundary condition.
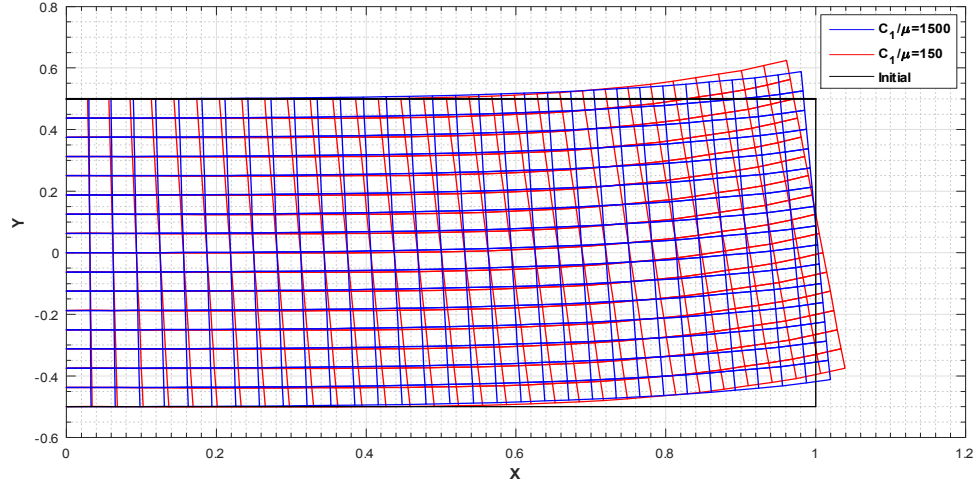
Figure 4.7: Deformed configurations with respect to C_1/μ when $M/\mu = 50$ and $C_2/\mu = 100$.

4.4 Boundary conditions

Admissible boundary conditions arising from second gradient continua are well discussed in [59]-[90]. Here, we reframed the works in the present setting for the sake of consistency and completeness. From Eq. (4.15), we have

$$\dot{E} = \int_\Omega P_{iA}\dot{F}_{iA}dA + \int_{\partial\Omega}\left(\frac{\partial W}{\partial G_{iAB}}u_{i,A}\right)N_BdS, \tag{4.34}$$

where

$$P_{iA} = \frac{\partial W}{\partial F_{iA}} - pF_{iA}^* - \left(\frac{\partial W}{\partial G_{iAB}}\right)_{,B}. \tag{4.35}$$
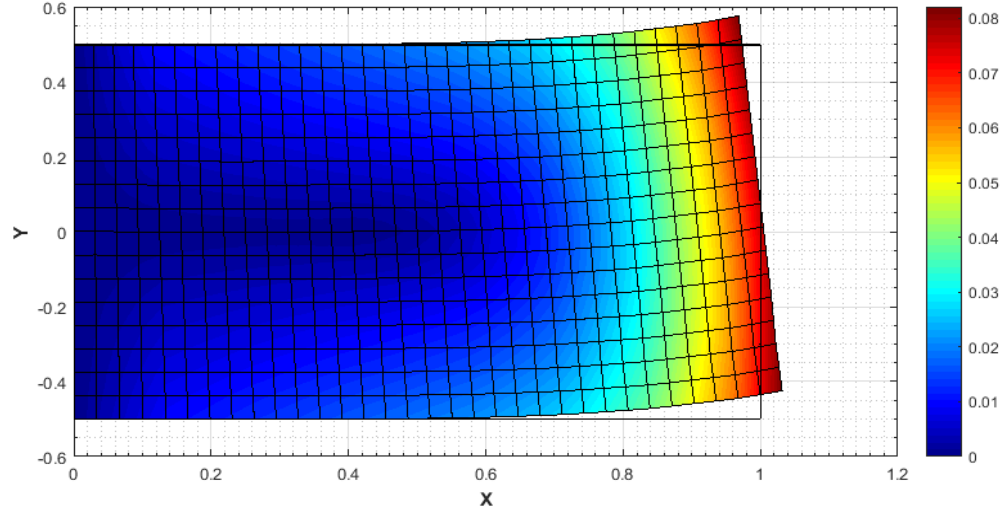
Figure 4.8: Deformation contour $(\sqrt{\chi_1^2 + \chi_2^2})$ when $C_1/\mu = 150$, $C_1/\mu = 100$ and $M/\mu = 30$.

Decomposing the above as in (4.13) (i.e. $P_{iA}u_{i,A} = (P_{iA}u_i)_{,A} - P_{iA,A}u_i$) yields

$$\dot{E} = \int_{\partial\Omega} P_{iA}u_i N_A dS - \int_{\Omega} P_{iA,A}u_i dA + \int_{\partial\Omega} \left(\frac{\partial W}{\partial G_{iAB}} u_{i,A} \right) N_B dS, \qquad (4.36)$$

and hence the Euler equation $P_{iA,A} = 0$ which holds in Ω. With this satisfied, Eq. (4.36) becomes

$$\dot{E} = \int_{\partial\Omega} P_{iA}u_i N_A dS + \int_{\partial\Omega} \left(\frac{\partial W}{\partial G_{iAB}} u_{i,A} \right) N_B dS. \qquad (4.37)$$

Now, we make use of the normal-tangent decomposition of $\nabla\mathbf{u}$ as;

$$\nabla\mathbf{u} = \nabla\mathbf{u}(\mathbf{T}\otimes\mathbf{T}) + \nabla\mathbf{u}(\mathbf{N}\otimes\mathbf{N}) = \mathbf{u}'\otimes\mathbf{T} + \mathbf{u}_{,\mathbf{N}}\otimes\mathbf{N}, \qquad (4.38)$$

where $\mathbf{T} = \mathbf{X}'(S) = \mathbf{k} \times \mathbf{N}$ is the unit tangent to $\partial\Omega$. $\mathbf{u}'$ and $\mathbf{u}_{,N}$ are the tangential and normal derivatives of $\mathbf{u}$ on $\partial\Omega$, respectively (i.e. $u_i' = u_{i,A}T_A$, $u_{i,N} = u_{i,A}N_A$).

Accordingly, Eq. (4.37) can be rewritten as

$$\dot{E} = \int_{\partial\Omega} P_{iA} u_i N_A dS + \int_{\partial\Omega} \frac{\partial W}{\partial G_{iAB}} \left(u_i' T_A N_B + u_{i,N} N_A N_B \right) dS. \tag{4.39}$$

Since

$$\frac{\partial W}{\partial G_{iAB}} T_A N_B u_i' = \left(\frac{\partial W}{\partial G_{iAB}} T_A N_B u_i \right)' - \left(\frac{\partial W}{\partial G_{iAB}} T_A N_B \right)' u_i, \tag{4.40}$$

we obtain

$$\begin{aligned}
\dot{E} &= \int_{\partial\Omega} \left\{ P_{iA} N_A - \left(\frac{\partial W}{\partial G_{iAB}} T_A N_B \right)' \right\} u_i dS \\
&\quad + \int_{\partial\Omega} \frac{\partial W}{\partial G_{iAB}} u_{i,N} N_A N_B dS + \int_{\partial\Omega} \left(\frac{\partial W}{\partial G_{iAB}} T_A N_B u_i \right)' dS. \tag{4.41}
\end{aligned}$$

In view of Eq. (4.17) (i.e. $W_{\mathbf{G}} = C_1 \mathbf{g}^1 \otimes \mathbf{L} \otimes \mathbf{L} + C_2 \mathbf{g}^2 \otimes \mathbf{M} \otimes \mathbf{M}$), Eq. (4.41) furnishes

$$\begin{aligned}
\dot{E} &= \int_{\partial\Omega} \left\{ P_{iA} N_A - \left(C_1 g_i^1 L_A T_A L_B N_B + C_2 g_i^2 M_A T_A M_B N_B \right)' \right\} u_i dS \\
&\quad + \int_{\partial\Omega} (C_1 g_i^1 L_A N_A L_B N_B + C_2 g_i^2 M_A N_A M_B N_B) u_{i,N} dS \\
&\quad - \sum \left\| (C_1 g_i^1 L_A T_A L_B N_B + C_2 g_i^2 M_A T_A M_B N_B) u_i \right\|, \tag{4.42}
\end{aligned}$$

where the double bar symbol refers to the jump across the discontinuities on the boundary $\partial\Omega$ (i.e. $\|*\| = (*)^+ - (*)^-$) and the sum refers to the collection of all discontinuities. Further, the principle of virtual work ($\dot{E} = P$) states that the admissible mechanical powers take the following form

$$P = \int_{\partial\Omega_t} t_i u_i dS + \int_{\partial\Omega} m_i u_{i,N} dS + \sum f_i u_i. \tag{4.43}$$

Consequently, by comparing Eqs. (4.42) and (4.43), we obtain

$$
\begin{aligned}
\mathbf{t} &= \mathbf{PN} - \frac{d}{dS}\left[C_1\mathbf{g}^1(\mathbf{L}\cdot\mathbf{T})(\mathbf{L}\cdot\mathbf{N}) + C_2\mathbf{g}^2(\mathbf{M}\cdot\mathbf{T})(\mathbf{M}\cdot\mathbf{N})\right], \\
\mathbf{m} &= C_1\mathbf{g}^1(\mathbf{L}\cdot\mathbf{N})^2 + C_2\mathbf{g}^2(\mathbf{M}\cdot\mathbf{N})^2, \\
\mathbf{f} &= C_1\mathbf{g}^1(\mathbf{L}\cdot\mathbf{T})(\mathbf{L}\cdot\mathbf{N}) + C_2\mathbf{g}^2(\mathbf{M}\cdot\mathbf{T})(\mathbf{M}\cdot\mathbf{N}).
\end{aligned}
\tag{4.44}
$$

which are expressions of edge tractions, edge moments and the corner forces, respectively. For example, if the fiber's directions are either normal or tangential to the boundary (i.e. $(\mathbf{L}\cdot\mathbf{T})(\mathbf{L}\cdot\mathbf{N}) = 0$ and $(\mathbf{M}\cdot\mathbf{T})(\mathbf{M}\cdot\mathbf{N}) = 0$), Eq. (4.44) further reduces to

$$
\begin{aligned}
t_i &= P_{iA}N_A, \\
m_i &= C_1 g_i^1 L_A N_A L_B N_B + C_2 g_i^2 M_A N_A M_B N_B, \\
f_i &= 0,
\end{aligned}
\tag{4.45}
$$

where

$$
\begin{aligned}
P_{iA} &= \mu F_{iA} - p F_{iA}^* - C_1 g_{i,B}^1 L_A L_B - C_2 g_{i,B}^2 M_A M_B, \\
g_i^1 &= F_{iA,B} L_A L_B \text{ and } g_i^2 = F_{iA,B} M_A M_B.
\end{aligned}
\tag{4.46}
$$

4.5 Linear Theory

We consider superposed "*small*" deformations as

$$
\boldsymbol{\chi} = \boldsymbol{\chi}_o + \varepsilon\dot{\boldsymbol{\chi}} \; ; |\varepsilon| \ll 1,
\tag{4.47}
$$

where $(*)_o$ denote configuration of $*$ evaluated at $\varepsilon = 0$ and $(\dot{*}) = \partial(*)/\partial\varepsilon$. In particular, we denote $\dot{\chi} = u$. Here caution needs to be taken that the present

notation is not confused with the one used for the variational computation. Details regarding the following developments can also be found in [91] where the authors discussed a compatible linear theory in a similar context. From Eq. (4.47), the deformation gradient tensor can be written by

$$\mathbf{F} = \mathbf{F}_o + \varepsilon \nabla \mathbf{u}, \text{ where } \dot{\mathbf{F}} = \nabla \mathbf{u}. \tag{4.48}$$

We assume that the body is initially undeformed and stress free at $\varepsilon = 0$ (i.e. $F_o = I$ and $P_o = 0$). Hence, Eq. (4.48) becomes

$$\mathbf{F} = \mathbf{I} + \varepsilon \nabla \mathbf{u}, \tag{4.49}$$

and successively obtain

$$\mathbf{F}^{-1} = \mathbf{I} - \varepsilon \nabla \mathbf{u} + o(\varepsilon), \tag{4.50}$$

and

$$J = \det \mathbf{F} = 1 + \varepsilon \operatorname{div} \mathbf{u} + o(\varepsilon). \tag{4.51}$$

Further, in view of Eq. (4.47), Eq. (4.20) can be rewritten as

$$Div(\mathbf{P}) = Div(\mathbf{P}_o) + \varepsilon Div(\dot{\mathbf{P}}) + o(\varepsilon) = \mathbf{0}. \tag{4.52}$$

By dividing the above by ε and letting $\varepsilon \to 0$, we have

$$Div(\dot{\mathbf{P}}) = 0, \tag{4.53}$$

which serves as the linearized Euler equation. Now, from Eq. (4.19), the induced variation of $\mathbf{P}$ with respect to ε is given by

$$\dot{\mathbf{P}} = W_{\mathbf{FF}} \dot{\mathbf{F}} - \dot{p} \mathbf{F}_o^* - p_o \dot{\mathbf{F}}^* - C_1 \nabla \dot{\mathbf{g}}^1 (\mathbf{L} \otimes \mathbf{L}) - C_2 \nabla \dot{\mathbf{g}}^2 (\mathbf{M} \otimes \mathbf{M}), \tag{4.54}$$

81

where, in the case of Neo-Hookean material (Eq. (4.21)); $W_{\mathbf{FF}} = \mu(\mathbf{e}_i \otimes \mathbf{E}_A \otimes \mathbf{e}_i \otimes \mathbf{E}_A)$. Thus, Eqs. (4.53-4.54) yield

$$Div(\mu \dot{\mathbf{F}}) - Div(\dot{p}\mathbf{F}_o^*) - Div(p_o \dot{\mathbf{F}}^*) - Div[C_1 \nabla \dot{\mathbf{g}}^1 (\mathbf{L} \otimes \mathbf{L}) + C_2 \nabla \dot{\mathbf{g}}^2 (\mathbf{M} \otimes \mathbf{M})] = 0.$$

(4.55)

However, from Eq. (4.47), the terms in the above further reduce to

$$Div(\mu \dot{\mathbf{F}}) = Div(\mu \nabla \mathbf{u}) = \mu u_{i,AA} \mathbf{e}_i,$$

(4.56)

$$Div(\dot{p}\mathbf{F}_o^*) = \mathbf{F}_o^* \nabla \dot{p} = \mathbf{I} \nabla \dot{p},$$

(4.57)

$$Div(\mathbf{F}^*) = 0,$$

where $\mathbf{I}\nabla\dot{p}$ is on the current basis (i.e. $\mathbf{I}\nabla\dot{p} = \dot{p}_{,i}\mathbf{e}_i$) and

$$Div(p_o \dot{\mathbf{F}}^*) = p_o Div(\dot{\mathbf{F}^*}) = 0,$$

(4.58)

$$p_o = \mu = \text{constant}$$

We mention here that $p_o = \mu$ to recover the initial stress free state at $\varepsilon = 0$ from the underlying finite deformation (i.e. $\mathbf{P}_o = \mu \mathbf{F}_o - p\mathbf{F}_o^* - C_1 \nabla \dot{\mathbf{g}}_o^1 (\mathbf{L} \otimes \mathbf{L}) - C_2 \nabla \dot{\mathbf{g}}_o^2 (\mathbf{M} \otimes \mathbf{M}) = \mathbf{0}$). In addition, since $\nabla \mathbf{L} = \nabla \mathbf{M} = 0$ for initially straight fibers, we evaluate

$$
\begin{aligned}
&Div(C_1 \nabla \dot{\mathbf{g}}^1 (\mathbf{L} \otimes \mathbf{L}) + C_2 \nabla \dot{\mathbf{g}}^2 (\mathbf{M} \otimes \mathbf{M})) \\
&= C_1 Div[u_{i,ABCD} L_A L_B L_C L_D (\mathbf{e}_i \otimes \mathbf{E}_D)] + C_2 Div[u_{i,ABCD} M_A M_B M_C M_D (\mathbf{e}_i \otimes \mathbf{E}_D)] \\
&= C_1 u_{i,ABCD} L_A L_B L_C L_D \mathbf{e}_i + C_2 u_{i,ABCD} M_A M_B M_C M_D \mathbf{e}_i,
\end{aligned}
$$

(4.59)

$$\dot{\mathbf{F}} = \nabla \mathbf{u}$$

Consequently, from Eqs. (4.55-4.59), the linearized Euler equation can be derived as

$$\mu u_{i,AA} - \dot{p}_{,i} - C_1 u_{i,ABCD} L_A L_B L_C L_D - C_2 u_{i,ABCD} M_A M_B M_C M_D = 0, \quad (4.60)$$

Also, in view of Eqs. (4.48-4.49) and (4.51), the condition of bulk incompressibility reduces to

$$\dot{(J-1)} = \mathbf{F}_o^* \cdot \dot{\mathbf{F}} = \operatorname{div} \mathbf{u} = \mathbf{0}. \quad (4.61)$$

In the case of an orthonormal family of fibers (i.e. $\mathbf{L} = \mathbf{E}_1, \ L_1 = 1, \ L_2 = 0, \ \mathbf{M} = \mathbf{E}_2, \ M_1 = 0, \ M_2 = 1$), Eq. (4.60) becomes

$$\dot{p}_{,i} = \mu u_{i,AA} - C_1 u_{i,1111} - C_2 u_{i,2222} \text{ for } i, A = 1, 2 \quad (4.62)$$

which, together with Eq. (4.61), serves as a compatible linear model of Eq. (4.26) for small deformations superposed on large. Finally, the boundary conditions in Eq. (4.44) can be linearized similarly as in the above ($\mathbf{t} = \mathbf{t}_o + \varepsilon \dot{\mathbf{t}} + o(e)$)

$$
\begin{aligned}
\dot{\mathbf{t}} &= \dot{\mathbf{P}}\mathbf{N} - \frac{d}{dS}\left[C_1 \dot{\mathbf{g}}^1 (\mathbf{L} \cdot \mathbf{T})(\mathbf{L} \cdot \mathbf{N}) + C_2 \dot{\mathbf{g}}^2 (\mathbf{M} \cdot \mathbf{T})(\mathbf{M} \cdot \mathbf{N}) \right], \\
\dot{\mathbf{m}} &= C_1 \dot{\mathbf{g}}^1 (\mathbf{L} \cdot \mathbf{N})^2 + C_2 \dot{\mathbf{g}}^2 (\mathbf{M} \cdot \mathbf{N})^2, \\
\dot{\mathbf{f}} &= C_1 \mathbf{g}^1 (\mathbf{L} \cdot \mathbf{T})(\mathbf{L} \cdot \mathbf{N}) + C_2 \dot{\mathbf{g}}^2 (\mathbf{M} \cdot \mathbf{T})(\mathbf{M} \cdot \mathbf{N}).
\end{aligned} \quad (4.63)
$$

In particular, if the fiber's directions are either normal or tangential to the boundary (i.e. $(\mathbf{L} \cdot \mathbf{T})(\mathbf{L} \cdot \mathbf{N}) = 0$ and $(\mathbf{M} \cdot \mathbf{T})(\mathbf{M} \cdot \mathbf{N}) = 0$), Eq. (4.63) reduces to

$$
\begin{aligned}
\dot{t}_i &= \dot{P}_{iA} N_A, \\
\dot{m}_i &= C_1 \dot{g}_i^1 L_A N_A L_B N_B + C_2 \dot{g}_i^2 M_A N_A M_B N_B, \\
\dot{f}_i &= 0,
\end{aligned} \quad (4.64)
$$

where

$$
\begin{aligned}
\dot{P}_{iA} &= \mu u_{i,A} - \dot{p}(F_{iA}^*)_o - p_o \dot{F}_{iA}^* - C_1 g_{i,B}^1 L_A L_B - C_2 g_{i,B}^2 M_A M_B, \\
\dot{g}_i^1 &= u_{i,AB} L_A L_B, \ \dot{g}_i^2 = F_{iA,B} M_A M_B,
\end{aligned}
\tag{4.65}
$$

and

$$
\begin{aligned}
(F_{iA}^*)_o &= \delta_{iA}, \tag{4.66} \\
(F_{iA})_o &= \delta_{iA} \ \text{ at } \varepsilon = 0.
\end{aligned}
$$

Further, since $J \partial F_{jB}^* / \partial F_{iA} = F_{jB}^* F_{iA}^* - F_{iB}^* F_{jA}^*$ at $\mathbf{F}_o = \mathbf{I}$, we obtain

$$
\begin{aligned}
(\partial F_{jB}^* / \partial F_{iA})_o &= \delta_{jB}\delta_{iA} - \delta_{iB}\delta_{jA} \tag{4.67} \\
(\mathbf{F}_{\mathbf{F}}^*[\dot{\mathbf{F}}])_{jB} &= (\delta_{jB}\delta_{iA} - \delta_{iB}\delta_{jA})u_{i,A}
\end{aligned}
$$

Thus

$$
\dot{F}_{iA}^* = (Div\mathbf{u})\delta_{iA} - u_{A,i} = -u_{A,i}, \tag{4.68}
$$

where $Div\mathbf{u} = \text{div } \mathbf{u} = 0$ from the Linearized incompressibility condition. We note that, in the superposed incremental deformations, there is no clear distinction between current and deformed configuration.

4.5.1   Solution to the linearized problem

We introduce scalar field ϕ as

$$
\mathbf{u} = \mathbf{k} \times \nabla\phi, \ \mathbf{k}(\text{unit normal}); \ u_i = \varepsilon_{\lambda i}\phi_{,\lambda}, \tag{4.69}
$$

so that Eq. (4.61) can be automatically satisfied. Thus, the linearized Euler equation Eq. (4.62) can be rewritten as

$$\dot{p}_{,i} = \mu \varepsilon_{\lambda i}(\phi_{,\lambda 11} + \phi_{,\lambda 22}) - C_1 \varepsilon_{\lambda i} \phi_{,\lambda 1111} - C_2 \varepsilon_{\lambda i} \phi_{,\lambda 2222}. \qquad (4.70)$$

By utilizing the compatibility condition of $\dot{p}_{,i}$ (i.e. $\dot{p}_{,ij} = \dot{p}_{,ji}$), we obtain the following partial differential equation solving for ϕ.

$$(\phi_{,1111} + 2\phi_{,1122} + \phi_{,2222}) - \frac{C_1}{\mu}(\phi_{,11} + \phi_{,22})_{,1111} - \frac{C_2}{\mu}(\phi_{,11} + \phi_{,22})_{,2222} = 0. \quad (4.71)$$

It is worth mentioning here that the solution of Eq. (4.71) is not accommodated by the conventional methods such as the Fourier transform and the separation of variables. Instead, we adopt the methods of iterative reduction and principle of eigenfunction expansion, and obtain the potential function for $\phi(x, y)$. The details which can be found in [85]-[87] are intentionally omitted for the sake of conciseness. The analytical solution ϕ is then converted through mapping $\boldsymbol{\chi} = (X_1 - \phi_{,2})\mathbf{e}_1 + (X_2 + \phi_{,1})\mathbf{e}_2$ to obtain the complete deformed configurations

(Figs. [4.9](#)-7). Accordingly, the general solution of Eq. ([4.71](#)) can be found as

$$
\begin{aligned}
\phi = \sum_{m=1}^{\infty} & \{ e^{\frac{\sqrt{2m\sqrt{\alpha_1}+1}}{2\sqrt{\alpha_1}}x} \left(A_m\cos(\frac{\sqrt{2m\sqrt{\alpha_1}-1}}{2\sqrt{\alpha_1}}x) + B_m\sin(\frac{\sqrt{2m\sqrt{\alpha_1}-1}}{2\sqrt{\alpha_1}}x) \right) \\
& e^{-\frac{\sqrt{2m\sqrt{\alpha_1}+1}}{2\sqrt{\alpha_1}}x} \left(C_m\cos(\frac{\sqrt{2m\sqrt{\alpha_1}-1}}{2\sqrt{\alpha_1}}x) + D_m\sin(\frac{\sqrt{2m\sqrt{\alpha_1}-1}}{2\sqrt{\alpha_1}}x) \right) \} \times \\
& \{ E_m\cosh(\frac{\sqrt{1+\sqrt{4\alpha_2 m^2+1}}}{\sqrt{2\alpha_2}}y) + F_m\sinh(\frac{\sqrt{1+\sqrt{4\alpha_2 m^2+1}}}{\sqrt{2\alpha_2}}y) + \\
& G_m\cos(\frac{\sqrt{\sqrt{4\alpha_2 m^2+1}-1}}{\sqrt{2\alpha_2}}y) + H_m\sin(\frac{\sqrt{\sqrt{4\alpha_2 m^2+1}-1}}{\sqrt{2\alpha_2}}y) \} \\
+ \sum_{n=1}^{\infty} & \{ e^{\frac{\sqrt{2n\sqrt{\alpha_2}+1}}{2\sqrt{\alpha_2}}x} \left(A_n\cos(\frac{\sqrt{2n\sqrt{\alpha_2}-1}}{2\sqrt{\alpha_2}}y) + B_n\sin(\frac{\sqrt{2n\sqrt{\alpha_2}-1}}{2\sqrt{\alpha_2}}y) \right) \\
& e^{-\frac{\sqrt{2n\sqrt{\alpha_2}+1}}{2\sqrt{\alpha_2}}x} \left(C_n\cos(\frac{\sqrt{2n\sqrt{\alpha_2}-1}}{2\sqrt{\alpha_2}}y) + D_n\sin(\frac{\sqrt{2n\sqrt{\alpha_2}-1}}{2\sqrt{\alpha_2}}y) \right) \} \times \\
& \{ E_n\cosh(\frac{\sqrt{1+\sqrt{4\alpha_1 n^2+1}}}{\sqrt{2\alpha_1}}x) + F_n\sinh(\frac{\sqrt{1+\sqrt{4\alpha_1 n^2+1}}}{\sqrt{2\alpha_1}}x) + \\
& G_n\cos(\frac{\sqrt{\sqrt{4\alpha_1 n^2+1}-1}}{\sqrt{2\alpha_1}}x) + H_n\sin(\frac{\sqrt{\sqrt{4\alpha_1 n^2+1}-1}}{\sqrt{2\alpha_1}}x) \},
\end{aligned} \tag{4.72}
$$

where $\alpha_1 = C_1/\mu$ and $\alpha_2 = C_2/\mu$. The unknown constant real numbers A_m, $B_m, C_m, D_m, E_m, F_m, G_m, H_m, A_n, B_n, C_n, D_n, E_n, F_n, G_n$ and H_n can be completely determined by imposing admissible boundary conditions as depicted in Eqs. ([4.63](#)-[4.68](#)). The corresponding stress fields can also be obtained through Eqs. ([4.65](#)) and ([4.69](#)-[4.70](#)). For example, in the case of symmetric bending (see Fig. [4.6](#).), where

$$
\mathbf{\dot{m}} = \dot{m}_1\mathbf{e}_1 + \dot{m}_2\mathbf{e}_2, \ \dot{m}_1 = C_1 u_{1,11} = -\phi_{,211} = 5 \approx \sum_{n=1}^{30} \frac{20}{\pi n}(-1)^{\frac{n-1}{2}}\cos(\frac{\pi n}{2d})y\mathbf{e}_m,
$$

$$
\dot{m}_2 = 0. \tag{4.73}
$$

and for top and bottom surfaces, we impose

$$\dot{\mathbf{m}} = \dot{m}_1\mathbf{e}_1 + \dot{m}_2\mathbf{e}_2, \ \dot{m}_2 = C_2 u_{2,22} = \phi_{,122} = 0.001 = \sum_{m=1}^{30} \frac{0.004}{\pi m}(-1)^{\frac{m-1}{2}} \cos(\frac{\pi m}{2c})x,$$

$$\dot{m}_1 = 0. \tag{4.74}$$

4.6 Linearized Problem Result

The applied moment is approximated using Fourier series (see Eq. (4.73-4.74)) indicating fast convergence and the corresponding results are summarized through Figs. 4.9-7. Despite the inherent complexities of the present PDE (e.g. non-smooth/singular behavior of the potential as approaching a boundary, discontinuities on the corner vertices), the solution is smooth and stable throughout the entire domain of interest and displays good agreement with both the experiments [84] and the corresponding numerical results for a "*small*" deformation regime (Figs. 4.9-7 and 4.11-4.15).
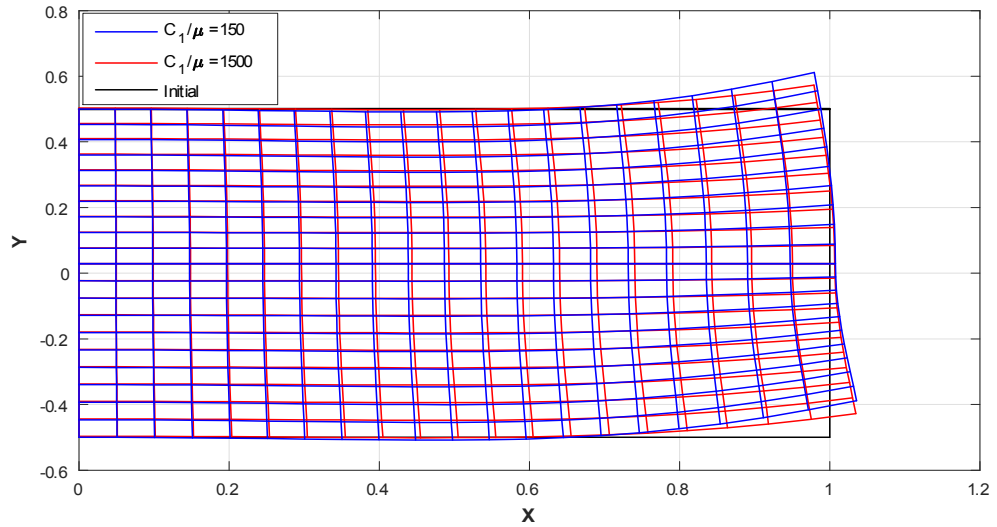
Figure 4.9: Deformed configurations with respect to C_1/μ when $M/\mu = 50$ and $C_2/\mu = 100$.
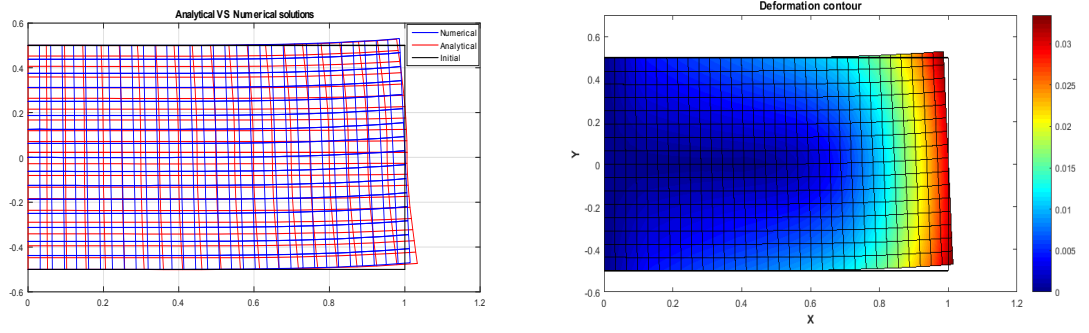
Figure 4.10: Deformed configurations when $\dfrac{C_1}{\mu} = 150, \dfrac{C_2}{\mu} = 100, \dfrac{M}{\mu} = 10$.
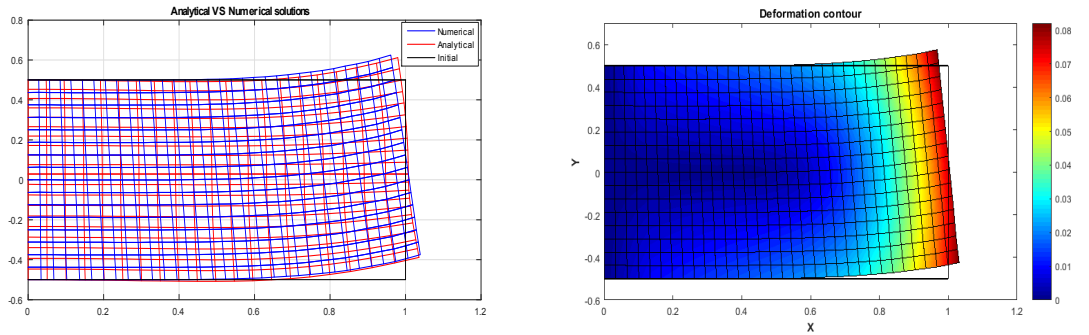
Figure 4.11: Deformed configurations when $\dfrac{C_1}{\mu} = 150, \dfrac{C_2}{\mu} = 100, \dfrac{M}{\mu} = 30$
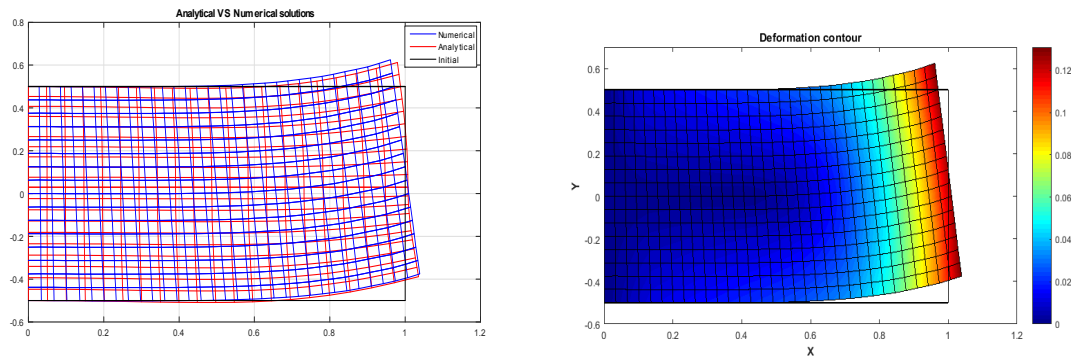
Figure 4.12: Deformed configurations when $\dfrac{C_1}{\mu} = 150, \dfrac{C_2}{\mu} = 100, \dfrac{M}{\mu} = 50$.

4.7 Model verification and validation via experimental results

A comparison with experimental results is performed in this section to determine the accuracy and utility of the proposed model. Two sets of experiments are considered for the purpose; one from the inhouse experimental setting and the other from the work of [84].

4.7.1 3 points bending test: CNC fiber composite

In the experiment, a composite reinforced with CNC fibers ($C_1 = 150 GPa$, $\mu = 1 GPa$) is placed on 3 point bending (at $-10mm, 0$, and $10mm$) and the out of plane direction (x_3) is aligned with the loading cylinder (Fig. 4.10). The applied loads and resulting displacements are simultaneously recorded via the MTS road cell and data logger. This setting is a special case of the proposed model when $c \gg d$ and $C_1/\mu = 150$ with vanishing C_2/μ (Fig. 4.6). The obtained solution successfully predicts the normal deflections of the CNC composite strip with a configuration factor $= 0.526[L]^2$ between the applied load and input stress on each simulation ($\sigma_{input} \times = Load_{applied}$; Table 4.1). Detailed discussions regarding the second-gradient theory and it's applications in the relevant experiments can be found in [93]-[95]. In addition, using a commercial image processing tool, the experimental deformed profiles are also obtained (maximum deflections at $2.55mm$ and $3mm$) and compared with the theoretical predictions. The resulting deformation profiles from both the experiments and theoretical simulations demonstrate a close correspondence throughout the domain of interest (Fig. 4.11).

4.7.2 Bending test of bidirectional fiber composites

With regard to the bending test of bidirectional fiber composite reinforced with E glass and T700S carbon fibers, we took the experimental results from the work
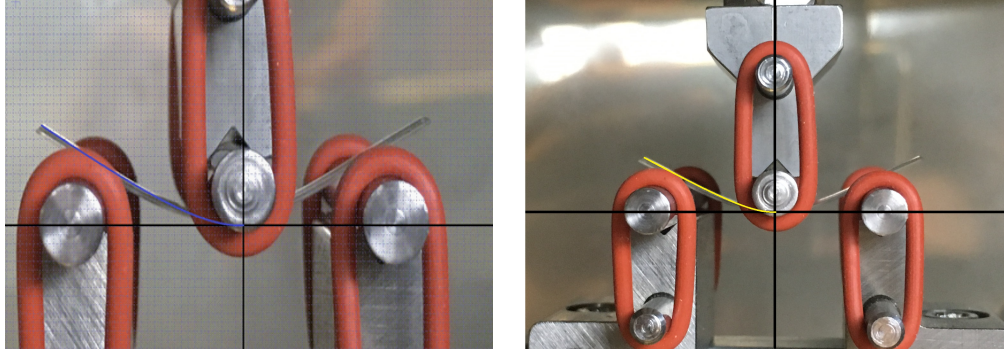
Figure 4.10: Experimental result and image processing (2.55mm 3mm): CNC fiber composite.(Dr. Ayranci and Ms. Garance)

Table 4.1: Maximum deflections: Experimental results VS Theoretical predictions

$\text{Load}_{applied}$ (N)	Experiment (mm)	Theory (mm)
0.1	0.349	0.339
0.2	0.682	0.667
0.3	1.001	1.001
0.4	1.329	1.335
0.5	1.659	1.669
0.6	2.002	2.003
0.7	2.380	2.336

of Dong and Davies ([84]; Fig. 4.7). Three experimental samples are considered: carbon-carbon fiber; carbon-glass fiber; and glass-glass fiber composites with fiber's volume fraction 37.2%, 32.9% and 30.9%, respectively. These fibers are mounted in the matrix material in the same manner as illustrated in Fig. 4.6. In each simulation, the material properties of carbon and glass fibers are accommodated by the parameters C_1 and C_2 (e.g. $C_1 = \text{carbon} = 4900MPa$, $C_2 = \text{glass} = 2240MPa$ for a carbon-glass fiber composite). The carbon-class fiber composite case with volume fraction 32.9% is used for benchmarking data in the identification of the configuration factor = 0.936 (Fig. 4.12). The factor is then uniformly applied for the other simulations, with the effects of different fibers' volume fractions taken into account. It is clear from Figs. 4.12-4.13 that predictions from both the nonlinear and linear theory demonstrate a close agreement with the experimental data. In addition, the proposed model assimilates the results presented in [77] which demonstrates good agreement up to linear regime (Fig. 4.14). These, in turn,
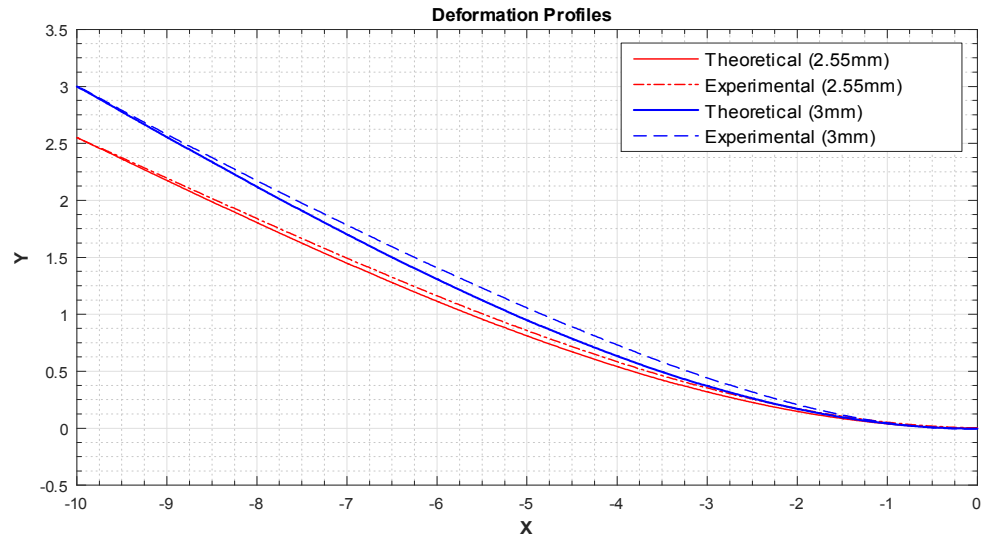
Figure 4.11: Deformation profiles: Theoretical predictions VS Experimental results.

suggest that the second-gradient of the deformations, incorporated in the present model, accurately represents fiber's resistant to flexure. Overall, the proposed models perform well in the prediction of the mechanical behavior of fiber reinforced composites and therefore they can be easily adopted in field exercises. In particular, the one from the linear theory is more useful, as it provides an explicit form of solution rather than a discretized solution.
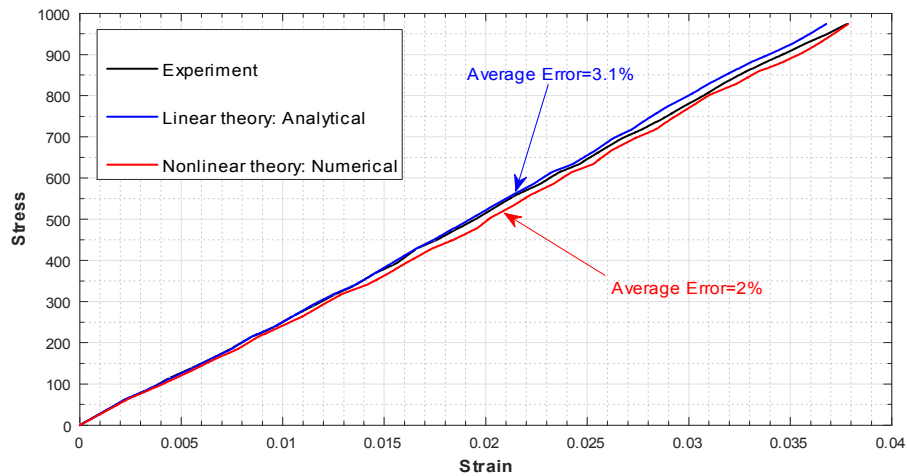
Figure 4.12: Strain-stress curve: Carbon-glass fiber composite
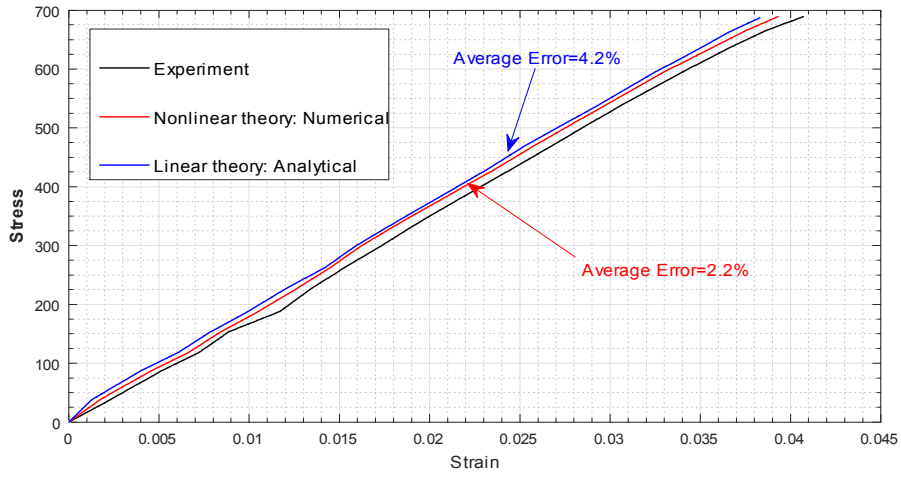
Figure 4.13: Strain-stress curve: Glass-glass fiber composite.
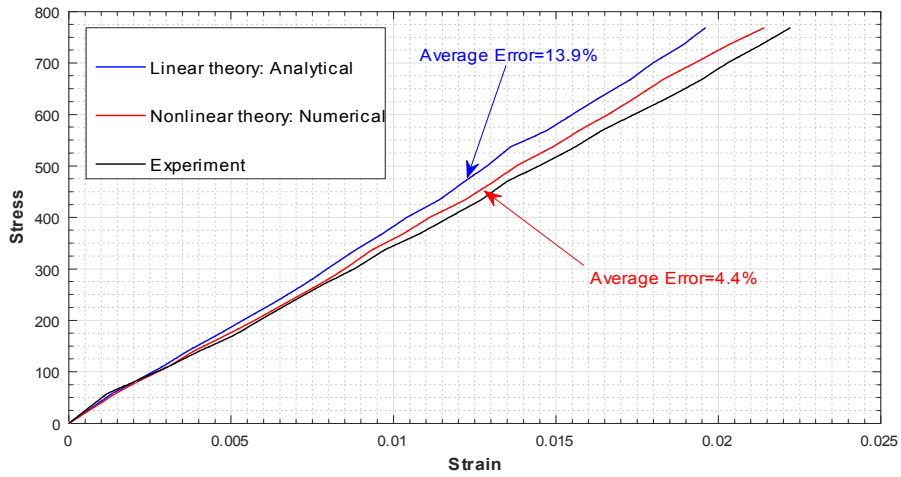
Figure 4.14: Strain-stress curve: Carbon-carbon fiber composite.
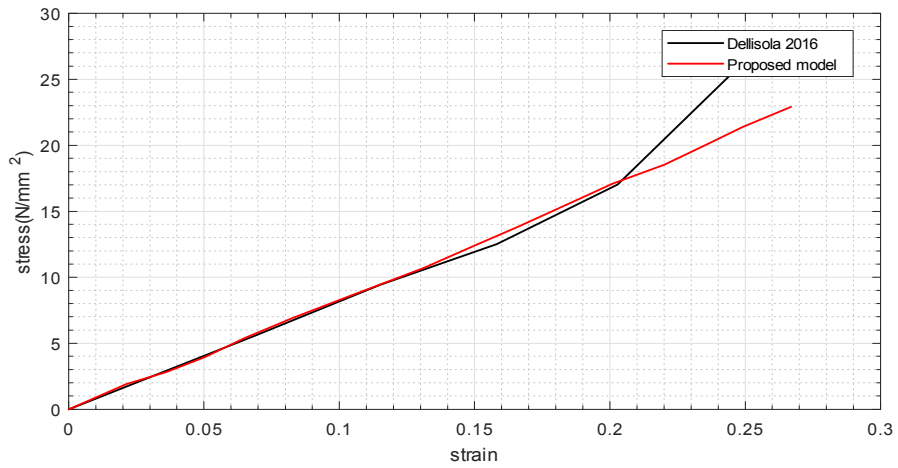
Figure 4.15: Strain-stress curve: Proposed model VS dell′Isola 2016

92

Chapter 5

Mechanics of bidirectional fiber-reinforced composite with fiber resistant to flexure & extension

We formulate the constitutive relations by applying the variational principle on the first and second gradient of deformations, respectively in sections 5.1 and 5.2. We then in section 5.2.1, consider a special case of a Neo-Hookian material reinforced with bidirectional fibers and successively derive systems of coupled Partial Differential Equations. In section 5.3, we present rigorous derivation of the necessary boundary conditions. The solutions of the resulting PDEs are obtained via the Finite Element Analysis in section 5.4, which demonstrate excellent correspondence with exiting theoretical and experimental results More importantly, the plane bias extension test and predicts smooth transitions of the corresponding shear strain fields as opposed to the first-gradient theory. In addition, we develop a compatible linear theory and analytical solution in sections 5.5 and 5.6.

5.1   Kinematics and Equilibrium equations

Let $\mathbf{L}$ and $\mathbf{M}$ are the unit tangent to the fiber's trajectory in the reference configuration and $\mathbf{l}$ and $\mathbf{m}$ are their counterparts in the deformed configuration. The

93

orientation of particular bidirectional fibers is then given by

$$\lambda = |\boldsymbol{\eta}| = \frac{ds}{dS}, \ \mu = |\boldsymbol{\tau}| = \frac{du}{dU} \text{ and } \mathbf{l} = \boldsymbol{\eta}\lambda^{-1}, \ \mathbf{m} = \boldsymbol{\tau}\mu^{-1}, \qquad (5.1)$$

where

$$\mathbf{FL} = \lambda\mathbf{l} \text{ and } \mathbf{FM} = \mu\mathbf{m}, \qquad (5.2)$$

and $\mathbf{F}$ is the gradient of the deformation function $(\boldsymbol{\chi}(\mathbf{X}))$. Eq.(5.2) can be derived by taking the derivative of $\mathbf{r}(s(S)) = \boldsymbol{\chi}(\mathbf{X}(S))$ with respect to arclength parameters S and ultimately s, upon making the identifications $\mathbf{L} = \frac{d\mathbf{X}}{dS}$ and $\mathbf{l} = \nabla\frac{d\boldsymbol{\chi}}{ds}$ and similarly for $\mathbf{M}$ ($\mathbf{M} = \frac{d\mathbf{X}}{dU}$ and $\mathbf{m} = \nabla\frac{d\boldsymbol{\chi}}{du}$). Here, $\frac{d(*)}{dS}, \frac{d(*)}{dU}$ and $\frac{d(*)}{ds}, \frac{d(*)}{du}$ refer to the arclength derivatives of $(*)$ along fibers' directions in the reference and deformed configurations, respectively. Without loss of generality, it is assumed that bidirectional fibers are initially orthonormal:

$$\mathbf{M} \cdot \mathbf{L} = \mathbf{0}. \qquad (5.3)$$

Combining Eqs. (5.2-5.3) furnishes a useful fiber decomposition of the deformation gradient that

$$\mathbf{F} = \lambda\mathbf{l} \otimes \mathbf{L} + \mu\mathbf{m} \otimes \mathbf{M}. \qquad (5.3\text{-}1)$$

Therefore, we have, for example, $\mathbf{L} = L_A\mathbf{E}_A$ and $\mathbf{l} = l_i\mathbf{e}_i$ to yield

$$\lambda l_i = F_{iA}L_A, \qquad (5.3\text{-}2)$$

where $\{\mathbf{E}_A\}$, $\{\mathbf{e}_i\}$ are orthonormal bases in the reference and deformed configurations.

The expressions for geodesic curvatures of a parametric curve $(\mathbf{r}(s, u))$ are

obtained from Eq. (5.2) that

$$\mathbf{g}_1 = \frac{d^2\mathbf{r}(S)}{dS^2} = \frac{d(\frac{\mathbf{r}(S)}{dS})}{dS} = \frac{\partial(\mathbf{FL})}{\partial\mathbf{X}}\frac{d\mathbf{X}}{dS} = \nabla[\mathbf{FL}]\mathbf{L}, \tag{5.4}$$

and

$$\mathbf{g}_2 = \frac{d^2\mathbf{r}(U)}{dU^2} = \frac{d(\frac{\mathbf{r}(U)}{dU})}{dU} = \frac{\partial(\mathbf{FM})}{\partial\mathbf{X}}\frac{d\mathbf{X}}{dU} = \nabla[\mathbf{FM}]\mathbf{M}. \tag{5.5}$$

In general, most of the fibers are straight prior to deformations. Even for slightly curved fibers, they can be idealized as 'fairly straight' fibers considering their length scales with respect to that of matrix materials. This suggests that the gradients of unit tangents in the reference configuration are identically vanishes (i.e. $\nabla\mathbf{L} = \nabla\mathbf{M} = \mathbf{0}$). Accordingly, Eqs. (5.4-5.5) becomes

$$\begin{aligned} \mathbf{g}_1 &= \nabla\mathbf{F}(\mathbf{L}\otimes\mathbf{L}) \\ \mathbf{g}_2 &= \nabla\mathbf{F}(\mathbf{M}\otimes\mathbf{M}) \end{aligned} \tag{5.6}$$

We introduce the convention of the second gradient of deformations as

$$\nabla\mathbf{F} \equiv \mathbf{G}, \tag{5.6-1}$$

where the compatibility condition of $\mathbf{G}$ is given by

$$G_{iAB} = F_{iA,B} = F_{iB,A} = G_{iBA}. \tag{5.7}$$

Thus

$$\begin{aligned} \mathbf{g}_1 &= \mathbf{G}(\mathbf{L}\otimes\mathbf{L}) = \mathbf{g}_1(\mathbf{G}) \\ \mathbf{g}_2 &= \mathbf{G}(\mathbf{M}\otimes\mathbf{M}) = \mathbf{g}_2(\mathbf{G}). \end{aligned} \tag{5.8}$$

In addition, Eqs. (5.1-5.2) furnish

$$\lambda^2 = \mathbf{FL} \cdot \mathbf{FL} = \mathbf{F}^T \mathbf{FL} \cdot \mathbf{L} = (\mathbf{F^T F}) \cdot \mathbf{L} \otimes \mathbf{L}, \tag{5.9}$$

and similarly for

$$\mu^2 = (\mathbf{F^T F}) \cdot \mathbf{M} \otimes \mathbf{M}. \tag{5.10}$$

The forgoing developments suggest that the mechanical responses of fibers-matrix systems can be described by the following energy function

$$\begin{aligned} W(\mathbf{F}, \mathbf{G}) &= \widehat{W}(\mathbf{F}) + W(\mathbf{G}), \\ W(\mathbf{G}) &\equiv \frac{1}{2} C_1(\mathbf{F}) |\mathbf{g}_1|^2 + \frac{1}{2} C_2(\mathbf{F}) |\mathbf{g}_2|^2, \end{aligned} \tag{5.11}$$

where $\mathbf{F}$ is the gradient of the deformation function $(\boldsymbol{\chi}(\mathbf{X}))$ and $\mathbf{G}$ is the gradient of $\mathbf{F}$ (i.e. $\mathbf{G} = \nabla \mathbf{F}$). $C_i(\mathbf{F})$ refers to the material property of fibers which, in general, independent of the deformation gradient (i.e. $C_i(\mathbf{F}) = C_i$). Eq. (5.11) presumes that fiber's bending energy is solely accounted by the second gradient of deformations as depicted in Eq. (5.8)). This concept has been widely and successfully adopted in relevant subjects ([8] and [47]).

Fibers' stretch can be computed as

$$\varepsilon_1 = \frac{1}{2} \left(\lambda^2 - 1 \right) = \frac{1}{2} [(\mathbf{F^T F}) \cdot \mathbf{L} \otimes \mathbf{L} - 1], \tag{5.12}$$

and

$$\varepsilon_2 = \frac{1}{2} \left(\mu^2 - 1 \right) = \frac{1}{2} [(\mathbf{F^T F}) \cdot \mathbf{M} \otimes \mathbf{M} - 1]. \tag{5.13}$$

Clearly, the stretches of fibers' are $\mathbf{F}$ dependent. Eqs. (5.12-5.13) lead to the expression of

$$\widehat{W}(\mathbf{F}) = W(I, \varepsilon_1, \varepsilon_2), \tag{5.14}$$

where $I = tr\mathbf{C}$ and $\mathbf{C} = \mathbf{F^T F}$ is the right Cauchy–Green deformation tensor which

is also dependent on $\mathbf{F}$. Consequently, the energy functional (5.11) can be written explicitly as

$$\widehat{W}(\mathbf{F})+W(\mathbf{G}) = W\left(I, \varepsilon_1, \varepsilon_2, \mathbf{g}_1, \mathbf{g}_2\right) = W\left(I, \varepsilon_1, \varepsilon_2\right)+\frac{1}{2}C_1 \left|\mathbf{g}_1\right|^2+\frac{1}{2}C_2 \left|\mathbf{g}_2\right|^2. \quad (5.15)$$

In order to compute variational derivatives of the response function, we use chain rule

$$\frac{\partial W}{\partial F_{iA}} \dot{F}_{iA} + \frac{\partial W}{\partial G_{iAB}} \dot{G}_{iAB} = \dot{W}, \qquad (5.16)$$

where the superposed dot refers to derivatives with respect to a parameter at a certain fixed value (e.g. $\varepsilon = 0$) that labels a one-parameter family of deformations. Accordingly, in view of equation (5.15), we obtain

$$\dot{W} = \dot{W}(I, \varepsilon_1, \varepsilon_2, \mathbf{g}_1, \mathbf{g}_2) = W_I \dot{I} + W_{\varepsilon_1}\dot{\varepsilon}_1 + W_{\varepsilon_2}\dot{\varepsilon}_2 + W_{\mathbf{g}_1} \cdot \dot{\mathbf{g}}_1 + W_{\mathbf{g}_2} \cdot \dot{\mathbf{g}}_2, \quad (5.17)$$

in which we have used the fact that W depends on the deformation through I, ε_1, ε_2, $\mathbf{g}_1$ and $\mathbf{g}_1$; ultimately $\mathbf{F}$ and $\mathbf{G}$. The required expressions can be equated in terms of $\mathbf{F}$ that

$$\dot{I} = [tr(\mathbf{C})]\dot{} = (\mathbf{I} \cdot \mathbf{C})\dot{} = \mathbf{I} \cdot \dot{\mathbf{C}} = 2\mathbf{F} \cdot \dot{\mathbf{F}}. \qquad (5.18)$$

Further, Eq. (5.9) yields

$$\dot{\varepsilon}_1 = \dot{\lambda}\lambda = \mathbf{FL} \cdot \dot{\mathbf{F}}\mathbf{L} = tr(\mathbf{FL} \otimes \dot{\mathbf{F}}\mathbf{L}) = tr((\mathbf{FL} \otimes \mathbf{L})\dot{\mathbf{F}}^T) = \mathbf{FL} \otimes \mathbf{L} \cdot \dot{\mathbf{F}}. \quad (5.19)$$

and similarly for

$$\dot{\varepsilon}_2 = \dot{\mu}\mu = \mathbf{FM} \otimes \mathbf{M} \cdot \dot{\mathbf{F}}. \qquad (5.20)$$

In particular, the variational computations with respect to the second gradient of deformations is equivalent to (see, Eq. 5.11_2)

$$\dot{W}(\mathbf{G}) = W_{\mathbf{G}} \cdot \dot{\mathbf{G}} = C_1\mathbf{g}_1 \cdot \dot{\mathbf{g}}_1 + C_2\mathbf{g}_2 \cdot \dot{\mathbf{g}}_2, \qquad (5.21)$$

where $\dot{\mathbf{g}}_1 = \dot{\mathbf{G}}(\mathbf{L} \otimes \mathbf{L})$ and $\dot{\mathbf{g}}_2 = \dot{\mathbf{G}}(\mathbf{M} \otimes \mathbf{M})$ in the case of initially straight fibers (i.e. $\dot{\mathbf{L}} = \dot{\mathbf{M}} = \mathbf{0}$). Therefore, by invoking the above

$$W_{\mathbf{G}} \cdot \dot{\mathbf{G}} = \dot{\mathbf{G}} \cdot (C_1 \mathbf{g}_1 \otimes \mathbf{L} \otimes \mathbf{L} + C_2 \mathbf{g}_2 \otimes \mathbf{M} \otimes \mathbf{M}). \tag{5.22}$$

Consequently, we derive that

$$\frac{\partial W}{\partial G_{iAB}} = C_1 (g_1)_i L_A L_B + C_2 (g_2)_i M_A M_B. \tag{5.23}$$

The constraint of bulk incompressibility can be accommodated by introducing the following form of an augmented energy potential;

$$U(I, \varepsilon_1, \varepsilon_2, \; \mathbf{g}_1, \; \mathbf{g}_2) = W(I, \varepsilon_1, \varepsilon_2, \mathbf{g}_1, \mathbf{g}_2) - p(J - 1). \tag{5.24a}$$

Since $\dot{J} = \frac{\partial J}{\partial \mathbf{F}} \cdot \dot{\mathbf{F}} = J\left(\mathbf{F}^{-1}\right)^T \cdot \dot{\mathbf{F}} = \mathbf{F}^* \cdot \dot{\mathbf{F}}$, Eqs. (5.18-5.20) and Eq. (5.24a) furnish

$$\dot{U} = 2W_I \mathbf{F} \cdot \dot{\mathbf{F}} + W_{\varepsilon_1} \mathbf{F} \mathbf{L} \otimes \mathbf{L} \cdot \dot{\mathbf{F}} + W_{\varepsilon_2} \mathbf{F} \mathbf{M} \otimes \mathbf{M} \cdot \dot{\mathbf{F}} - p \mathbf{F}^* \cdot \dot{\mathbf{F}} + C_1 \mathbf{g}_1 \cdot \dot{\mathbf{g}}_1 + C_2 \mathbf{g}_2 \cdot \dot{\mathbf{g}}_2. \tag{5.25a}$$

But from (5.21-5.22), the above reduces to

$$\dot{U} = (2W_I \mathbf{F} + W_{\varepsilon_1} \mathbf{F} \mathbf{L} \otimes \mathbf{L} + W_{\varepsilon_2} \mathbf{F} \mathbf{M} \otimes \mathbf{M} - p \mathbf{F}^*) \cdot \dot{\mathbf{F}} + W_{\mathbf{G}} \cdot \dot{\mathbf{G}}, \tag{5.26}$$

or in component form;

$$\dot{U} = (2W_I F_{iA} + W_{\varepsilon_1} F_{iB} L_A L_B + W_{\varepsilon_2} F_{iB} M_A M_B - p F_{iA}^*) \dot{F}_{iA} + \frac{\partial W}{\partial G_{iAB}} \dot{G}_{iAB}. \tag{5.26-1}$$

Eq. 5.26 reflects the fact that material response of the matrix material and stretch of fibers are computed via the first gradient $\mathbf{F}$, and bending resistant of fibers is accommodated by the second gradient $\mathbf{G}$ (see, also, [8]).

5.2 Equilibrium

The derivation of the Euler equation and boundary conditions arising in second-gradient elasticity is well studied [10]-[11] and [46]. We reformulate the results in the present context for the sake of clarity and completeness. The weak form of the equilibrium equations is given by the virtual-work statement

$$\dot{E} = P, \tag{5.27}$$

where P is the virtual power of the applied loads and the superposed dot refers to the variational and/or Gateâux derivative;

$$E = \int_\Omega U\left(\mathbf{F}, \mathbf{G}\right) dA \tag{5.28}$$

is the strain energy. In the above (Eq. 5.28), the conservative loads are characterized by the existence of a potential L such that $P = \dot{L}$. Therefore, the problem of determining equilibrium deformations is reduced, in the present case, to the problem of minimizing the potential energy $E - L$.

Accordingly, we have

$$\dot{E} = \int_\Omega \dot{U}\left(\mathbf{F}, \mathbf{G}\right) dA, \tag{5.29}$$

where the expression of $\dot{U}$ is given by (5.26). From Eq. (5.7), the energy variations with respect to the second gradient of deformations (i.e. $\dot{W}(\mathbf{G}) = W_\mathbf{G} \cdot \dot{\mathbf{G}}$), can be rewritten as

$$W_\mathbf{G} \cdot \dot{\mathbf{G}} = \frac{\partial W}{\partial G_{iAB}}\dot{G}_{iAB} = \frac{\partial W}{\partial G_{iAB}}\dot{F}_{iA,B} = \frac{\partial W}{\partial G_{iAB}}u_{i,AB}. \tag{5.30}$$

and

$$\frac{\partial W}{\partial G_{iAB}}u_{i,AB} = \left(\frac{\partial W}{\partial G_{iAB}}u_{i,A}\right)_{,B} - \left(\frac{\partial W}{\partial G_{iAB}}\right)_{,B}u_{i,A}, \tag{5.31}$$

where $u_i = \dot{\chi}_i$ is the variation of the position field. Substituting Eqs. (5.26, 5.31) into the above yields

$$
\begin{aligned}
\dot{E} &= \int_\Omega [(2W_I F_{iA} + W_{\varepsilon_1} F_{iB} L_A L_B + W_{\varepsilon_2} F_{iB} M_A M_B - p F_{iA}^*) u_{i,A} \\
&\quad + \left(\frac{\partial W}{\partial G_{iAB}} u_{i,A} \right)_{,B} - \left(\frac{\partial W}{\partial G_{iAB}} \right)_{,B} u_{i,A}] dA
\end{aligned}
\tag{5.32}
$$

Thus, we obtain

$$
\begin{aligned}
\dot{E} &= \int_\Omega [2W_I F_{iA} + W_{\varepsilon_1} F_{iB} L_A L_B + W_{\varepsilon_2} F_{iB} M_A M_B - p F_{iA}^* \\
&\quad - \left(\frac{\partial W}{\partial G_{iAB}} \right)_{,B}] u_{i,A} dA + \int_{\partial\Omega} \frac{\partial W}{\partial G_{iAB}} u_{i,A} N_B dS,
\end{aligned}
\tag{5.33}
$$

where $\mathbf{N}$ is the rightward unit normal to $\partial\Omega$ in the scence of Green-Stokes theorem. Also, for initially straight fibers (i.e. $\dot{\mathbf{L}} = \dot{\mathbf{M}} = \mathbf{0}$), $Div(W_{\mathbf{G}})$ reduces to

$$
\begin{aligned}
Div(W_{\mathbf{G}}) &= C_1(g_1)_{i,B} L_A L_B (\mathbf{e}_i \otimes \mathbf{E}_A) + C_2(g_2)_{i,B} M_A M_B (\mathbf{e}_i \otimes \mathbf{E}_A) \\
&= [C_1(g_1)_{i,B} L_A L_B + C_2 g_{i,B}^2 M_A M_B](\mathbf{e}_i \otimes \mathbf{E}_A), \\
\left(\frac{\partial W}{\partial G_{iAB}} \right)_{,B} &= C_1(g_1)_{i,B} L_A L_B + C_2 g_{i,B}^2 M_A M_B.
\end{aligned}
\tag{5.34}
$$

Consequently, Eq. 5.33 furnishes

$$
\dot{E} = \int_\Omega P_{iA} \dot{F}_{iA} dA + \int_{\partial\Omega} \frac{\partial W}{\partial G_{iAB}} \dot{F}_{iA} N_B dS,
\tag{5.35}
$$

where

$$
P_{iA} = 2W_I F_{iA} + W_{\varepsilon_1} F_{iB} L_A L_B + W_{\varepsilon_2} F_{iB} M_A M_B - p F_{iA}^* - C_1(g_1)_{i,B} L_A L_B - C_2(g_2)_{i,B} M_A M_B,
\tag{5.36}
$$

and hence the Euler equation is obtained by

$$P_{iA,A} = 0 \text{ or } Div(\mathbf{P}) = 0 \tag{5.37}$$

which holds in Ω.

5.2.1 Neo-Hookean type materials

In the case of incompressible neo-Hookean type materials, the energy density function is given by

$$W^1(I) = \mu(I - 3). \tag{5.38}$$

Further, in order to accommodate fiber's resistant to extension, we propose the following augmented energy potential of quadratic form;

$$W^2(\varepsilon_1, \varepsilon_2) = E_1 \frac{1}{2}\varepsilon_1^2 + E_2 \frac{1}{2}\varepsilon_2^2. \tag{5.38-1}$$

Combining Eqs. $(5.38_{1,2})$ yields

$$W(I, \varepsilon_1, \varepsilon_2) = W^1(I) + W^2(\varepsilon_1, \varepsilon_2) = \mu(I - 3) + E_1 \frac{1}{2}\varepsilon_1^2 + E_2 \frac{1}{2}\varepsilon_2^2. \tag{5.38-2}$$

We now substitute the above into Eq. (5.15) and thereby obtain

$$W\left(I, \varepsilon_1, \varepsilon_2, \mathbf{g}_1, \mathbf{g}_2\right) = W(I, \varepsilon_1, \varepsilon_2) + W(\mathbf{G}) = \mu I + \frac{1}{2}E_1\varepsilon_1^2 + \frac{1}{2}E_2\varepsilon_2^2 + \frac{1}{2}C_1\left|\mathbf{g}_1\right|^2 + \frac{1}{2}C_2\left|\mathbf{g}_2\right|^2, \tag{5.39}$$

where μ and C_i are the material constant of the matrix and fibers, respectively. Further, the required expressions are computed via Eqs. (5.12-5.13) and 5.38 that

$$W_I = \mu, W_{\varepsilon_1} = E_1\varepsilon_1 = \frac{1}{2}E_1\left(\mathbf{FL} \cdot \mathbf{FL} - 1\right) \tag{5.40}$$

$$W_{\varepsilon_2} = E_2\varepsilon_2 = \frac{1}{2}E_2\left(\mathbf{FM} \cdot \mathbf{FM} - 1\right).$$

Thus, Eqs. (5.38) becomes

$$
\begin{aligned}
P_{iA} &= 2\mu F_{iA} + \frac{E_1}{2}(F_{jC}F_{jD}L_CL_D - 1)F_{iB}L_AL_B + \frac{E_2}{2}(F_{jC}F_{jD}M_CM_D - 1)F_{iB}M_AM_B \\
&\quad -pF_{iA}^* - C_1(g_1)_{i,B}L_AL_B - C_2(g_2)_{i,B}M_AM_B,
\end{aligned}
\tag{5.41}
$$

and the corresponding Euler equation is evaluated as

$$
\begin{aligned}
P_{iA,A} &= 0 = 2\mu F_{iA,A} - pF_{iA}^* + \frac{E_1}{2}(F_{iB,A}F_{jC}F_{jD} + F_{iB}F_{jC,A}F_{jD} \\
&\quad + F_{iB}F_{jC}F_{jD,A})L_AL_BL_CL_D + \frac{E_2}{2}(F_{iB,A}F_{jC}F_{jD} + F_{iB}F_{jC,A}F_{jD} \\
&\quad + F_{iB}F_{jC}F_{jD,A})M_AM_BM_CM_D - \frac{E_1}{2}F_{iB,A}L_AL_B \\
&\quad - \frac{E_2}{2}F_{iB,A}M_AM_B - C_1(g_1)_{i,AB}L_AL_B - C_2(g_2)_{i,AB}M_AM_B,
\end{aligned}
\tag{5.42}
$$

where $F_{iA,A}^* = 0$ (Piola's identity).

Now consider a fiber-reinforced material which consists of initially orthonormal set of fibers,

$$
\begin{aligned}
\mathbf{L} &= \mathbf{E}_1, \ L_1 = 1, \ L_2 = 0, \\
\mathbf{M} &= \mathbf{E}_2, \ M_1 = 0, \ M_2 = 1,
\end{aligned}
\tag{5.43}
$$

and is subjected to finite plane deformations. Accordingly, Eq. (5.42) reduces to

$$
\begin{aligned}
P_{iA,A} &= 0 = 2\mu F_{iA,A} - pF_{iA}^* + \frac{E_1}{2}(F_{i1,1}F_{j1}F_{j1} + F_{i1}F_{j1,1}F_{j1} + F_{i1}F_{j1}F_{j1,1}) \\
&\quad + \frac{E_2}{2}(F_{i2,2}F_{j2}F_{j2} + F_{i2}F_{j2,2}F_{j2} + F_{i2}F_{j2}F_{j2,2}) \\
&\quad - \frac{E_1}{2}F_{i1,1} - \frac{E_2}{2}F_{i2,2} - C_1(g_1)_{i,11} - C_2(g_2)_{i,22},
\end{aligned}
\tag{5.44}
$$

where

$$(g_1)_i = F_{i1,1}, \ (g_2)_i = F_{i2,2}, \tag{5.45}$$

$$F_{iA} = \frac{\partial \chi_i}{\partial X_A} \text{ and } F_{iA}^* = \varepsilon_{ij} \varepsilon_{AB} F_{jB}.$$

In the above, ε_{ij} is the $2-$D permutation; $\varepsilon_{12} = -\varepsilon_{21} = 1, \varepsilon_{11} = -\varepsilon_{22} = 0$. Consequently, from Eq. (5.44-5.45) together with the constraint of the bulk incompressibility (det $\mathbf{F}$ =1), we derive the following coupled PDE system solving for χ_1, χ_2 and p.

$$
\begin{aligned}
0 &= 2\mu \left(\chi_{1,11} + \chi_{1,22} \right) - p_{,1} \chi_{2,2} + p_{,2} \chi_{2,1} - \frac{E_1}{2} \chi_{1,11} - \frac{E_2}{2} \chi_{1,22} \\
&\quad + \frac{E_1}{2} (3\chi_{1,11}\chi_{1,1}\chi_{1,1} + \chi_{1,11}\chi_{2,1}\chi_{2,1} + 2\chi_{2,11}\chi_{1,1}\chi_{2,1}) \\
&\quad + \frac{E_2}{2} (3\chi_{1,22}\chi_{1,2}\chi_{1,2} + \chi_{1,22}\chi_{2,2}\chi_{2,2} + 2\chi_{2,22}\chi_{1,2}\chi_{2,2}) - C_1\chi_{1,1111} - C_2\chi_{1,2222} \\
0 &= 2\mu \left(\chi_{2,11} + \chi_{2,22} \right) + p_{,1} \chi_{1,2} - p_{,2} \chi_{1,1} - \frac{E_1}{2} \chi_{2,11} - \frac{E_2}{2} \chi_{2,22} \\
&\quad + \frac{E_1}{2} (3\chi_{2,11}\chi_{2,1}\chi_{2,1} + \chi_{2,11}\chi_{1,1}\chi_{1,1} + 2\chi_{1,11}\chi_{1,1}\chi_{2,1}) \\
&\quad + \frac{E_2}{2} (3\chi_{2,22}\chi_{2,2}\chi_{2,2} + \chi_{2,22}\chi_{1,2}\chi_{1,2} + 2\chi_{1,22}\chi_{1,2}\chi_{2,2}) - C_1\chi_{2,1111} - C_2\chi_{2,2222} \\
1 &= \chi_{1,1}\chi_{2,2} - \chi_{1,2}\chi_{2,1}. \tag{5.46}
\end{aligned}
$$

5.3 Boundary conditions

Writing $P_{iA}u_{i,A} = (P_{iA}u_i)_{,A} - P_{iA,A}u_i$, we have from Eq. (5.35) that

$$\dot{E} = \int_{\partial\Omega} P_{iA}u_i N_A dS - \int_{\Omega} P_{iA,A}u_i dA + \int_{\partial\Omega} \left(\frac{\partial W}{\partial G_{iAB}} u_{i,A} \right) N_B dS, \tag{5.47}$$

where the Green-stoke's theorem is applied in the first term of Eq. (5.47). Since the Euler equation $P_{iA,A} = 0$ holds in Ω, the above reduces to

$$\dot{E} = \int_{\partial\Omega} P_{iA}u_i N_A dS + \int_{\partial\Omega} \left(\frac{\partial W}{\partial G_{iAB}} u_{i,A} \right) N_B dS. \qquad (5.48)$$

In addition, decomposing $\nabla \mathbf{u}$ in normal and tangential directions furnishes

$$\nabla\mathbf{u} = \nabla\mathbf{u}(\mathbf{T} \otimes \mathbf{T}) + \nabla\mathbf{u}(\mathbf{N} \otimes \mathbf{N}) = \mathbf{u}' \otimes \mathbf{T} + \mathbf{u}_{,\mathbf{N}} \otimes \mathbf{N}, \qquad (5.49)$$

where $\mathbf{T} = \mathbf{X}'(S) = \mathbf{k} \times \mathbf{N}$ is the unit tangent to $\partial\Omega$. $\mathbf{u}'$ and $\mathbf{u}_{,N}$ are the tangential and normal derivatives of $\mathbf{u}$ on $\partial\Omega$, respectively (i.e. $u_i' = u_{i,A}T_A$, $u_{i,N} = u_{i,A}N_A$). Hence Eq. (5.48) becomes

$$\dot{E} = \int_{\partial\Omega} P_{iA}u_i N_A dS + \int_{\partial\Omega} \frac{\partial W}{\partial G_{iAB}} \left(u_i' T_A N_B + u_{i,N} N_A N_B \right) dS. \qquad (5.50)$$

By decomposing the second term of Eq. (5.50) as in Eq. (5.48), we obtain

$$\frac{\partial W}{\partial G_{iAB}} T_A N_B u_i' = \left(\frac{\partial W}{\partial G_{iAB}} T_A N_B u_i \right)' - \left(\frac{\partial W}{\partial G_{iAB}} T_A N_B \right)' u_i, \qquad (5.51)$$

and therefore,

$$\begin{aligned}
\dot{E} &= \int_{\partial\Omega} [P_{iA}N_A - \left(\frac{\partial W}{\partial G_{iAB}} T_A N_B \right)'] u_i dS + \int_{\partial\Omega} \frac{\partial W}{\partial G_{iAB}} u_{i,N} N_A N_B dS \\
&\quad + \int_{\partial\Omega} \left(\frac{\partial W}{\partial G_{iAB}} T_A N_B u_i \right)' dS. \qquad (5.52)
\end{aligned}$$

In view of Eq. (5.22) (i.e. $\frac{\partial W}{\partial G_{iAB}} = C_1(g_1)_i L_A L_B + C_2(g_2)_i M_A M_B$), Eq. (5.52) can be rewritten as

$$
\begin{aligned}
\dot{E} &= \int_{\partial\Omega} [P_{iA}N_A - \left(C_1 g_i^1 L_A T_A L_B N_B + C_2 g_i^2 M_A T_A M_B N_B\right)']u_i dS \\
&+ \int_{\partial\Omega} (C_1(g_1)_i L_A N_A L_B N_B + C_2(g_2)_i M_A N_A M_B N_B)u_{i,N} dS \\
&- \sum \|(C_1(g_1)_i L_A T_A L_B N_B + C_2(g_2)_i M_A T_A M_B N_B)u_i\|,
\end{aligned}
\tag{5.53}
$$

where the double bar symbol refers to the jump across the discontinuities on the boundary $\partial\Omega$ (i.e. $\|*\| = (*)^+ - (*)^-$) and the sum refers to the collection of all discontinuities. It is concluded from (5.27) that admissible powers are of the from

$$
P = \int_{\partial w_t} t_i u_i dS + \int_{\partial w} m_i u_{i,N} dS + \sum f_i u_i.
\tag{5.54}
$$

Therefore, by comparing (5.53) and (5.54), we obtain

$$
\begin{aligned}
t_i &= P_{iA}N_A - \frac{d}{dS}[C_1(g_1)_i L_A T_A L_B N_B + C_2(g_2)_i M_A T_A M_B N_B], \\
m_i &= C_1(g_1)_i L_A N_A L_B N_B + C_2(g_2)_i M_A N_A M_B N_B, \\
f_i &= C_1(g_1)_i L_A T_A L_B N_B + C_2(g_2)_i M_A T_A M_B N_B,
\end{aligned}
\tag{5.55}
$$

which are the expressions of edge tractions, edge moments and corner forces, respectively. For example, if the fiber's directions are either normal or tangential to the boundary (i.e. $(\mathbf{L} \cdot \mathbf{T})(\mathbf{L} \cdot \mathbf{N}) = 0$ and $(\mathbf{M} \cdot \mathbf{T})(\mathbf{M} \cdot \mathbf{N}) = 0$), (5.55) further reduces to

$$
\begin{aligned}
t_i &= P_{iA}N_A, \\
m_i &= C_1(g_1)_i L_A N_A L_B N_B + C_2(g_2)_i M_A N_A M_B N_B, \\
f_i &= 0,
\end{aligned}
\tag{5.56}
$$

where

$$
\begin{aligned}
P_{iA} &= 2W_I F_{iA} + W_{\varepsilon_1} F_{iB} L_A L_B + W_{\varepsilon_2} F_{iB} M_A M_B - p F_{iA}^* \\
&\quad - C_1 (g_1)_{i,B} L_A L_B - C_2 (g_2)_{i,B} M_A M_B, \\
(g_1)_i &= F_{iA,B} L_A L_B, \\
(g_2)_i &= F_{iA,B} M_A M_B.
\end{aligned}
\tag{5.57}
$$

Consequently, by imposing the admissible boundary conditions (Eq. 5.56), solutions of the PDE system (Eq. 5.46) can be obtained via commercial packages.

5.4 Finite element analysis of the 4th order coupled PDE

Details regarding Finite Element Analysis (FEA) formulations are presented in this section. It is not trivial to demonstrate numerical analysis procedures for coupled PDE systems, especially for those with high order terms, since the piece wise linear function adopted in FE analysis has limited differentiability up to second order.

For pre processing, Eq. (5.46) can be recast as

$$
\begin{aligned}
0 &= 2\mu\,(Q+H) - AS + BD - C_1 Q_{,11} - C_2 H_{,22} - \frac{E_1}{2}Q - \frac{E_2}{2}H \\
&\quad + \frac{E_1}{2}(3QC^2 + QD^2 + 2RCD) + \frac{E_2}{2}(3HG^2 + HS^2 + 2TGS), \\
0 &= 2\mu\,(R+T) + AG - BC - C_1 R_{,11} - C_2 T_{,22} - \frac{E_1}{2}R - \frac{E_2}{2}T \\
&\quad + \frac{E_1}{2}(3RD^2 + RC^2 + 2QDC) + \frac{E_2}{2}(3TS^2 + \chi_{2,22}G^2 + 2HSG), \\
0 &= C\chi_{2,2} - D\chi_{1,2} - 1,\ \ 0 = Q - \chi_{1,11},\ \ 0 = R - \chi_{2,11}, \\
0 &= C - \chi_{1,1},\ \ 0 = D - \chi_{2,1},\ \ 0 = T - \chi_{2,22}, \\
0 &= S - \chi_{2,2},\ \ 0 = G - \chi_{1,2},\ \ 0 = H - \chi_{1,22}, \\
0 &= A - \mu(\chi_{1,11} + \chi_{1,22}) - CR_{,11},\ \ 0 = B - \mu(\chi_{2,11} + \chi_{2,22}) - CQ_{,11}.
\end{aligned}
\tag{5.58}
$$

where $A = p_{,1}$, $B = p_{,2}$, $Q = \chi_{1,11}$, $R = \chi_{2,11}$, $T = \chi_{2,22}$, $H = \chi_{1,22}$, $C = \chi_{1,1}$, $D = \chi_{2,1}$, $S = \chi_{2,2}$ and $G = \chi_{1,2}$. The above non-linear terms can be treated as, for example:

$$
\begin{aligned}
-A\chi_{2,2} + B\chi_{2,1} &\implies -A_0\chi_{2,2} + B_0\chi_{2,1}, \\
A\chi_{1,2} - B\chi_{1,1} &\implies A_0\chi_{1,2} - B_0\chi_{1,1}, \\
C\chi_{2,2} - D\chi_{2,1} &\implies C_0\chi_{2,2} - D_0\chi_{2,1}, \\
3QCC + QDD + 2RCD &\implies 3QC_0^2 + QD_0^2 + 2RC_0D_0, \\
3RDD + RCC + 2QDC &\implies 3RD_0^2 + RC_0^2 + 2QD_0C_0, \\
3HGG + HSS + 2TGS &\implies 3HG_0^2 + HS_0^2 + 2TG_0S_0, \\
3TSS + TGG + 2HSG &\implies 3TS_0^2 + TG_0^2 + 2HS_0G_0.
\end{aligned}
\tag{5.59}
$$

where the values of A, B, C, D, Q, R, T, H, S and G continue to be refreshed based on their previous estimations A_o, B_o, C_0, D_0, Q_0, R_0, T_0, H_0, S_0, G_0) as

iteration progresses. Thus, the weak form of Eq. (5.58) is obtained by

$$
\begin{aligned}
0 &= \int_\Omega w_1 (2\mu\,(Q+H) - A_0 S + B_0 D - C_1 Q_{,11} - C_2 H_{,22} - \frac{E_1}{2}Q - \frac{E_2}{2}H \\
&\quad + \frac{E_1}{2}(3QC_0^2 + QD_0^2 + 2RC_0 D_0) + \frac{E_2}{2}(3HG_0^2 + HS_0^2 + 2TG_0 S_0))d\Omega, \\
0 &= \int_\Omega w_2 (2\mu\,(R+T) + A_0 G - B_0 C - C_1 R_{,11} - C_2 T_{,22} - \frac{E_1}{2}R - \frac{E_2}{2}T \\
&\quad + \frac{E_1}{2}(3RD_0^2 + RC_0^2 + 2QD_0 C_0) + \frac{E_2}{2}(3TS_0^2 + TG_0^2 + 2HS_0 G_0))d\Omega, \\
0 &= \int_\Omega w_3(C\chi_{2,2} - D\chi_{1,2} - 1)d\Omega, \ 0 = \int_\Omega w_4(Q - \chi_{1,11})d\Omega, \\
0 &= \int_\Omega w_5(R - \chi_{2,11})d\Omega, \ 0 = \int_\Omega w_6(C - \chi_{1,1})d\Omega, \\
0 &= \int_\Omega w_7(D - \chi_{2,1})d\Omega, \ 0 = \int_\Omega w_8(T - \chi_{2,22})d\Omega, \\
0 &= \int_\Omega w_9(S - \chi_{2,2})d\Omega, \ 0 = \int_\Omega w_{10}(G - \chi_{1,2})d\Omega, \\
0 &= \int_\Omega w_{11}(H - \chi_{1,22})d\Omega, \ 0 = \int_\Omega w_{12}(A - \mu(\chi_{1,11} + \chi_{1,22}) - CR_{,11})d\Omega, \\
0 &= \int_\Omega w_{13}(B - \mu(\chi_{2,11} + \chi_{2,22}) - CQ_{,11})d\Omega, \quad (5.60)
\end{aligned}
$$

where the unknowns (e. g. χ_1, χ_2, Q_1, R_1, A, B etc...) can be written in the form of Lagrangian polynomial such that $(*) = \sum_{j=1}^n [(*)_j \Psi_j(x,y)]$. The corresponding test function w is given by

$$
w = \sum_{i=1}^n w_i \Psi_i(x,y), \quad (5.61)
$$

where w_i is weight of the test function and $\Psi_i(x,y)$ are the shape functions that

$$
\begin{bmatrix}
1 & 5 & 9 & 13 \\
2 & 6 & 10 & 14 \\
3 & 7 & 11 & 15 \\
4 & 8 & 12 & 16
\end{bmatrix}
=
\begin{bmatrix}
f_1 \\
f_2 \\
f_3 \\
f_4
\end{bmatrix}
\begin{bmatrix} g_1 & g_2 & g_3 & g_4 \end{bmatrix}, \quad (5.62)
$$

where

$$
\begin{aligned}
f_1(x) &= \frac{\left(x - \frac{c}{3}\right)\left(x - \frac{2c}{3}\right)(x - c)}{\left(-\frac{c}{3}\right)\left(-\frac{2c}{3}\right)(-c)}, \quad f_2(x) = \frac{x\left(x - \frac{2c}{3}\right)(x - c)}{\left(\frac{c}{3}\right)\left(-\frac{c}{3}\right)\left(-\frac{2c}{3}\right)}, \\
f_3(x) &= \frac{x\left(x - \frac{c}{3}\right)(x - c)}{\left(\frac{2c}{3}\right)\left(\frac{c}{3}\right)\left(-\frac{c}{3}\right)}, \quad f_4(x) = \frac{x\left(x - \frac{c}{3}\right)\left(x - \frac{2c}{3}\right)}{\left(\frac{c}{3}\right)\left(\frac{2c}{3}\right)(c)} \\
g_1(y) &= \frac{\left(y - \frac{d}{3}\right)\left(y - \frac{2d}{3}\right)(y - d)}{\left(-\frac{d}{3}\right)\left(-\frac{2d}{3}\right)(-d)}, \quad g_2(y) = \frac{y\left(y - \frac{2d}{3}\right)(y - d)}{\left(\frac{d}{3}\right)\left(-\frac{d}{3}\right)\left(-\frac{2d}{3}\right)}, \\
g_3(y) &= \frac{y\left(y - \frac{d}{3}\right)(y - d)}{\left(\frac{2d}{3}\right)\left(\frac{d}{3}\right)\left(-\frac{d}{3}\right)}, \quad g_4(y) = \frac{y\left(y - \frac{d}{3}\right)\left(y - \frac{2d}{3}\right)}{\left(\frac{d}{3}\right)\left(\frac{2d}{3}\right)(d)}.
\end{aligned}
\tag{5.62-1}
$$

Using Lagrangian polynomial representation, the first of Eq. (5.60) can be rewritten as

$$
\begin{aligned}
0 &= \sum_{i,j=1}^{n} \left[\int_{\Omega}\left(2\mu\Psi_i\Psi_j + C_1\Psi_{i,1}\Psi_{j,1} - \frac{E_1}{2}\Psi_i\Psi_j\right)d\Omega\right]Q_j \\
&+ \sum_{i,j=1}^{n} \left[\int_{\Omega}\left(2\mu\Psi_i\Psi_j + C_2\Psi_{i,2}\Psi_{j,2} - \frac{E_2}{2}\Psi_i\Psi_j\right)d\Omega\right]H_j \\
&+ \sum_{i,j=1}^{n} \left[\int_{\Omega} A_0\Psi_i\Psi_j d\Omega\right]S_j - \sum_{i,j=1}^{n} \left[\int_{\Omega} B_0\Psi_i\Psi_j d\Omega\right]D_j \\
&+ \sum_{i,j=1}^{n} \left[\frac{E_1}{2}\int_{\Omega} 3\Psi_i\Psi_j C_0^2\}d\Omega\right]Q_j + \sum_{i,j=1}^{n} \left[\frac{E_1}{2}\int_{\Omega} \Psi_i\Psi_j D_0^2 d\Omega\right]Q_j \\
&+ \sum_{i,j=1}^{n} \left[\frac{E_1}{2}\int_{\Omega} 2\Psi_i\Psi_j C_0 D_0 d\Omega\right]R_j + \sum_{i,j=1}^{n} \left[\frac{E_2}{2}\int_{\Omega} 3\Psi_i\Psi_j S_0^2 d\Omega\right]H_j \\
&+ \sum_{i,j=1}^{n} \left[\frac{E_2}{2}\int_{\Omega} \Psi_i\Psi_j G_0^2 d\Omega\right]H_j + \sum_{i,j=1}^{n} \left[\frac{E_2}{2}\int_{\Omega} 2\Psi_i\Psi_j G_0 S_0 d\Omega\right]T_j \\
&- \int_{\partial\Gamma}(C_1\Psi_i Q_{,1} + C_2\Psi_i H_{,2})N d\Gamma,
\end{aligned}
\tag{5.63}
$$

and similarly for the rest of equations. In the above, Ω, $\partial\Gamma$ and $\mathbf{N}$ are the domain of interest, the associated boundary, and the rightward unit normal to the boundary $\partial\Gamma$ in the sense of the Green-stoke's theorem, respectively. Finally, we obtain the systems of equations $[\mathbb{K}][\mathbb{E}] = [\mathbb{F}]$. Here $[\mathbb{K}]$ and $[\mathbb{F}]$ are $[13{\times}12]$ and $[12{\times}1]$ matrices,

respectively and $[\mathbb{E}]$ is $[13 \times 1]$ matrix with unknowns (e. g. χ_1, χ_2, Q_1, R_1, A, B etc...). The expressions of $[K^{ij}]$ and $[F_i]$ can be obtained via the standard Finite Element Analysis procedures. For example,

$$\left[K^{11}\right] = \int_\Omega [2\mu\Psi_i\Psi_j + C_1\Psi_{i,1}\Psi_{j,1} - \frac{E_1}{2}\Psi_i\Psi_j + \frac{E_1}{2}(3\Psi_i\Psi_j C_0^2 + \Psi_i\Psi_j D_0^2)]d\Omega, \quad (5.63\text{-}1)$$

and

$$F_1 = -\int_{\partial\Gamma}(C_1\Psi_i Q_{,1} + C_2\Psi_i H_{,2})Nd\Gamma. \quad (5.63\text{-}2)$$
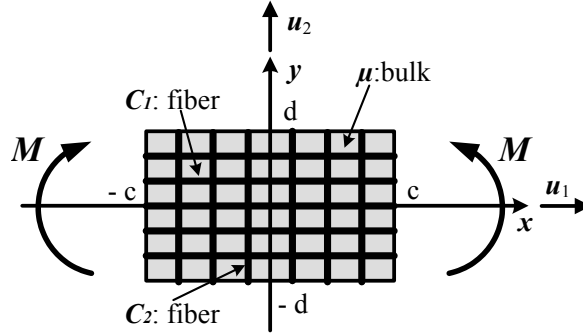
Schematic of problem for bidirectional fiber reinforced with Moment (M) boundary condition

Figs. 5.1~5.3 illustrate the fiber composite's deformation profiles under the axial tension. The expression of applied load tension is obtained from Eq. 5.41 that

$$P_{11} = 2\mu\chi_{1,1} + \frac{E_1}{2}(\chi_{1,1}\chi_{1,1} + \chi_{2,1}\chi_{2,1} - 1)\chi_{1,1} - p\chi_{2,2} - C_1\chi_{1,111}. \quad (5.64)$$

It is clear from Fig. 5.1 that the axial extension is sensitive to the fibers' elastic resistance in x direction (i.e. C_1, E_1). More precisely, the net amount of axial extension decreases with increasing values of C_1 and E_1. In particular, we simulate the plane bias extension test in order to examine the effects of second-gradients of deformations onto the shear responses of the bidirectional fiber composites. The corresponding shear strains are computed via the relation $\phi' = \frac{u_2''(1+u_1') - u_2'u_1''}{u_2'^2 + (1+u_1')^2}$,

where ϕ' is the rate of shear angle change. The results in Figs. 5.2-5.3 clearly indicate that the proposed model successfully predicts the smooth transitions of the shear strain fields unlike those described by the first-order theory where a significant discontinuity is in present (Fig. 5.4). The compatible results, in the case of meshed structures, can be found in the work of [17]-[19] which also demonstrate a close agreement with the presented results (See, for example, Fig. 14 in [19]). In the simulations, we consider the case where an elastic solid is reinforced with bidirectional fibers and subjected to finite plane deformations (either axial stretch or bending is considered) as illustrated in Fig. 5.60. In the assimilation of fiber
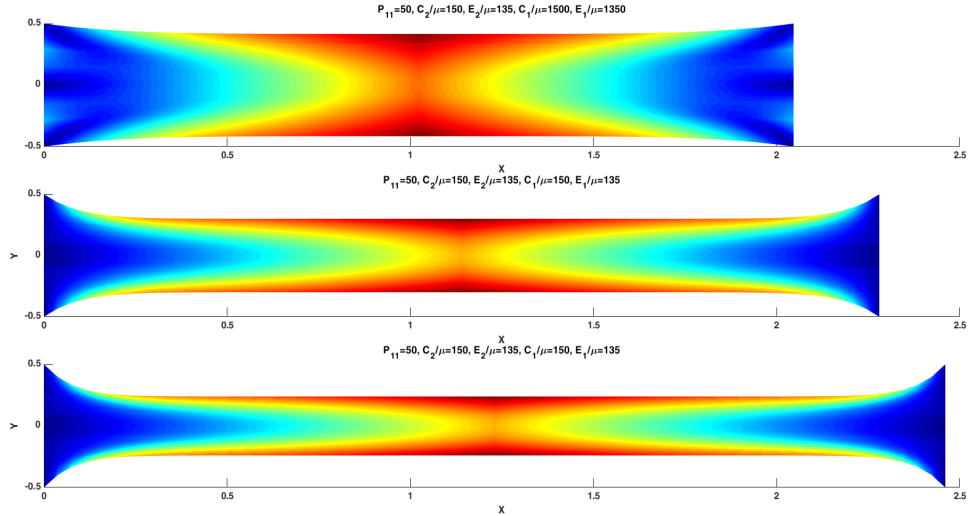
Figure 5.1: Deformation contour ($\sqrt{\chi_1^2 + \chi_2^2}$) with respect to C_1/μ, when $P_{11}/\mu = 50$, $C_2/\mu = 150$ and $E_2/\mu = 135$

composite subject to flexure, we consider a rectangular fiber composites where one end is fixed and the other end is subjected to constant bending in order to examine fibers' reinforcing effects against to flexure. The corresponding boundary conditions are imposed as; $\chi_{1,11} = -M/\mu$, $\chi_{2,11} = 0$, $\chi_2 = 0$ and $\chi_1 = 0$ at $x = 0$ and $\chi_{1,11} = -M/\mu$, $\chi_{2,11} = 0$, $\chi_{2,1} = 0$ and $\chi_{1,1} = 0$ at $x = c$. For the upper $(y = d)$ and bottom $(y = -d)$ faces, compatible boundary conditions are prescribed where we impose zero moment (i.e. $\chi_{2,22} = 0$ on the designated boundary). The resulting deformed profiles and contours demonstrate smooth
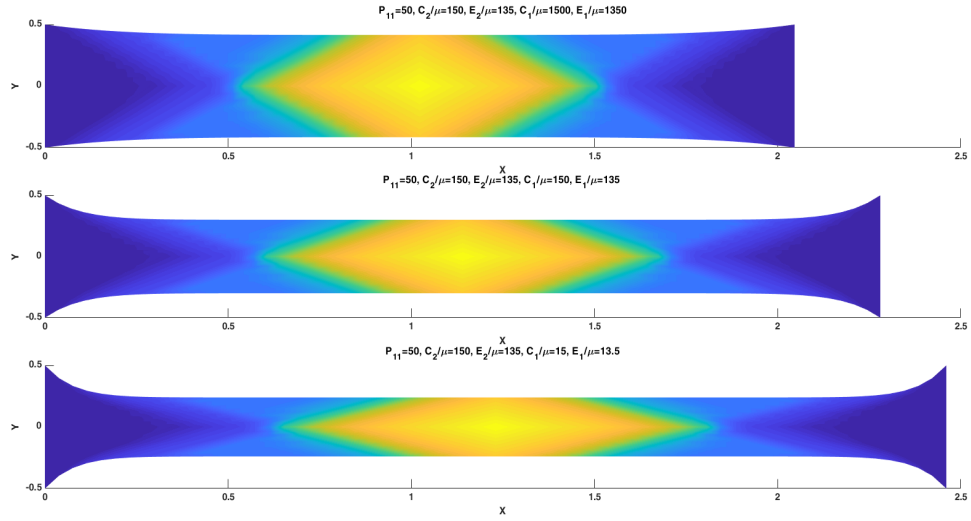
Figure 5.2: Shear strain contour with respect to C_1/μ. when $P_{11}/\mu = 50$, $C_2/\mu = 150$ and $E_2/\mu = 135$.
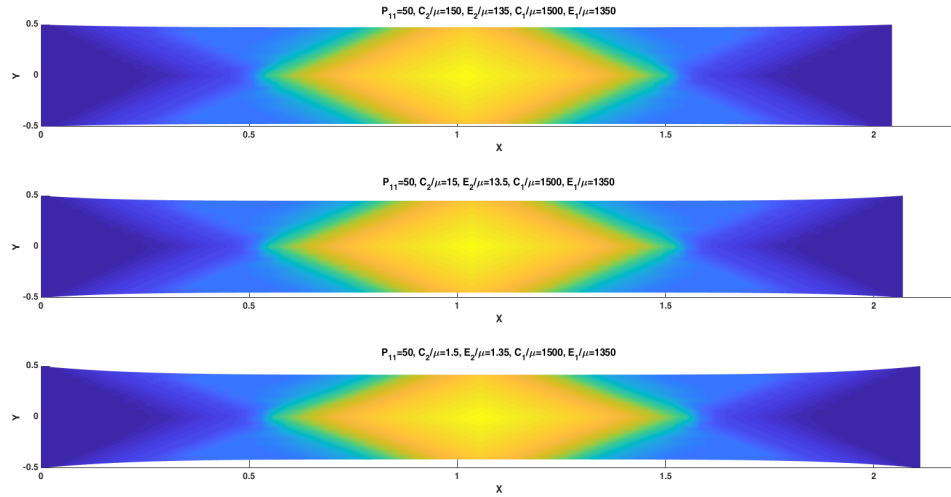
Figure 5.3: Shear strain contour with respect to C_2/μ. when $P_{11}/\mu = 50$, $C_1/\mu = 1500$ and $E_2/\mu = 1350$.

transitions as they approach to the boundary (see, Figs. 5.5). Further, Fig. 5.5 illustrates that the magnitude of deformation decreases as fiber's bending stiffness increases.

Comparisons with experimental results is also performed to determine the accuracy and utility of the proposed model. Three sets of experiments are considered for the purpose; two from inhouse setting and the other from the work of Dong. For
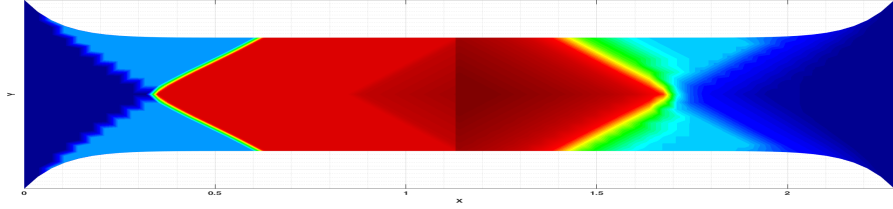
Figure 5.4: Shear strain contour: 1st gradient (left) VS 2rd gradient (right)
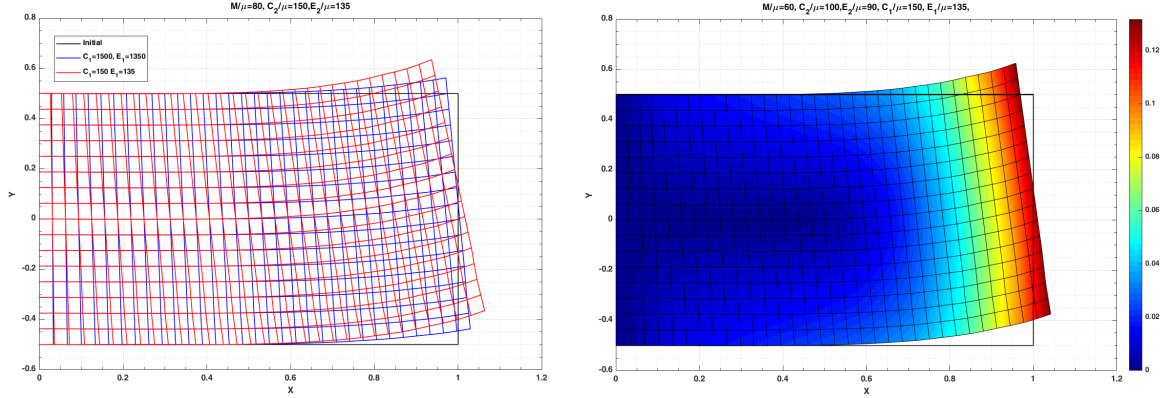
Figure 5.5: Deformed configurations with respect to C_1/μ when $M/\mu=80$ and deformation magnitude contour when $M/\mu=60$

inhouse experiments, we considered; 3 point bending test of a crystalline nanocellulose (CNC) fiber composite ($C_1 = 150GPa, E_1 = 135GPa, \mu = 1GPa$) and an impact bending test of a Nylon-6 Fiber Neoprene Rubber Composite ($C_1 = 2000Mpa$, $E_1 = 1300Mpa, \mu = 2Mpa$). In the tests, the out of plane direction (x_3) is aligned with the loading cylinder and/or line of impact (see, Fig. 5.6). These are special cases of the proposed model, when $c \gg d$ with vanishing C_2/μ and E_2/μ (see, Fig. 5.62-1). The solutions from our model successfully predict the deformations of both the CNC composites and the Nylon-6 Fiber Neoprene Rubber Composite with maximum error less than 3% (Fig. 5.7).

The above results, in turn, suggest that the proposed model accurately describes fiber's elastic resistant to flexures and extension through the first and second gradient of deformations. Lastly, we mention that the presented solution accommodate the results from [80] in the limited of vanishing fibers elastic resistance in y direction (i.e $C_2 = 0, \ E_2 = 0$) in the limit of vanishing material parameters.
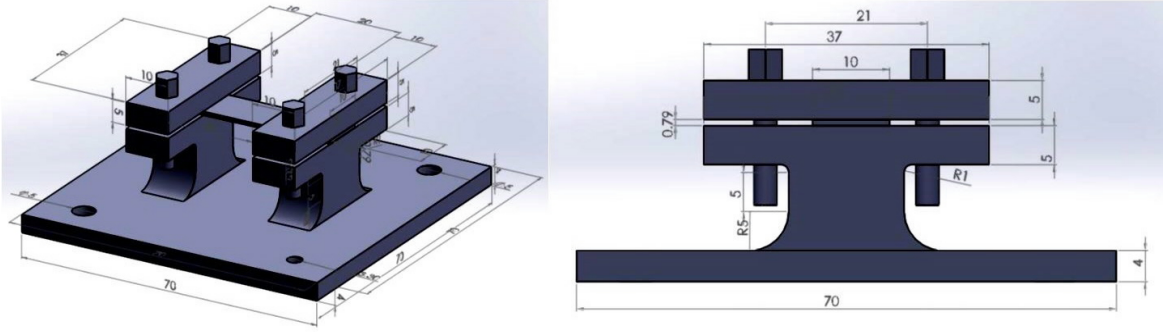
Figure 5.6: Experimental setting: Nylon−6 Fiber Neoprene Rubber Composite.
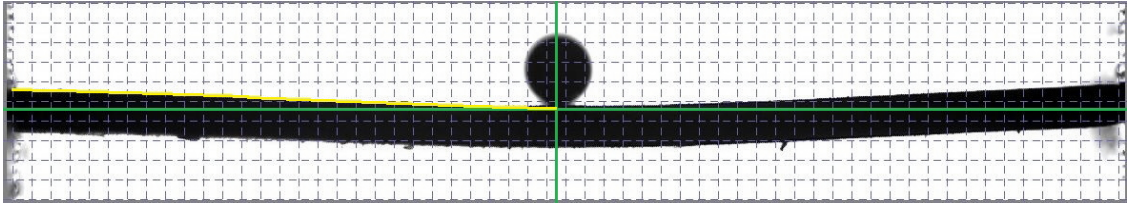
Figure 5.7: Deformation profiles: Experimental results

(See Fig. 5.9).

5.5   Linear Theory

We consider superposed "*small*" deformations described as

$$\boldsymbol{\chi} = \boldsymbol{\chi}_o + \epsilon \dot{\boldsymbol{\chi}} \; ; |\epsilon| \ll 1, \tag{5.65}$$

where $(*)_o$ denote configuration of $*$ evaluated at $\epsilon = 0$ and $(\dot{*}) = \partial(*)/\partial\varepsilon$. In particular, we denote $\dot{\boldsymbol{\chi}} = \mathbf{u}$ in forthcoming derivations where applicable. Here caution needs to be taken that the present notation is not confused with the one used for the variational computation. From Eq. (5.65), the deformation gradient tensor is given by

$$\mathbf{F} = \mathbf{F}_o + \epsilon \nabla \mathbf{u}, \text{ where } \dot{\mathbf{F}} = \nabla \mathbf{u}. \tag{5.66}$$
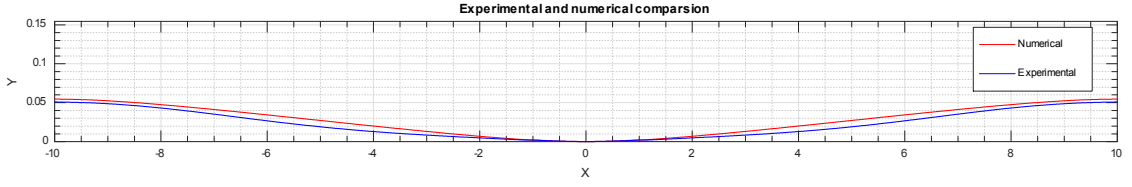
Figure 5.8: Deformation profiles: Theoretical results.
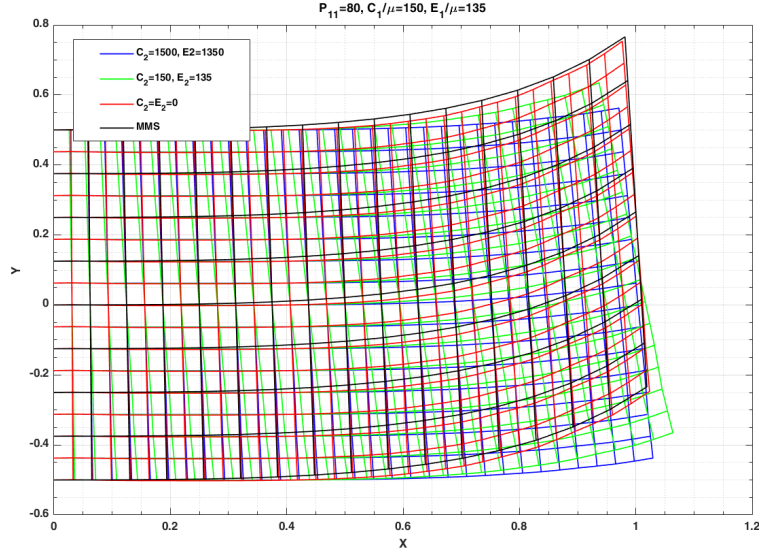
Figure 5.9: Deformation profiles: Proposed model VS Zeidi & Chunil. 2017

We assume that the body is initially undeformed and stress free (i.e. at $\varepsilon = 0$, $\mathbf{F}_o = \mathbf{I}$ and $\mathbf{P}_o = \mathbf{0}$). Hence, Eq. (5.66) becomes

$$\mathbf{F} = \mathbf{I} + \epsilon \nabla \mathbf{u}, \tag{5.67}$$

and successively obtain

$$\mathbf{F}^{-1} = \mathbf{I} - \epsilon \nabla \mathbf{u} + o(\epsilon) \text{ and } J = \det \mathbf{F} = 1 + \epsilon \operatorname{div} \mathbf{u} + o(\epsilon). \tag{5.68a}$$

Further, in view of Eq. (5.65), Eq. (5.37) can be approximated as

$$Div(\mathbf{P}) = Div(\mathbf{P}_o) + \epsilon Div(\dot{\mathbf{P}}) + o(\epsilon) = \mathbf{0}. \tag{5.69}$$

Dividing the above by ϵ and letting $\epsilon \to 0$, we obtain

$$Div(\dot{\mathbf{P}}) = 0 \text{ or } \dot{P}_{iA,A} = 0 \tag{5.70}$$

which serves as the compatible linearized Euler equation. Now, from Eq. (5.36), the induced variation of $\mathbf{P}$ with respect to ϵ can be evaluated as

$$
\begin{aligned}
\dot{P}_{iA} = {} & 2(W_{II}\dot{I} + W_{I\varepsilon_1}\dot{\varepsilon}_1 + W_{I\varepsilon_2}\dot{\varepsilon}_2)(F_{iA})_o + 2(W_I)_o\dot{F}_{iA} - \dot{p}(F^*_{iA})_o - p_o\dot{F}^*_{iA} \\
& + [(W_{I\varepsilon_1}\dot{I} + W_{\varepsilon_1\varepsilon_1}\dot{\varepsilon}_1 + W_{\varepsilon_1\varepsilon_2}\dot{\varepsilon}_2)(F_{iB})_o + (W_{\varepsilon_1})_o\dot{F}_{iB} - C_1(\dot{g}_1)_{i,B}]L_AL_B \\
& + [(W_{I\varepsilon_2}\dot{I} + W_{\varepsilon_1\varepsilon_2}\dot{\varepsilon}_1 + W_{\varepsilon_2\varepsilon_2}\dot{\varepsilon}_2)(F_{iB})_o + (W_{\varepsilon_2})_o\dot{F}_{iB} - C_2(\dot{g}_2)_{i,B}]M_AM_B \tag{5.71}
\end{aligned}
$$

In the case of Neo-Hookean material (Eq. (5.38)) (e.g. $W_{II} = 0$, $W_{I\varepsilon_1} = 0$, $W_{I\varepsilon_2} = 0$ etc...), the above reduces to

$$
\begin{aligned}
\dot{P}_{iA} = {} & 2\mu\dot{F}_{iA} - \dot{p}(F^*_{iA})_o - p_o\dot{F}^*_{iA} + [E_1\dot{\varepsilon}_1(F_{iB})_o + E_1(\varepsilon_1)_o\dot{F}_{iB} - C_1(\dot{g}_1)_{i,B}]L_AL_B \\
& + [E_2\dot{\varepsilon}_2(F_{iB})_o + E_2(\varepsilon_2)_o\dot{F}_{iB} - C_2(\dot{g}_2)_{i,B}]M_AM_B, \tag{5.72}
\end{aligned}
$$

Evaluating limits at $\epsilon = 0$, we have

$$
\begin{aligned}
\dot{P}_{iA} = {} & 2\mu\dot{F}_{iA} - \dot{p}\delta_{iA} - p_o\dot{F}^*_{iA} + [E_1\dot{\varepsilon}_1\delta_{iB} - C_1(\dot{g}_1)_{i,B}]L_AL_B \\
& + [E_2\dot{\varepsilon}_2\delta_{iB} - C_2(\dot{g}_2)_{i,B}]M_AM_B, \tag{5.73}
\end{aligned}
$$

where $p_o = 2\mu$ to recover the initial stress free state at $\epsilon = 0$ (i.e. $P_{iA} = 0$ at $\epsilon = 0$). In addition, we approximate the fiber's extensions as

$$\dot{\varepsilon}_1 = \mathbf{FL} \otimes \mathbf{L} \cdot \dot{\mathbf{F}} \simeq \mathbf{L} \otimes \mathbf{L} \cdot \dot{\mathbf{F}} = \dot{F}_{jC}L_jL_C, \tag{5.74}$$

and subsequently formulate

$$(2\mu\dot{F}_{iA}),_A = 2\mu\dot{F}_{iA,A}, \;\; (p_o\dot{F}^*_{iA}),_A = 0, \;\; (\dot{p}\delta_{iA}),_A = \dot{p}_{,i}$$

$$(E_1\dot{\varepsilon}_1\delta_{iB}L_AL_B),_A = (E_1\dot{\varepsilon}_1L_iL_B),_A = E_1\dot{F}_{jA,B}L_iL_jL_AL_B, \text{ and}$$

$$(C_1(\dot{g}_1)_{i,B}L_AL_B),_A = (C_1\dot{F}_{iC,BD}L_CL_DL_AL_B),_A = C_1\dot{F}_{iA,BCD}L_AL_BL_CL_D \quad (5.75)$$

Similar scheme can be applied for $\dot{\varepsilon}_2$ and $(\dot{g}_2)_i$. Therefore, from Eqs. (5.70 and 5.73-5.75), the Euler equation for small deformations is given by

$$\begin{aligned}
0 = \;& \dot{P}_{iA,A} = 2\mu\dot{F}_{iA,A} - \dot{p}_{,i} + E_1\dot{F}_{jA,B}L_iL_jL_AL_B - C_1\dot{F}_{iA,BCD}L_AL_BL_CL_D \\
& + E_2\dot{F}_{jA,B}M_iM_jM_AM_B - C_2\dot{F}_{iA,BCD}M_AM_BM_CM_D, \quad (5.76)
\end{aligned}$$

where, we make use of the identities $Div(\dot{*}) = \dot{Div(*)}$, $(p_o),_A = 0$ and $(\dot{g}_1)_{i,B} = (\dot{F}_{iC,D}L_CL_D),_B = \dot{F}_{iC,BD}L_CL_D$. Alternatively, from Eq. (5.68a), the above can be rewritten as

$$\begin{aligned}
\dot{p}_{,i} = \;& 2\mu u_{i,AA} + E_1 u_{j,AB}L_iL_jL_AL_B - C_1 u_{i,ABCD}L_AL_BL_CL_D \\
& + E_2 u_{j,AB}M_iM_jM_AM_B - C_2 u_{i,ABCD}M_AM_BM_CM_D. \quad (5.77)
\end{aligned}$$

We note here that, the current and deformed configurations are commute in the case of superposed incremental deformations (i.e. $\mathbf{e}_\alpha = \mathbf{E}_\alpha$). For an orthonormal family of fibers (i.e. $\mathbf{L} = \mathbf{E}_1$, $L_1 = 1$, $L_2 = 0$, $\mathbf{M} = \mathbf{E}_2$, $M_1 = 0$, $M_2 = 1$), Eq. (5.77) furnishes

$$\dot{p}_{,i} = 2\mu u_{i,AA} + E_1 u_{1,11}\delta_{i1} - C_1 u_{i,1111} + E_2 u_{2,22}\delta_{i2} - C_2 u_{i,2222}. \quad (5.78)$$

Further, in view of Eqs. (5.66-5.68a), the condition of bulk incompressibility reduces to

$$(J-1)^{\cdot} = \mathbf{F}^*_o \cdot \dot{\mathbf{F}} = \text{div } \mathbf{u} = \mathbf{0}. \quad (5.79)$$

which, together with the Eq. (5.77), serves as a compatible form of the equilibrium equation (5.46) for small deformations. Lastly, the boundary conditions in Eq. (5.55) can be approximated similarly as in the above (e.g. $\mathbf{t} = \mathbf{t}_o + \varepsilon\dot{\mathbf{t}} + o(e)$ etc...)

$$
\begin{aligned}
\dot{t}_i &= \dot{P}_{iA}N_A - \frac{d}{dS}[C_1(\dot{g}_1)_i L_A T_A L_B N_B + C_2(\dot{g}_2)_i M_A T_A M_B N_B], \\
\dot{m}_i &= C_1(\dot{g}_1)_i L_A N_A L_B N_B + C_2(\dot{g}_2)_i M_A N_A M_B N_B, \\
\dot{f}_i &= C_1(\dot{g}_1)_i L_A T_A L_B N_B + C_2(\dot{g}_2)_i M_A T_A M_B N_B,
\end{aligned}
\tag{5.80}
$$

In particular, if the fiber's directions are either normal or tangential to the boundary (i.e. $(\mathbf{L} \cdot \mathbf{T})(\mathbf{L} \cdot \mathbf{N}) = 0$ and $(\mathbf{M} \cdot \mathbf{T})(\mathbf{M} \cdot \mathbf{N}) = 0$), Eq. (5.80) yields

$$
\begin{aligned}
\dot{t}_i &= \dot{P}_{iA}N_A, \\
\dot{m}_i &= C_1(\dot{g}_1)_i L_A N_A L_B N_B + C_2(\dot{g}_2)_i M_A N_A M_B N_B, \\
\dot{f}_i &= 0,
\end{aligned}
\tag{5.81}
$$

where

$$
\begin{aligned}
\dot{P}_{iA} &= 2\mu\dot{F}_{iA} - \dot{p}\delta_{iA} - p_o\dot{F}^*_{iA} + E_1\dot{F}_{jB}L_iL_jL_AL_B - C_1(\dot{g}_1)_{i,B}L_AL_B \\
&\quad + E_2\dot{F}_{jB}M_iM_jM_AM_B - C_2(\dot{g}_2)_{i,B}M_AM_B, \\
(\dot{g}_1)_i &= \dot{F}_{iC,D}L_CL_D \text{ and } (\dot{g}_2)_i = \dot{F}_{iC,D}M_CM_D.
\end{aligned}
\tag{5.82}
$$

In addition, since $J\partial F^*_{jB}/\partial F_{iA} = F^*_{jB}F^*_{iA} - F^*_{iB}F^*_{jA}$ at $\epsilon = 0$, we obtain

$$
(\partial F^*_{jB}/\partial F_{iA})_o = \delta_{jB}\delta_{iA} - \delta_{iB}\delta_{jA} \text{ and } (\mathbf{F}^*_{\mathbf{F}}[\dot{\mathbf{F}}])_{jB} = (\delta_{jB}\delta_{iA} - \delta_{iB}\delta_{jA})u_{i,A}, \tag{5.83}
$$

Therefore,

$$
\dot{F}^*_{iA} = (Div\mathbf{u})\delta_{iA} - u_{A,i} = -u_{A,i}, \tag{5.84}
$$

where $Div\mathbf{u} = 0$ from the linearized incompressibility condition.

5.6 Solution to the linearized problem

We introduce scalar field ϕ as

$$\mathbf{u} = \mathbf{k} \times \nabla\phi;\ u_i = \varepsilon_{\lambda i}\phi_{,\lambda}, \tag{5.85}$$

so that Eq. (5.79) can be automatically satisfied (i.e. $\phi_{,12} - \phi_{,21} = 0$). Thus, the linearized Euler equation Eq. (5.78) can be rewritten as

$$\dot{p}_{,i} = 2\mu\varepsilon_{\lambda i}(\phi_{,\lambda 11}+\phi_{,\lambda 22})-E_1\phi_{,211}\delta_{i1}-C_1\varepsilon_{\lambda i}\phi_{,\lambda 1111}-E_2\phi_{,122}\delta_{i2}-C_2\varepsilon_{\lambda i}\phi_{,\lambda 2222}. \tag{5.86}$$

By utilizing the compatibility condition of $\dot{p}_{,i}$ (i.e. $\dot{p}_{,ij} = \dot{p}_{,ji}$), we obtain the following partial differential equation solving for ϕ.

$$2\mu(\phi_{,1111}+2\phi_{,1122}+\phi_{,2222})-C_1(\phi_{,11}+\phi_{,22})_{,1111}-C_2(\phi_{,11}+\phi_{,22})_{,2222}-\phi_{,1122}(E_1+E_2) = 0, \tag{5.87}$$

The above further reduces to

$$\Delta[\Delta\phi - \alpha_1\phi_{,1111} - \alpha_2\phi_{,2222}] - (\beta_1 + \beta_2)\phi_{,1122} = 0, \tag{5.88}$$

where $\alpha_1 = \frac{C_1}{2\mu} > 0$, $\alpha_2 = \frac{C_2}{2\mu} > 0$, $\beta_1 = \frac{E_1}{2\mu} > 0$, $\beta_2 = \frac{E_2}{2\mu} > 0$. We note here that the solution of Eq. (5.88) is not accommodated by the conventional methods such as the Fourier transform and the separation of variables. Instead, we adopt the methods of iterative reduction and principle of eigenfunction expansion, and obtain the potential function for $\phi(x,\ y)$. Details are reserved the sake of conciseness

which can be found in [85]-[87]. The general solution of Eq. (5.88) is obtained as

$$
\begin{aligned}
\phi(x,y) \;=\; & \sum_{m=1}^{\infty}[\{A_m\exp\left(xT\right)+B_m\exp\left(-xT\right)+\exp(a_mx)(C_m\cos b_mx+D_m\sin b_mx)+ \\
& \exp(-a_mx)(E_m\cos b_mx+F_m\sin b_mx)\}\times(\sin my)],
\end{aligned}
\tag{5.89}
$$

where

$$
a_m \;=\; \sqrt{\dfrac{\sqrt{\left(\frac{\sqrt{3}}{2}\left(\frac{P}{Q}+\,Q\right)\right)^2+\left(-\frac{Q}{2}+\frac{P}{2Q}-\frac{B}{3A}\right)^2}+\left(-\frac{Q}{2}+\frac{P}{2Q}-\frac{B}{3A}\right)}{2}},
$$

$$
b_m \;=\; \sqrt{\dfrac{\sqrt{\left(\frac{\sqrt{3}}{2}\left(\frac{P}{Q}+\,Q\right)\right)^2+\left(-\frac{Q}{2}+\frac{P}{2Q}-\frac{B}{3A}\right)^2}-\left(-\frac{Q}{2}+\frac{P}{2Q}-\frac{B}{3A}\right)}{2}},
$$

$$
P \;=\; \dfrac{C}{3A}-\dfrac{B^2}{9A^2},\; T=\sqrt{Q-\dfrac{P}{Q}-\dfrac{B}{3A}},
$$

$$
Q \;=\; \sqrt[3]{\left(\left(\dfrac{C}{3A}-\dfrac{B^2}{9A^2}\right)^3+\left(\dfrac{B^3}{27A^3}+\dfrac{D}{2A}-\dfrac{B.C}{6A^2}\right)^2\right)^{\frac{1}{2}}-\dfrac{B^3}{27A^3}-\dfrac{D}{2A}+\dfrac{BC}{6A^2}}
\tag{5.89-1}
$$

and

$$
m=\dfrac{\pi n}{2d},\; A=-\alpha_1,\; B=(1-m^2),\; C=-m^2(\alpha_2m^2-\beta_1-\beta_2+2),\; D=-m^4(\alpha_2m^2+1)
\tag{5.89-2}
$$

The unknown constant real numbers $A_m, B_m, C_m, D_m, E_m,$ and F_m can be completely determined by imposing admissible boundary conditions as depicted in Eqs. (5.81-5.84). The analytical solution ϕ is then converted through mapping $\boldsymbol{\chi}=(X_1-\phi_{,2})\mathbf{e}_1+(X_2+\phi_{,1})\mathbf{e}_2$ to obtain the complete deformed configurations (see, for example, Fig. 5.10). In addition, the corresponding stress fields can also be obtained through Eqs. (5.82) and (5.85-5.86). For example, in the cases of fiber composites subjected to lateral extension and/or flexure (Fig. 5.62-1), the expressions of the corresponding boundary conditions can be obtained from Eqs.

(5.81-5.82 and 5.85) that

$$\text{Extension} \implies \dot{P}_{11} = 2\mu u_{1,1} - \dot{p} - 2\mu u_{2,2} + E_1 u_{1,1} - C_1 u_{1,111}$$

$$\text{Flexure} \implies \dot{\mathbf{m}} = \dot{m}_1 \mathbf{e}_1 + \dot{m}_2 \mathbf{e}_2, \ \dot{m}_1 = C_1 u_{1,11} \text{ and} \dot{m}_2 = 0 \qquad (5.90)$$

where $u_{1,1} = -\phi_{,21}$, $u_{1,11} = -\phi_{,211}$, $u_{1,111} = -\phi_{,2111}$ and similarly for u_2 (Eq. 5.85). In the analysis, the applied tensions and moments are approximated via Fourier series as;

$$\dot{P}_{11} = 2\mu u_{1,1} - \dot{p} - 2\mu u_{2,2} + E_1 u_{1,1} - C_1 u_{1,111} = 50 \cong \sum_{l=1}^{30} \frac{200}{\pi l} (-1)^{\frac{l-1}{2}} \cos(\frac{\pi l}{2d}) y,$$

$$(5.91)$$

and

$$\dot{\mathbf{m}} = \dot{m}_1 \mathbf{e}_1 + \dot{m}_2 \mathbf{e}_2, \ \dot{m}_1 = C_1 u_{1,11} = 80 \cong \sum_{n=1}^{30} \frac{20}{\pi n} (-1)^{\frac{n-1}{2}} \cos(\frac{\pi n}{2d}) y \mathbf{e}_m,$$

$$\dot{m}_2 = 0, \qquad (5.92)$$

which ensure fast convergence (within 30 iterations). Despite the presence of sharp corners, where singular behaviors of response functions are often observed, the obtained solutions are smooth and stable throughout the entire domain of interest (Fig. 5.10) with reasonable sensitivity to the fiber's resistant to both the extension and flexure. More precisely, Figs. 5.11-5.12 indicate the inverse correlations between the magnitude of deformations and fiber's material constants.

In particular, the linear solution displays good agreements with the nonlinear solutions and experiments [[84]] for small deformations superposed on large (Fig. 4.13) while it demonstrate discrepancies in the predictions of large deformation analyses (Fig. 5.13). Overall, the proposed models perform well in the prediction of the mechanical behavior of fiber-reinforced composites and therefore they can be easily adopted in field exercises.
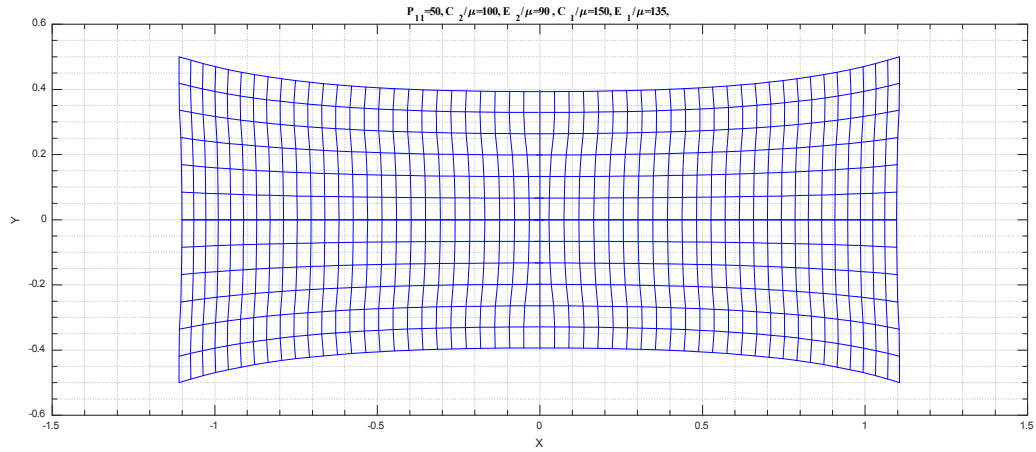
Figure 5.10: Deformed configurations under axial loading $P_{11}/\mu = 50$
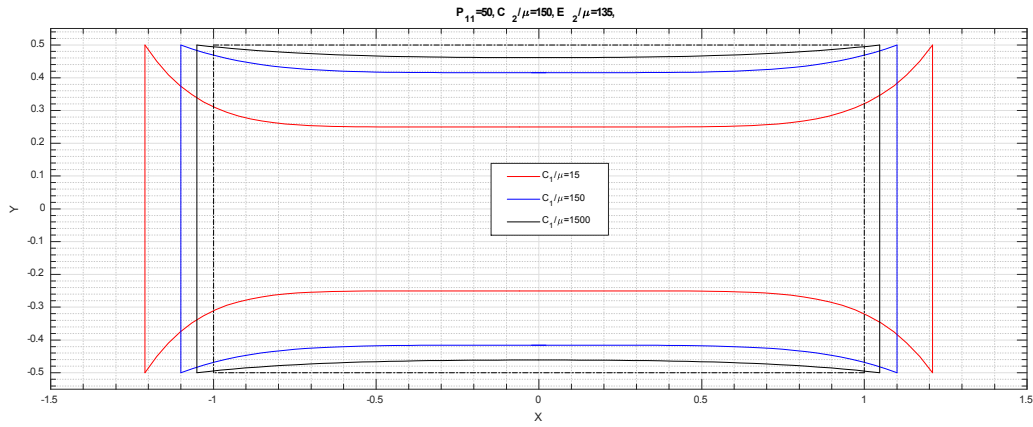
Figure 5.11: Deformed configurations with respect to E_1/μ when $P_{11}/\mu = 50$.
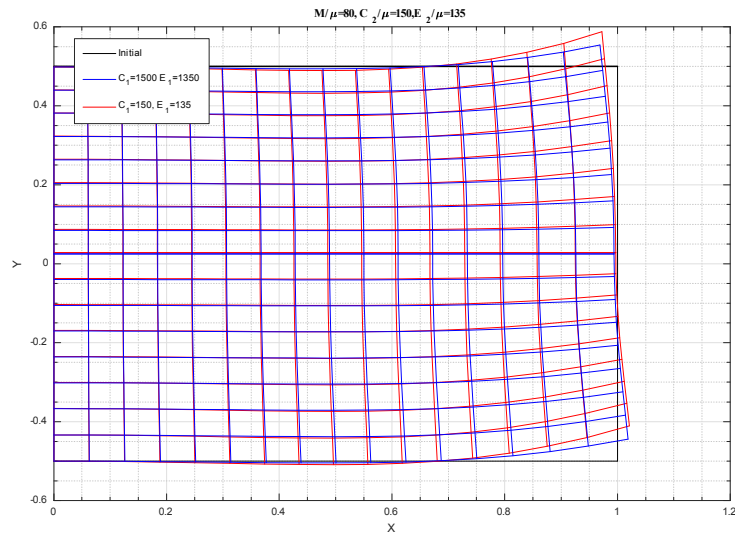
Figure 5.12: Deformed configurations with respect to E_1/μ when $P_{11}/\mu = 50$
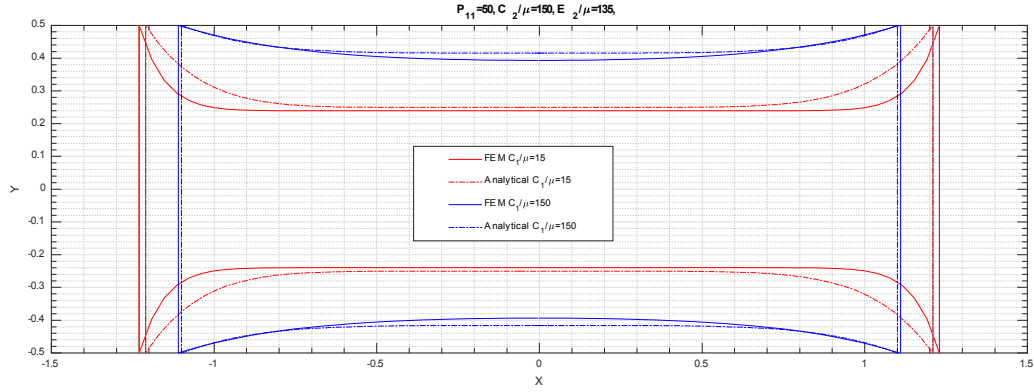
Figure 5.13: Analytical VS nonlinear solutions: Extension $P_{11} = 50$
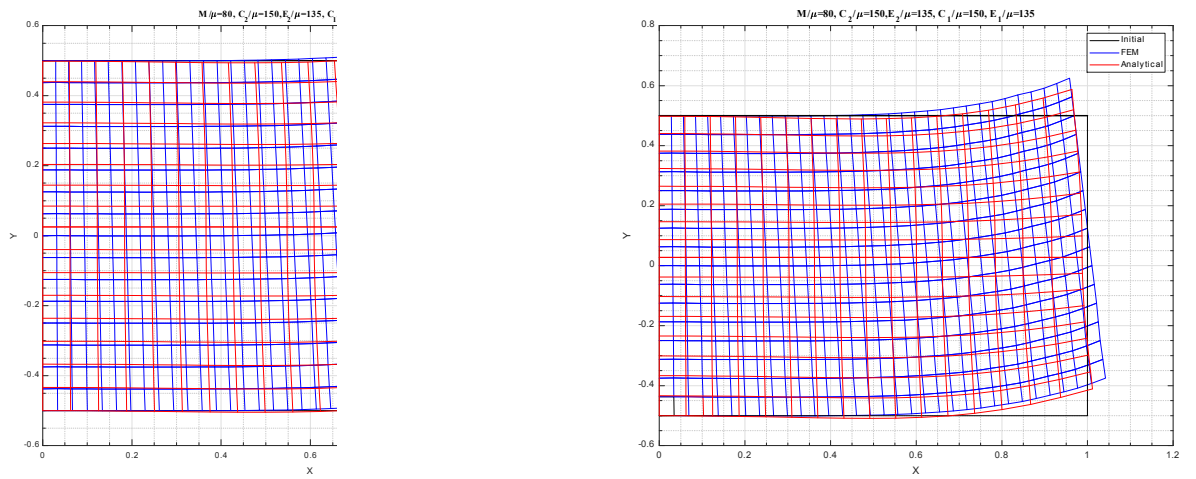
Figure 5.14: Analytical VS nonlinear solutions: Flexure M/μ=50

Chapter 6

Conclusions and future works

6.1 Conclusions

In this thesis, we have presented a continuum model for the mechanics of elastic solid reinforced with both unidirectional (see chapter 2 and 3) and bidirectional (see chapter 4 and 5) fibers in finite plane elastostatics. The primary goal of this thesis is to find analytical and numerical solutions of differential equations which are obtained from the gradient elasticity theory. Our works lead to the following conclusions:

- We have developed analytical and numerical solution for these models. The fibers are idealized as continuously distributed spatial the Kirchhoff rods and their elastic resistant to stretch and flexure are incorporated into the models via the gradient of deformations. Then, the Euler equation and necessary boundary conditions are derived. These lead to 4th order nonlinear coupled PDE systems from which a set of numerical solutions describing mechanical responses of fiber composites are obtained.

- Especially, we examined the plane bias extensions (see chapter 5) in the case of bidirectional fiber-reinforced composites and demonstrate that the proposed model successfully predicts the continuous distributions of shear

strain fields through the second gradient of deformations. Also, a compatible linear theory, including boundary conditions, is developed and used to obtain complete analytical solutions. The results obtained from the linear theory demonstrate close agreement with the both numerical predictions and experiments for the small deformation regime. In addition, the analytical solution for bending exhibits smooth behavior as it approaches the boundary despite the influences of sharp corners, where singular behaviors of response functions are often observed.

- We have developed a FEM code to solve 4th order nonlinear coupled PDE systems. The numerical results are compared with the results in literatures (FEniCS Project) showing a good agreement (see chapter 4).

- The results are compared with several experimental data demonstrating that the proposed model successfully predicts the deformed configurations of a Crystalline Nanocellulose (CNC) fiber composite subjected to three point bending, and also corresponds with the experimental results for T700S carbon-E glass fiber composites (see chapter 4 and 5).

- Lastly, we mention that the proposed model can be used as an alternative 2D Cosserat theory of non-linear elasticity.

The hardest parts of this thesis were obtaining analytical and numerical solutions of differential equations. This is due to the fact that the conventional methods, Fourier transform and the method of separation of variable, are not applicable. Instead, we adopt iterative reduction and eigenfunction expansion methods (modified separation of variable methods; see, [85] and [87]) and successfully obtained complete analytical solutions for the small deformations superposed on large. Also, due to the complex nature of the resulting PDEs, it was not possible to obtain solutions using the commercial numerical softwares (e.g. COMSOL, Abaqus). To overcome the difficulties, we developed our own numerical schemes through which complete numerical solutions are obtained.

The thesis initiates the research subject on modeling biomaterials and soft materials which are very popular these days. While writing the thesis, I have a great passion and motivation to pursue my Ph.D. study in the field of soft material.

6.2 Future Works

- This work can be extended by using the Mooney-Rivlin model energy functions, for the analysis of soft composite materials such as carbon fiber rubber composite and human composite tissues.

- As we discussed, so far we studied up to the second order gradient theory. We can develop third gradient elastic theory in the application of microstructured continua (see [24]).

- In this work we developed a model for fiber reinforced composite. As we illustrated in the introduction, we can also model cracks with this theory in the future.

BIBLIOGRAPHY

[1] Spencer, A.J.M., "Deformations of Fibre-Reinforced Materials," *Oxford University Press* (1972).

[2] Pipkin, A.C., "Stress analysis for fiber-reinforced materials," *Adv. Appl. Mech.* **19**, 1-51 (1979) http://doi.org/10.1016/S0065-2156(08)70308-9

[3] W. Voigt, "Theoretical Studies on the Elasticity Relationships of Crystals," *Abh. Gesch. Wissenschaften* **34** (1887).

[4] F. Moravec, M. Holecek, "Microstructure-dependent Nonlinear Viscoelasticity due to Extracellular Flow within Cellular Structures," *Int. J. Solids and Struct.* **47**, 1876-1887 (2010) https://doi.org/10.1016/j.ijsolstr.2010.03.024

[5] J. F. Mulhern, T. G. Rogers, A.J.M. Spencer, "A continuum theory of a plastic-elastic fibre-reinforced material," *Int. J. Engng Sci.* **7**, 129-152 (1969) https://doi.org/10.1016/0020-7225(69)90053-6

[6] Pipkin, A.C., Rogers, T.G., "Plane deformations of incompressible fiber-reinforced materials," *ASME J. Appl. Mech.* **38**(8), 634-640 (1971) http://doi.org/10.1115/1.3408866

[7] Mulhern, J.F., Rogers, T.G., Spencer, A.J.M., "A continuum model for fibre-reinforced plastic materials," *Proc. R. Soc. Lond. A.* **301**(1467), 473-492 (1967) https://doi.org/10.1098/rspa.1967.0220

[8] Spencer, A.J.M., Soldatos, K.P., "Finite deformations of fibre-reinforced elastic solids with fibre bending stiffness," *Int. J. Non-Linear Mech.* **42**, 355-368 (2007) https://doi.org/10.1016/j.ijnonlinmec.2007.02.015

[9] D.J. Steigmann,F. dell'Isola, "Mechanical response of fabric sheets to three-dimensional bending, twisting, and stretching," *Acta Mechanica Sinica* **31**(3), 373-382 (2015) https://doi.org/10.1007/s10409-015-0413-x

[10] R.A. Toupin, "Theories of elasticity with couple stress," *Arch. Ration. Mech. Anal.* **17**, 85-112 (1964) https://hal.archives-ouvertes.fr/hal-00853382/en

[11] W.T. Koiter, "Couple-stresses in the theory of elasticity," *Proc. K. Ned. Akad. Wetensc. B* **67**, 17-44 (1964).

[12] H.C. Park, R.S. Lakes, "Torsion of a micropolar elastic prism of square cross section," *Int. J. Solids Struct.* **23,** 485–503 (1987) https://doi.org/10.1016/0020-7683(87)90013-8

[13] I. Munch, P. Neff, W. Wagner, "Transversely isotropic material: nonlinear Cosserat vs. classical approach," *Continuum Mech. Therm.* **23,** 27–34 (2011) https://doi.org/10.1007/s00161-010-0150-0

[14] P. Neff, "Existence of minimizers for a finite-strain micro-morphic elastic solid," *Proc. Roy. Soc. Edinburgh A* **136**, 997–1012 (2006) https://doi.org/10.1017/S0308210500004844

[15] E. Fried, M.E. Gurtin, "Gradient nanoscale polycrystalline elasticity: intergrain interactions and triple-junction conditions," *J. Mech. Phys. Solids* **57,** 1749–1779 (2009) https://doi.org/10.1016/j.jmps.2009.06.004

[16] Steigmann, D.J., "Theory of elastic solids reinforced with fibers resistant to extension, flexure and twist," *Int. J. Non-Linear mech.* **47**, 743-742 (2012). http://doi.org/10.1016/j.ijnonlinmec.2012.04.007

[17] dell'Isola, F., Cuomo, M., Greco, L., Della Corte, A., "Bias extension test for pantographic sheets: numerical simulations based on second gradient shear energies," *J. Eng. Math.* **103**(1), 127-157 (2017). http://doi.org/10.1007/s10665-016-9865-7

[18] Turco, E., et al., "Non-standard coupled extensional and bending bias tests for planar pantographic lattices. Part I: numerical simulations," *Z. Angw. Math. Phys* **67**(5), 122 (2016) https://doi.org/10.1007/s00033-016-0713-4

[19] F. dell'Isola, A. Della Corte, L. Greco, A. Luongo, "Plane bias extension test for a continuum with two inextensible families of fibers: a variational treatment with Lagrange multipliers and a perturbation solution," *Int. J. Solids Struct.* **81**, 1–12 (2016) https://doi.org/10.1016/j.ijsolstr.2015.08.029

[20] Cuomo, M., dell'Isola, F.,Greco, L., "Simplified analysis of a generalized bias-test for fabricswith two families of inextensible fibres," *Z. Angw. Math. Phys.* **39** (2016). https://doi.org/10.1007/s00033-016-0653-z

[21] Rivlin, R. S., "The solution of problems in second order elasticity theory," *J. Ration. Mech. Anal.* **2**, 53-81 (1953) http://doi.org/10.1007/978-1-4612-2416-7_20

[22] Ericksen, JL and Rivlin, RS., "Large elastic deformations of homogeneous anisotropic materials," *J Ration Mech Anal.* **3**, 281-301 (1954) https://doi.org/10.1007/978-1-4612-2416-7_32

[23] Boisse, P., Hamila, N., & Madeo, A., "Modelling the development of defects during composite reinforcements and prepreg forming," *Phil. Trans. R. Soc. A*, **374**(2071), 20150269 (2016), https://doi.org/10.1098/rsta.2015.0269

[24] Dell'Isola, Francesco, Alessandro Della Corte, and Ivan Giorgio, "Higher-gradient continua: The legacy of Piola, Mindlin, Sedov and Toupin and some future research perspectives," *Math. Mech. Solids* **22**(4), 852-872 (2017) http://doi.org/10.1177/1081286515616034

[25] Dahler, JS, and Scriven, LE., "Theory of structured continua. IGeneral consideration of angular momentum and polarization," *Proc Roy Soc London* **275**, 504–527 (1963) http://doi.org/10.1098/rspa.1963.0183

[26] Green, AE, and Rivlin, RS., "Multipolar continuum mechanics," *Arch Rat Mech Anal* **17**, 113–147 (1964) http://doi.org/10.1007/978-1-4612-2416-7_114

[27] Mindlin, RD., "Second gradient of strain and surface-tension in linear elasticity," *Int J Solid Struct.* **1**(4), 417–438 (1965) http://doi.org/10.1016/0020-7683(65)90006-5

[28] E. Cosserat and F. Cosserat, "Theorie des corps deformables. Hermann, Paris, (1909).

[29] Reissner, E., "A further note on finite-strain force and moment stress elasticity," *Z. angew. Math. Phys.* **38**, 665-673 (1987) http://doi.org/10.1007/BF00948288

[30] Adkins, JE., "Finite plane deformation of thin elastic sheet reinforced with inextensible cords," *Phil Trans Roy Soc Series A* **249,** 125 (1956) http://doi.org/10.1098/rsta.1956.0017

[31] R.D. Mindlin, Tiersten, H.F., "Effects of couple-stresses in linear elasticity," *Arch. Ration. Mech. Anal.* **11**, 415-448 (1962) https://doi.org/10.1007/BF00253946

[32] LI. Sedov, "Mathematical methods for constructing new models of contin-

uous media," *Russ. Math. Surv.* **20**(5), 123–182 (1965) https://doi.org/10.1070/RM1965v020n05ABEH001191

[33] Cowin, SC., "Bone poroelasticity," *J. Biomech.* **32**(3), 217–238 (1999) https://doi.org/10.1016/S0021-9290(98)00161-4

[34] Federico, S., & Gasser, T. C., "Nonlinear elasticity of biological tissues with statistical fibre orientation," *J Roy. Soc. Interface*, **7**(47), 955-966 (2010).

[35] Lekszycki, T, and dell'Isola, F., "A mixture model with evolving mass densities for describing synthesis and resorption phenomena in bones reconstructed with bio-resorbable materials," *ZAMM J Appl. Math. Mech.* **92**(6), 426–444 (2012) http://doi.org/10.1002/zamm.201100082

[36] Andreaus, U, Giorgio, I, and Lekszycki, T., "A 2D continuum model of a mixture of bone tissue and bio-resorbable material for simulating mass density redistribution under load slowly variable in time," *ZAMM J. Appl. Math. Mech.* **94**(12), 978–1000 (2014) http://doi.org/10.1002/zamm.201200182

[37] Madeo, A, Placidi, L, and Rosi, G., "Towards the design of metamaterials with enhanced damage sensitivity: Second gradient porous materials," *Res Nondes Eval* **25**(2), 99-124 (2014) https://doi.org/10.1080/09349847.2013.853114

[38] Biomedical Tissue Research, University of York, https://www.york.ac.uk/res/bonefromblood/background/boneremodelling.html, 2007

[39] Alessi, R, Marigo, JJ, and Vidoli, S., "Gradient damage models coupled with plasticity and nucleation of cohesive cracks," *Arch. Rat. Mech. Anal.* **214**(2), 575–615 (2014) https://doi.org/10.1007/s00205-014-0763-8

[40] Cazzani, A, and Rovati, M., "Sensitivity analysis and optimum design of elastic-plastic structural systems," *Meccanica* **26**(2-3), 173–178 (1991) https://doi.org/10.1007/BF00429886

[41] Francfort, GA, and Marigo, JJ., "Cracks in fracture mechanics: A time indexed family of energy minimizers. In: IUTAM symposium on variations of domain and free-boundary problems in solid mechanics, 197–202 (1999).

[42] G.A. Maugin, A.V. Metrikine, "Mechanics of Generalized Continua: One Hundred Years After the Cosserats," *Springer*, New York (2010).

[43] P. Neff, "A finite-strain elastic–plastic Cosserat theory for polycrystals with grain rotations," *Int. J. Eng. Sci.* **44,** 574–594 (2006) https://doi.org/10.1016/j.ijengsci.2006.04.002

[44] S.K. Park, X.-L. Gao, "Variational formulation of a modified couple-stress theory and its application to a simple shear problem," *Z. Angew. Math. Phys* **59**, 904–917 (2008) https://doi.org/10.1007/s00033-006-6073-8

[45] C. Truesdell, W. Noll, "The non-linear field theories of mechanics, in:S. Flugge (Ed.)," *Handbuch der Physik, vol. III/3*, Springer, Berlin (1965).

[46] P. Germain, "The method of virtual power in continuum mechanics, part 2: microstructure," *SIAM J. Appl. Math.* **25**, 556-575 (1973) https://doi.org/10.1137/0125053

[47] F. dell'Isola, D.J. Steigmann, "A Two-dimensional gradient-elasticity theory for woven fabrics," *J. Elast.* **118**(1), 113-125 (2015) https://doi.org/10.1007/s10659-014-9478-1

[48] R.W. Ogden, "Non-Linear Elastic Deformations," *Ellis Horwood Ltd.*, Chichester, England (1984).

[49] Spencer, AJM, "Deformations of Fibre-Reinforced Materials," *Oxford University Press* (1972).

[50] Pipkin, AC, "Stress analysis for fiber-reinforced materials," *Advances in Appl Mech* **19,** 1–51 (1979).

[51] Dow, N, F. (1963) Gen. Elect. Co. Report No. R63-SD-61.

[52] Mulhern, JF and Rogers, TG. and Spencer, AJM, "A continuum theory of a plastic-elastic fibre-reinforced material," *Int J Engng Sci* **7**, 129-152 (1969).

[53] Spencer, AJM and Soldatos, KP, "Finite deformations of fibre-reinforced elastic solids with fibre bending stiffness," *Int J Non-Linear Mech* **42**, 355—368 (2007) https://doi.org/10.1016/j.ijnonlinmec.2007.02.015

[54] Steigmann, DJ., "Theory of elastic solids reinforced with fibers resistant to extension, flexure and twist," *Int J Non-Linear Mech.* **47**, 743–742 (2012) https://doi.org/10.1016/j.ijnonlinmec.2012.04.007

[55] Pietraszkiewicz, W and Eremeyev, VA., "On natural strain measures of the non- linear micropolar continuum," *Int. J. Solids Struct.* **46**, 774–787 (2009) https://doi.org/10.1016/j.ijsolstr.2008.09.027

[56] Boutin, C., "Microstructural effects in elastic composites," *Int. J. Solids and Struct.* **33**(7), 1023-1051 (1996) https://doi.org/10.1016/0020-7683(95)00089-5

[57] Dell'Isola, F, and Placidi, L., "Variational principles are a powerful tool also for formulating field theories. In: dell'Isola F., Gavrilyuk S. (eds) Variational Models and Methods in Solid and Fluid Mechanics. CISM Courses and Lectures," Vienna, Springer, 1-15 (2012) https://doi.org/10.1007/978-3-7091-0983-0_1

[58] Forest, S., "Homogenization methods and the mechanics of generalised continua part 2," T*heor. Appl. Mech.* **28**, 113-143 (2002) https://doi.org/10.2298/TAM0229113F

[59] Auffray, N., dell'Isola, F., Eremeyev, V., Madeo, A., Rosi, G., "Analytical continuum mechanics à la Hamilton-Piola: least action principle for second gradient continua and capillary fluids," *Mech. Math. of Solids* **20**(4), 375-417 (2015) https://doi.org/10.1177/1081286513497616

[60] Rinaldi, A, and Placidi, L., "A microscale second gradient approximation of the damage parameter of quasi-brittle heterogeneous lattices," *ZAMM J Appl Math Mech.* **94**(10), 862-877 (2014) https://doi.org/10.1002/zamm.201300028

[61] Contrafatto, L, and Cuomo, M., "A new thermodynamically consistent continuum model for hardening plasticity coupled with damage," *Int. J. Solid Struct.* **39**(25), 6241-6271 (2002) https://doi.org/10.1016/S0020-7683(02)00470-5

[62] Jasiuk, I, and Ostoja-Starzewski, M., "Modeling of bone at a single lamella level," *Biomech. Model Mechanobio.* **3**(2), 67-74 (2004) https://doi.org/10.1007/s10237-004-0048-5

[63] Carcaterra, A, and Akay, A., "Theoretical foundations of apparent-damping phenomena and nearly irreversible energy exchange in linear conservative systems," J Acoust Soc. Am **121**(4), 1971–1982 (2007) https://doi.org/10.1121/1.2697030

[64] dell'Isola, F, Steigmann, D, and Della Corte, A., "Synthesis of complex structures. Designing micro-structure to deliver targeted macro-scale response," *Appl Mech Rev.* (2015) http://doi.org/10.1115/1.4032206

[65] Auffray, N, dell'Isola, F, Eremeyev, VA, et al., "Analytical continuum mechanics á la Hamilton–Piola least action principle for second gradient continua and capillary fluids," *Math Mech Solid* (2013) https://doi.org/10.1177/1081286513497616

[66] Casal, P., "Theory of second gradient and capillarity," *CR Hebd Sean Acad Sci Ser A* **274**(22), 1571-1574 (1972).

[67] Ferretti, M, Madeo, A, dell'Isola, F, et al., "Modeling the onset of shear boundary layers in fibrous composite reinforcements by second-gradient theory," *Z Angew Math Phys* **65**(3): 587–612 (2014) https://doi.org/10.1007/s00033-013-0347-8

[68] Lekszycki, T, and dell'Isola, F., "A mixture model with evolving mass densities for describing synthesis and resorption phenomena in bones reconstructed with bio-resorbable materials," *ZAMM J Appl Math Mech.* **92**(6), 426-444 (2012) https://doi.org/10.1002/zamm.201100082

[69] Placidi, L., Greco, L., Bucci, S., Turco, E., & Rizzi, N.L., "A second gradient formulation for a 2D fabric sheet with inextensible fibres," *Z. ang. Math. Phys.*, **67**(5), 114 (2016) https://doi.org/10.1007/s00033-016-0701-8

[70] S. W. Hahm, D. Y. Khang, "Crystallization and Microstructure-dependent Elastic Moduli of Ferroelectric P(VDF–TrFE) Thin Films," *Soft Matter* **6**, 5802-5806 (2010) https://doi.org/10.1039/C0SM00350F

[71] Placidi, L., Barchiesi, E., Turco, E., & Rizzi, N.L., "A review on 2D models for the description of pantographic fabrics," *Z. ang. Math. Phy.* **67**(5), 121 (2016) https://doi.org/10.1007/s00033-016-0716-1

[72] Cuomo, M., dell'Isola, F., Greco, L., Rizzi, N.L., "First versus second gradient energies for planar sheets with two families of inextensible fibres: Investigation on deformation boundary layers, discontinuities and geometrical instabilities," *Composites Part B Engineering*, **115**, 423-448 (2017) https://doi.org/10.1016/j.compositesb.2016.08.043

[73] J. Monecke, Microstructure Dependence of Material Properties of Composites," *Phys. Stat. Sol. (b)* **154**, 805-813 (1989) https://doi.org/10.1002/pssb.2221540239

[74] dell'Isola, F., Cuomo, M., Greco, L., Della Corte, A., "Bias extension test for pantographic sheets: numerical simulations based on second gradient shear energies," *J. Eng. Math.* 1-31 (2016) http://doi.org/10.1007/s10665-016-9865-7

[75] dell'Isola, F., Della Corte, A., Greco, L., Luongo, A., "Plane bias extension test for a continuum with two inextensible families of fibers: A variational treatment with Lagrange multipliers and a perturbation solution," *Int. J. Solids Struct.*, **81**, 1-12 (2016) https://doi.org/10.1016/j.ijsolstr.2015.08.029

[76] dell'Isola, F., Lekszycki, T., Pawlikowski, M.,Grygoruk, R., Greco, L., "Designing a light fabric metamaterial being highly macroscopically tough under directional extension: first experimental evidence," *Z. ang. Math. Physik ZAMP* **66**(6), 3473-3498 (2015) https://doi.org/10.1007/s00033-015-0556-4

[77] dell'Isola, F., Giorgio, I., Pawlikowski, M., Rizzi, N.L., "Large deformations of planar extensible beams and pantographic lattices: heuristic homogenization, experimental and numerical examples of equilibrium," *Proc. Roy. Soc. of London A* **472**(2185), 20150790 (2016) http://doi.org/10.1098/rspa.2015.0790

[78] M. Zeidi, Chun il Kim, "Mechanics of fiber composites with fibers resistant to extension and flexure," *Math. Mech. Solids* (2017) http://doi.org/10.7939/R3Z892V17

[79] M. Zeidi, Chun il Kim, "Finite plane deformations of elastic solids reinforced with fibers resistant to flexure: Complete solution," *Arch. Appl. Mech.* (2017) http://doi.org/10.1007/s00419-018-1344-3

[80] Zeidi, M., Kim, C., "Mechanics of fiber composites with fibers resistant to extension and flexure," *Math. Mech. Solids* (2017) http://doi.org/10.7939/R3Z892V17

[81] L.D. Landau, E.M. Lifshitz, "Theory of Elasticity, 3rd edition," Pergamon, Oxford (1986).

[82] Dill, E.H., "Kirchhoff's theory of rods," *Arch. Hist. Exact Sci.* **44,** 1-23 (1992) https://doi.org/10.1007/BF00379680

[83] S.S. Antman, "Nonlinear Problems of Elasticity," *Springer*, Berlin (2005).

[84] Dong, C., Davies, I.J., "Flexural strength of bidirectional hybrid epoxy composites reinforced by E glass and T700S carbon fibres," C*omposites: Part B* **72,** 65-71 (2015) https://doi.org/10.1016/j.compositesb.2014.11.031

[85] W.W. Read, "Analytical solutions for a Helmholtz equation with dirichlet boundary donditions and arbitrary boundaries," *Mathl. Comput. Modeling* **24**(2), 23-34 (1996) https://doi.org/10.1016/0895-7177(96)00087-8

[86] W.W. Read, "Series solutions for Laplace's equation with nonhomogeneous mixed boundary conditions and irregular boundaries," **17**(12), 9-19 (1993) https://doi.org/10.1016/0895-7177(93)90023-R

[87] Huang, Y., Zhang, X., "General analytical solution of transverse vibration for orthotropic rectangular thin plates," **1**(2), 78-82 (2002) https://doi.org/10.1007/BF02935845

[88] Turco, Emilio, et al., "Non-standard coupled extensional and bending bias tests for planar pantographic lattices. Part I: numerical simulations," *Z. ang. Math. und Phys.* **67**(5), 122 (2016) https://doi.org/10.1007/s00033-016-0713-4

[89] Turco, E., Barcz, K., Luigi Rizzi, N., "Non-standard coupled extensional and bending bias tests for planar pantographic lattices. Part II: comparison with experimental evidence," *Z. ang. Math. und Phys.* **67**(5) (2016) https://doi.org/10.1007/s00033-016-0714-3

[90] dell'Isola, F., Andreaus, U., Placidi, L., "At the origins and in the vanguard of peridynamics, non-local and higher gradient continuum mechanics. An underestimated and still topical contribution of Gabrio Piola," *Mech. Math. of Solids* **20** (8), 887-928 (2015) https://doi.org/10.1177/1081286513509811

[91] Boutin, C., dell'Isola, F., Giorgio, I., Placidi, L., "Linear pantographic sheets: Asymptotic micro-macro models identification," *Math. Mech. Complex Systems* **5**(2), 127-162 (2017) http://doi.org/10.2140/memocs.2017.5.127

[92] Mulhern, JF and Rogers, TG, and Spencer, AJM., "A continuum model for fibre-reinforced plastic materials," *Proc R Soc Lond A* **301**, 473-492 (1967).

[93] Spagnuolo, M., Barcz, K., Pfaff, A., dell'Isola, F., Franciosi, P., "Qualitative pivot damage analysis in aluminum printed pantographic sheets: Numerics and experiments," *Mechanics Research Communications* **83**, 47-52 (2017) http://doi.org/10.1016/j.mechrescom.2017.05.005

[94] dell'Isola, F., Steigmann, D.J., Della Corte, A., "Synthesis of fibrous complex structures: designing microstructure to deliver targeted macroscale response," *Applied Mechanics Reviews* **67**(6), 060804 (2016) http://doi.org/10.1115/1.4032206

[95] Turco, E., Golaszewski, M., Cazzani, A., & Rizzi, N.L., "Large deformations induced in planar pantographic sheets by loads applied on fibers: experimental validation of a discrete Lagrangian model," *Mechanics Research Communications* **76**, 51-56 (2016) http://doi.org/10.1016/j.mechrescom.2016.07.001

[96] Abali, B.E., Muller, W.H., dell'Isola, F., "Theory and computation of higher gradient elasticity theories based on action principles," *Archive of Applied Mechanics* **87**(9), 1495-1510 (2017) https://doi.org/10.1007/s00419-017-1266-5

[97] M. Cuomo, F. dell'Isola, L. Greco, "Simplified analysis of a generalized bias-test for fabrics with two families of inextensible fibres," *Z. ang. Math. Phys.* (2016) http://doi.org/10.1007/s00033-016-0653-z

[98] B.E. Abali, "Technical University of Berlin, Institute of Mechanics, Chair of Continuums Mechanics and Material Theory.Computational Reality," (2017) http://www.lkm.tu-berlin.de/ComputationalReality

[99] Alnaes, M.S., Blechta, J., Hake, J., Johansson, A., Kehlet, B., Logg, A., Richardson, C., Ring, J., Rognes, M.E., Wells, G.N., "The FEniCS Project Version 1.5," *Arch. of Numerical Software* **3** (2015). http://doi.org/10.11588/ans.2015.100.20553

[100] F. Dell'Isola, I. Giorgio, M. Pawlikowski, & N.L. Rizzi, "Large deformations of planar extensible beams and pantographic lattices: heuristic homogenization, experimental and numerical examples of equilibrium," P*roc. R. Soc. A* **472**(2185), 20150790 (2016) https://doi.org/10.1098/rspa.2015.0790

[101] N. Auffray, F dell'Isola, VA Eremeyev., "Analytical continuum mechanics á la Hamilton–Piola least action principle for second gradient continua and capillary fluids," *Math Mech Solid* (2013). https://doi.org/10.1177/1081286513497616

[102] Zeidi, M., Kim, C., "Finite plane deformations of elastic solids reinforced with fibers resistant to flexure: complete solution," *Arch. Appl. Mech.* (2017). http://doi.org/10.1007/s00419-018-1344-3

[103] Zeidi, M., Kim, C., "Mechanics of an elastic solid reinforced with bidirectional fiber in finite plane elastostatics: complete analysis," *Continuum Mech. Thermodyn* (2018) http://doi.org/10.1007/s00033-016-0653-z

[104] C. Boutin, P. Royer, and JL. Auriault, "Acoustic absorption of porous surfacing with dual porosity," *Int J Solid Struct* **35**(34), 4709–4737 (1998) https://doi.org/10.1016/S0020-7683(98)00091-2

[105] Y. Yang, A. Misra, "Higher-order stress-strain theory for damage modeling implemented in an element-free Galerkin formulation," *Comput Model Eng Sci* **64**(1), 1–36 (2010) https://hal.archives-ouvertes.fr/hal-00556175

[106] C.I. Kim, M. Zeidi, "Gradient elasticity theory for fiber composites with fibers resistant to extension and flexure," *Int J Eng Science*, (2018) https://doi.org/10.1016/j.ijengsci.2018.06.002